



5-2017

# Thermodynamic Characterization and Isothermal Separability of Heavy Fission Product Chelates for Post-Detonation Nuclear Forensic Analysis

Steven Adam Stratz

*University of Tennessee, Knoxville*, [ssstratz@vols.utk.edu](mailto:ssstratz@vols.utk.edu)

---

## Recommended Citation

Stratz, Steven Adam, "Thermodynamic Characterization and Isothermal Separability of Heavy Fission Product Chelates for Post-Detonation Nuclear Forensic Analysis." PhD diss., University of Tennessee, 2017.  
[https://trace.tennessee.edu/utk\\_graddiss/4428](https://trace.tennessee.edu/utk_graddiss/4428)

This Dissertation is brought to you for free and open access by the Graduate School at Trace: Tennessee Research and Creative Exchange. It has been accepted for inclusion in Doctoral Dissertations by an authorized administrator of Trace: Tennessee Research and Creative Exchange. For more information, please contact [trace@utk.edu](mailto:trace@utk.edu).

To the Graduate Council:

I am submitting herewith a dissertation written by Steven Adam Stratz entitled "Thermodynamic Characterization and Isothermal Separability of Heavy Fission Product Chelates for Post-Detonation Nuclear Forensic Analysis." I have examined the final electronic copy of this dissertation for form and content and recommend that it be accepted in partial fulfillment of the requirements for the degree of Doctor of Philosophy, with a major in Nuclear Engineering.

Howard L. Hall, Major Professor

We have read this dissertation and recommend its acceptance:

Lawrence H. Heilbronn, Robert M. Counce, Joseph R. Stainback

Accepted for the Council:

Dixie L. Thompson

Vice Provost and Dean of the Graduate School

(Original signatures are on file with official student records.)

---

# Thermodynamic Characterization and Isothermal Separability of Heavy Fission Product Chelates for Post-Detonation Nuclear Forensic Analysis

A Dissertation Presented for the

Doctor of Philosophy

Degree

The University of Tennessee, Knoxville

Steven Adam Stratz

May 2017

Copyright © 2017 by Steven Adam Stratz

All rights reserved.

## ACKNOWLEDGEMENTS

I would first like to thank my major advisor and postdoc advisor, Dr. Howard Hall and Dr. John Auxier II, who helped guide me through my degree and research. Their experience and guidance have been of great assistance, and I would not be where I am today without them. I would further like to thank my committee members, Dr. Lawrence Heilbronn, Dr. Joseph Stainback IV, and Dr. Robert (Pete) Counce, for their enthusiasm in the classroom and time spent helping me to further develop and enhance this research.

I would also like to thank the Department of Nuclear Engineering, particularly Mrs. Gisela Goertz, for continued administrative support and assistance when things did not go as planned. Her willingness to help a graduate student through paperwork, travel, and life in general is unmatched in the administrative world.

I would further like to thank the Institute for Nuclear Security, particularly Mrs. Kristin England, for complete and uninhibited support throughout this degree. Her continuous investment in the lives of her students is extremely admirable.

I would also like to thank my undergraduate assistants, Mr. Colton Oldham (Dept. of Nuclear Engineering), Mr. Matthew Marsh (Dept. of Chemistry), Ms. Ashlyn Jones (Dept. of Chemistry), and Mr. Austin Mullen (Dept. of Nuclear Engineering), for their dedication and willingness to complete any and all tasks I asked of them. Without their orchestrated efforts and individual areas of expertise, this research would have taken much more time to complete, and for that I am very thankful.

Lastly, my gratitude would not be complete without the acknowledgement of my friends and family who formed my support network throughout this difficult period. I would particularly

like to thank my mom and dad, Denise and Steve Stratz, for their unending support and love. I would also like to thank Benjamin Vaught, Robert Schafer, Emilie Fenske, Jonathan Gill, Nicole Huchet, Nancy Carder, Amalie Zeitoun, and Jeffrey Morrison for their ever-present encouragement and motivation.

## **ABSTRACT**

Nuclear terrorism, one of the most critical threats to national security, exhibits complexities that do not exist with similar threats from sanctioned state actors. Responding to a domestic nuclear terrorism strike is difficult when the original source of the weapon may be unknown, given that terrorist organizations (at the time of writing) do not themselves have nuclear technology sufficient to design and build nuclear weapons. Consequently, the development of forensic techniques to help source and characterize nuclear weapons after detonation has recently become an area of interest. This relatively new field of science, known as post-detonation nuclear forensics, aims to ascertain weapon characteristics with both speed and precision while maintaining the highest level of accuracy achievable.

Weapon debris analysis employs chemical analytical techniques, among others, to obtain the technical information necessary for the attribution process. This work aims to reduce the time necessary for technical post-detonation forensic analysis by introducing gas-phase chemistry as an alternative to modern liquid-phase fission product separation techniques. This technique is intended to quantify and identify a certain class of fission products that appear in weapon debris in order to aid in weapon characterization. In particular, an organic ligand is attached to rare earth fission products to attempt separation of the products in the gas phase using isothermal chromatography. Successful, timely separation would contribute significantly to post-detonation forensic science, while even failed separations would contribute useful thermodynamic properties of these little-known complexes to the scientific community.

## **PREFACE**

This dissertation is an original intellectual product of the author, Steven Adam Stratz, performed under grant number DE-NA0001983 from the Stewardship Science Academic Alliances (SSAA) Program of the National Nuclear Security Administration (NNSA) and supported by the U.S. Department of Homeland Security (DHS) under grant award number 2012-DN-130-NF0001. The views and conclusions contained in this document are those of the author and should not be interpreted as representing the official policies, either expressed or implied, of the supporting entities.

Certain aspects of this work were performed in collaboration with the author's research group, including synthesis and characterization of the fission product complexes by Mr. Matthew Marsh, Mrs. Ashlyn Jones, Dr. Dan Hanson, Dr. John Auxier II, and the author, and the design and building of the updated coupled GC-ICP-TOF-MS system was performed by Mr. Colton Oldham, Mr. Austin Mullen, and the author. Two undergraduate research assistants, Mr. Austin Mullen and Mr. Colton Oldham, were instrumental in lab support during methodology development among various other supporting duties. Mr. Steven Jones was vital throughout many portions of this research in his capacity as the resident mass spectrometrists.

Portions of the text, as specified within the chapters, are quoted from scientific articles of which I am an author. Parts of the introductory text format are used from my master's thesis, completed at Tennessee Technological University and published in 2014.

All of the work presented henceforth was conducted at the University of Tennessee, Knoxville.



# TABLE OF CONTENTS

<b>CHAPTER 1 INTRODUCTION .....</b>	<b>1</b>
<i>1.1 Background: Nuclear Terrorism and Nuclear Forensics.....</i>	<i>1</i>
<i>1.2 Nuclear Debris Genesis and Analysis .....</i>	<i>1</i>
<i>1.3 Rare Earth Separations .....</i>	<i>3</i>
<i>1.4 Analytical Research Efforts .....</i>	<i>3</i>
<i>1.5 Complications with Current Practices in Post-Detonation Debris Analysis.....</i>	<i>4</i>
<i>1.6 Statement of the Problem.....</i>	<i>4</i>
<i>1.7 Statement of the Question .....</i>	<i>5</i>
<i>1.8 Objective of the Study .....</i>	<i>6</i>
<i>1.9 Dissertation Outline .....</i>	<i>6</i>
<b>CHAPTER 2 LITERATURE SURVEY .....</b>	<b>7</b>
<i>2.1 Essential Steps: Post-Detonation Nuclear Forensic Analysis.....</i>	<i>7</i>
<i>2.2 Synthesizing Nuclear Debris Surrogates for Analytical Development .....</i>	<i>8</i>
<i>2.3 Synthesis and Characterization of Ln[hfac]<sub>4</sub> Complexes .....</i>	<i>13</i>
<i>2.4 Modern Rare Earth Separations.....</i>	<i>15</i>
<i>2.5 Superheavy Element Thermochromatography .....</i>	<i>18</i>
<i>2.6 Separation Viability.....</i>	<i>21</i>
<i>2.7 Legal Requirements of TNF Data.....</i>	<i>21</i>
<i>2.8 Experimental Evaluation of Enthalpy and Entropy of Adsorption .....</i>	<i>23</i>
<b>CHAPTER 3 EXPERIMENTAL DEVELOPMENT .....</b>	<b>24</b>
<i>3.1 Scope.....</i>	<i>24</i>
<i>3.2 Synthesis and Characterization .....</i>	<i>25</i>
<i>3.3 Separation Chemistry .....</i>	<i>27</i>

3.4 Instrumentation.....	30
<b>CHAPTER 4 METHODOLOGY .....</b>	<b>37</b>
4.1 Engineering: Developing a Functional Coupling System .....	37
4.2 Injection Methodology.....	38
4.3 Proof of Concept: Separation Viability .....	39
4.4 Thermodynamic Measurements .....	43
4.5 Separation Optimization.....	47
4.6 Expected Results .....	53
<b>CHAPTER 5 RESULTS AND DISCUSSION.....</b>	<b>54</b>
5.1 Deposition Temperature Ranges of Individual $\text{Ln}[\text{hfac}]_4$ Complexes.....	54
5.2 Adsorption Plots .....	54
5.3 Enthalpy and Entropy of Adsorption of $\text{Ln}[\text{hfac}]_4$ Complexes .....	62
5.4 Monte Carlo Modeling using Adsorption Enthalpy Values.....	66
5.5 Thermodynamic Model .....	70
<b>CHAPTER 6 CONCLUSION .....</b>	<b>74</b>
6.1 Conclusion.....	74
6.2 Areas of Continuation.....	75
6.3 Legal Disclaimers and Acknowledgements .....	79
<b>REFERENCES.....</b>	<b>80</b>
<b>APPENDICES .....</b>	<b>87</b>
<b>APPENDIX A CHARACTERIZATION OF <math>\text{NH}_4[\text{LN}(\text{HFAC})_4]</math> COMPLEXES.....</b>	<b>88</b>
A.1 Characterization of $\text{Sm}[\text{hfac}]_4$ (1), $\text{Gd}[\text{hfac}]_4$ (2), $\text{Dy}[\text{hfac}]_4$ (3), and $\text{Tm}[\text{hfac}]_4$ (4) .....	88
A.2 Elemental Analysis .....	89

<i>A.3 FTIR</i> .....	90
<i>A.4 NMR</i> .....	90
<i>A.5 Melting Points</i> .....	90
<i>A.5 TGA</i> .....	91
<b>APPENDIX B ICP-MS SAMPLE INTEGRITY OF <math>\text{Ln}[\text{hfac}]_x</math> COMPLEXES</b> .....	<b>94</b>
<b>APPENDIX C MATLAB CODES AND MODELS</b> .....	<b>101</b>
<i>C.1 GCMS Readout Analysis</i> .....	101
<i>C.2 Thermodynamic Model</i> .....	105
<i>C.3 Monte Carlo Model<sup>12</sup></i> .....	111
<i>C.4 Experimental Data Analysis</i> .....	119
<b>APPENDIX D FRAGMENTATION PATTERNS</b> .....	<b>123</b>
<b>APPENDIX E THERMOGRAVIMETRIC ANALYSIS</b> .....	<b>130</b>
<b>VITA</b> .....	<b>135</b>

## LIST OF TABLES

Table 2.1 Characterization Techniques for Pre-Detonation Nuclear Materials (IAEA) <sup>15</sup> .....	8
Table 2.2 Characterization Techniques for Post-Detonation Nuclear Materials <sup>16</sup> .....	9
Table 3.1 Sample Contaminants .....	28
Table 3.2 Temperature Retention Volume Half-Values .....	30
Table 5.1 Pressure-Dependent Deposition Temperatures of Ln[hfac] <sub>4</sub> Complexes, °C .....	55
Table 5.2 Enthalpy and Entropy of Adsorption Values of Ln[hfac] <sub>4</sub> Complexes .....	62
Table 5.3 Simulated Monte Carlo Retention Times of Ln[hfac] <sub>4</sub> Complexes at 130°C .....	67
Table 5.4 Simulated Monte Carlo Retention Times of Ln[hfac] <sub>4</sub> Complexes at 193°C .....	68
Table 5.5 Thermodynamic Model Retention Time of Ln[hfac] <sub>4</sub> Complexes at 130°C.....	71
Table 5.6 Thermodynamic Model Retention Time of Ln[hfac] <sub>4</sub> Complexes at 193°C.....	71
Table A.1 Melting Points of NH <sub>4</sub> [Ln(hfac) <sub>4</sub> ] Complexes .....	92
Table A.2 Kinetic Thermodynamic Parameters of Complexes 1 – 4 using Coats-Redfern, Horowitz-Metzger, and Freeman Carroll.....	93
Table D.1 Possible FID Fragmentation Patterns of NH <sub>4</sub> [Ln(hfac) <sub>4</sub> ] Complexes* .....	123
Table E.1 Thermogravimetric Predictions of Enthalpy of Adsorption .....	130

# LIST OF FIGURES

Figure 1.1 Attribution Process.....	2
Figure 2.1 Trinity Test near Alamogordo, NM <sup>17</sup> .....	10
Figure 2.2 Trinitite Sample <sup>18</sup> .....	11
Figure 2.3 Synthetic Trinitite Sample <sup>4</sup> .....	12
Figure 2.4 Synthetic Urban Nuclear Melt Glass .....	13
Figure 2.5 Fission Product Spectrum <sup>23</sup> .....	14
Figure 2.6 Rare Earth Elements <sup>24</sup> .....	15
Figure 2.7 Large-Scale Ion Exchange Chromatography <sup>27</sup> .....	16
Figure 2.8 Cation Exchange Procedure <sup>31</sup> .....	17
Figure 2.9 Tiered Industrial Rare Earth Separation <sup>33</sup> .....	18
Figure 2.10 Author's Rendition of Sg Separation Procedure .....	20
Figure 3.1 Fully Synthesized RE Hfac Complexes.....	27
Figure 3.2 GC-ICP-TOF-MS Schematic (Version 1).....	32
Figure 3.3 GC-ICP-TOF-MS Front View (Version 1) .....	33
Figure 3.4 GC-ICP-TOF-MS Profile (Version 1).....	34
Figure 3.5 Coupling Oven (Version 2) .....	34
Figure 3.6 Assembled GC-ICP-TOF-MS (Version 2).....	35
Figure 3.7 ICP-TOF-MS Process <sup>58</sup> .....	35
Figure 4.1 Solid Injection of Pr[hfac] <sub>4</sub> .....	38

Figure 4.2 3D plot of GC-MS data from a sample injection of Sm, Dy, and Tm hfac .....	40
Figure 4.3 Custom Quartz Argon Heating Column.....	41
Figure 4.4 Quartz Argon Heating Coil Positioning .....	42
Figure 4.5 Stainless Steel Tube Oven Connection.....	42
Figure 4.6 Tm/Er Mixture Detection.....	44
Figure 4.7 Tm/Gd Mixture Detection.....	44
Figure 4.8 Gd/Ho/Tm/Lu Mixture Detection .....	45
Figure 5.1 Pr[hfac] <sub>4</sub> Adsorption Convergence Plot .....	56
Figure 5.2 Nd[hfac] <sub>4</sub> Adsorption Convergence Plot.....	56
Figure 5.3 Sm[hfac] <sub>4</sub> Adsorption Convergence Plot .....	57
Figure 5.4 Eu[hfac] <sub>4</sub> Adsorption Convergence Plot.....	57
Figure 5.5 Gd[hfac] <sub>4</sub> Adsorption Convergence Plot .....	58
Figure 5.6 Tb[hfac] <sub>4</sub> Adsorption Convergence Plot.....	58
Figure 5.7 Dy[hfac] <sub>4</sub> Adsorption Convergence Plot.....	59
Figure 5.8 Ho[hfac] <sub>4</sub> Adsorption Convergence Plot.....	59
Figure 5.9 Er[hfac] <sub>4</sub> Adsorption Convergence Plot .....	60
Figure 5.10 Tm[hfac] <sub>4</sub> Adsorption Convergence Plot.....	60
Figure 5.11 Yb[hfac] <sub>4</sub> Adsorption Convergence Plot.....	61
Figure 5.12 Lu[hfac] <sub>4</sub> Adsorption Convergence Plot.....	61
Figure 5.13 Enthalpy of Adsorption of Ln[hfac] <sub>4</sub> Complexes.....	63

<b>Figure 5.14 Entropy of Adsorption of Ln[hfac]<sub>4</sub> Complexes .....</b>	<b>63</b>
<b>Figure 5.15 Enthalpy of Adsorption vs. Enthalpy of Sublimation for Ln[hfac]<sub>4</sub> Complexes.....</b>	<b>64</b>
<b>Figure 5.16 Adsorption Enthalpy vs. Sublimation Enthalpy .....</b>	<b>64</b>
<b>Figure 5.17 Selected Adsorption Enthalpy vs. Sublimation Enthalpy .....</b>	<b>66</b>
<b>Figure 5.18 Gd[hfac]<sub>4</sub>, Ho[hfac]<sub>4</sub>, Tm[hfac]<sub>4</sub>, Lu[hfac]<sub>4</sub> Injections .....</b>	<b>69</b>
<b>Figure 5.19 Experimental vs. Theoretical Retention Times of Gd[hfac]<sub>4</sub> Samples.....</b>	<b>72</b>
<b>Figure 6.1 Injection Port Rendering .....</b>	<b>76</b>
<b>Figure 6.2 Quartz Separations Column Rendering .....</b>	<b>77</b>
<b>Figure 6.3 Tube Furnace Assembly Rendering.....</b>	<b>77</b>
<b>Figure 6.4 Vacuum Chamber Rendering.....</b>	<b>78</b>
<b>Figure 6.5 KCl Injector Rendering .....</b>	<b>78</b>
<b>Figure A.1 Crystal Structure of NH<sub>3</sub><sup>+</sup>(Gd[hfac]<sub>4</sub>) .....</b>	<b>89</b>
<b>Figure A.2 Melting Point Measurements of Pr(hfac)<sub>4</sub> .....</b>	<b>91</b>
<b>Figure B.1 La[hfac]<sub>4</sub> Mass Spectrum .....</b>	<b>94</b>
<b>Figure B.2 Pr[hfac]<sub>4</sub> Mass Spectrum.....</b>	<b>94</b>
<b>Figure B.3 Nd[hfac]<sub>4</sub> Mass Spectrum.....</b>	<b>95</b>
<b>Figure B.4 Sm[hfac]<sub>4</sub> Mass Spectrum .....</b>	<b>95</b>
<b>Figure B.5 Eu[hfac]<sub>4</sub> Mass Spectrum .....</b>	<b>96</b>
<b>Figure B.6 Gd[hfac]<sub>4</sub> Mass Spectrum .....</b>	<b>96</b>
<b>Figure B.7 Tb[hfac]<sub>4</sub> Mass Spectrum.....</b>	<b>97</b>

<b>Figure B.8 Dy[hfac]<sub>4</sub> Mass Spectrum .....</b>	<b>97</b>
<b>Figure B.9 Ho[hfac]<sub>4</sub> Mass Spectrum.....</b>	<b>98</b>
<b>Figure B.10 Er[hfac]<sub>4</sub> Mass Spectrum .....</b>	<b>98</b>
<b>Figure B.11 Tm[hfac]<sub>4</sub> Mass Spectrum.....</b>	<b>99</b>
<b>Figure B.12 Yb[hfac]<sub>4</sub> Mass Spectrum.....</b>	<b>99</b>
<b>Figure B.13 Lu[hfac]<sub>4</sub> Mass Spectrum.....</b>	<b>100</b>
<b>Figure E.1 Predicted Adsorption Enthalpy vs Atomic Radius .....</b>	<b>131</b>
<b>Figure E.2 (a) The TGA/DSC data for the NH<sub>4</sub>Lu[hfac]<sub>4</sub> compounds, (b) Coats-Redfern method, (c) Horowitz-Metzger method, and (d) Freeman Carroll method .....</b>	<b>131</b>
<b>Figure E.3 The average (of the HM and CR methods) Gibbs' free energy of sublimation (ordinate) is plotted as a function of the ionic radius (abscissa) .....</b>	<b>132</b>



# LIST OF EQUATIONS

Equation 3.1.....	29
Equation 3.2.....	29
Equation 3.3.....	29
Equation 4.1.....	47
Equation 4.2.....	48
Equation 4.3.....	49
Equation 4.4.....	49
Equation 4.5.....	49
Equation 4.6.....	49
Equation 4.7.....	50
Equation 4.8.....	50
Equation 4.9.....	50
Equation 4.10.....	51
Equation 4.11.....	51
Equation 4.12.....	51
Equation 4.13.....	51
Equation 4.14.....	52
Equation 5.1.....	65
Equation 5.2.....	66

<b>Equation E.1 .....</b>	<b>133</b>
<b>Equation E.2 .....</b>	<b>133</b>
<b>Equation E.3 .....</b>	<b>133</b>

## **LIST OF ABBREVIATIONS**

ACS – American Chemical Society

cm - Centimeter

CR – Coats-Redfern

CRM – Certified Reference Material

DHS – Department of Homeland Security

DOE – Department of Energy

DTA – Differential Thermogravimetric Analysis

FC – Freeman-Carroll

FTIR – Fourier Transform Infrared Spectroscopy

GC – Gas Chromatography

GCMS – Gas Chromatography Mass Spectrometer

HEU – Highly Enriched Uranium

HFAC - Hexafluoroacetylacetone

HM – Horowitz-Metzger

IAEA – International Atomic Energy Agency

IC – Isothermal Chromatography

ICP – Inductively Coupled Plasma

ID – Inner Diameter

IOS – International Organization for Standardization

min – Minutes

mL – Milliliters

mol - Moles

MP – Melting Point

NFAA – Nuclear Forensics and Attribution Act

NMR – Nuclear Magnetic Resonance

NNSA – National Nuclear Security Administration

MS – Mass Spectrometer

OTGC – Open Tubular Gas Chromatography

ppm – Parts per Million

ppt – Parts per Trillion

RE – Rare Earth

SADABS - Bruker/Siemens Area Detector Absorption

SC-XRD – Single Crystal X-ray Diffraction

SSAA – Stewardship Science Academic Alliances

STP – Standard Temperature and Pressure

TGA – Thermogravimetric Analysis

TNF – Technical Nuclear Forensics

TOF – Time of Flight

Ln – Lanthanide (denoting any element in the Rare Earth group)

La – Lanthinum

Pr – Praseodymium

Nd – Neodymium

Sm – Samarium

Eu – Europium

Gd – Gadolinium

Tb – Terbium

Dy – Dysprosium

Ho – Holmium

Er - Erbium

Tm – Thulium

Yb - Ytterbium

Lu - Lutetium

## LIST OF SYMBOLS

$\alpha$  – Alpha particle

$A$  – Thermogravimetric analysis pre-exponential factor (TGA method equations)

$A$  – Inner surface area of column (retention time equations)

$\beta$  - Beta particle

$\Delta H_{ads}$  – Enthalpy of adsorption

$\Delta H_{sub}$  – Enthalpy of sublimation

$\Delta S_{ads}$  – Entropy of adsorption

$\Delta T$  – Differential temperature

$D$  – Column diameter

$E^*$  - Activation energy

$\gamma$  - Gamma ray

$J$  – Joules

$KJ$  - Kilojoules

$K$  – Partition coefficient

$k$  – Boltzman's Constant

$L$  – Column length

$M_a$  – Mass of adsorbing material

$n$  – Reaction order

$\varphi$  - Free open cross-section of column

$R$  – Gas constant

$s$  – Open surface of column per 1m length

$s$  - Second

$T$  – Temperature

$t$  - time

$\bar{T}$  – Average temperature

$T_{iso}$  – Isothermal column temperature

$T_o$  – Standard temperature

$V$  – Inner volume of column

$v$  – Open volume of column per 1m length

$V_o\text{-bar}$  – Carrier gas flow rate at STP

$\nu_b$  – Phonon frequency

$Z$  – Thermogravimetric analysis pre-exponential factor

# **CHAPTER 1**

## **INTRODUCTION**

### **1.1 Background: Nuclear Terrorism and Nuclear Forensics**

In recent years, the United States has called upon the scientific community to address gaps in technology to improve the performance of forensics as a deterrent to nuclear terrorism.<sup>1</sup> The Nuclear Forensics and Attribution Act (NFAA),<sup>2</sup> enacted in 2010, is the legislative embodiment of this directive that stresses the technological readiness such a scenario necessitates, and has been approached through an interagency and academic collaboration.<sup>3</sup> Technical Nuclear Forensics (TNF) has been established as the specialized field of science to enhance this technology and analyze nuclear residues of interdicted (pre-detonation) or exploded (post-detonation) nuclear materials. Attribution of these materials employs TNF findings in concert with intelligence and law enforcement evidence to locate the source of these materials. Though the TNF community has made recent technological strides in identifying weapon characteristics from nuclear debris to supply timely, high-quality data in support of the attribution process, it is of continuing interest to develop techniques that can reduce the time required to perform analytical methods while retaining equivalent accuracy and precision to the established methods.

### **1.2 Nuclear Debris Genesis and Analysis**

In the aftermath of a nuclear detonation, a specialized type of debris is formed that effectively encapsulates weapon components and fission products in a solidified glassy matrix.<sup>4</sup> This debris,



or nuclear melt glass, is essential for nuclear forensic scientists to conclude weapon characteristics during post-detonation forensic analysis.<sup>5</sup> As modern non-state actors demonstrate a desire to obtain and deploy nuclear weapons,<sup>6</sup> particularly against the West,<sup>7</sup> a propensity for rapid analysis and attribution of the weapon is critical.<sup>8</sup> An attribution process to source and identify the origin of the weapon is desired; this attribution process is roughly outlined in Figure 1.1 below.

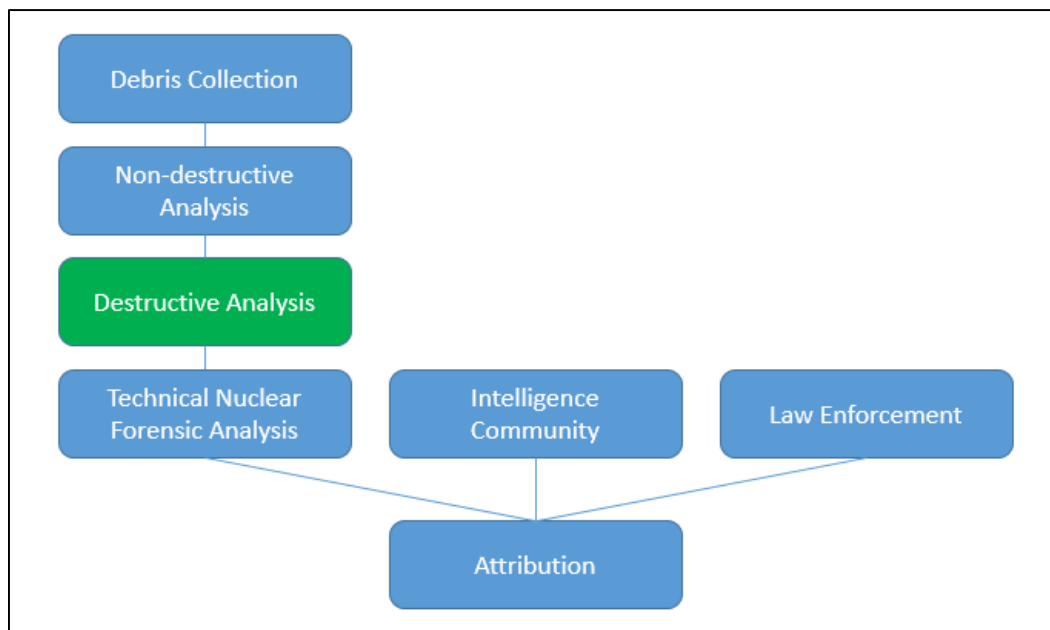


**Figure 1.1** Attribution Process

There are three main sources that are fused into an attribution decision originating from the intelligence community, law enforcement community, and scientists conducting technical nuclear forensic analysis of the debris. This dissertation will focus on methods to further

technology in the destructive analysis portion of technical nuclear forensic analysis (highlighted in green in Figure 1.1).

### **1.3 Rare Earth Separations**

Unfortunately, modern analysis techniques to identify and quantify species within the nuclear debris are non-trivial and require lengthy chemical processes during a stage when time is essential.<sup>9</sup> Therefore, advanced analytic techniques toward decreasing analysis time are highly desirable. In addition to nuclear forensic applications, which are the focus of this dissertation, chemical separations of rare earth elements are essential in many other fields including renewable energies, hybrid vehicles, and personal electronics, among many other consumer goods. This is readily accomplished using gas-phase separations, and if the separations prove feasible, applications outside the realm of nuclear security are prevalent in the rare earth (RE) industry.<sup>11</sup>

### **1.4 Analytical Research Efforts**

Recent research efforts have addressed temporal issues in RE separation techniques through the introduction of gas-phase chemistry as a practical option for chemical identification and separation; Garrison *et al.* showed theoretical indications that fission product separations are both possible and attainable from weapons debris in the gas phase,<sup>12</sup> and Hanson *et al.* took this theoretical model one step further and experimentally approached gas-phase separations of RE elements using thermochromatography.<sup>13</sup> This research aims to further the results of Hanson *et al.* using more precise custom-built instrumentation and optimizing an experiment for large-scale

multi-complex fission product separations while introducing isothermal chromatography in place of prior thermochromatographic experimentation. Collection methods for adsorptive thermodynamic measurements, however, were collected under thermochromatographic conditions and used for isothermal chromatography modeling.

### **1.5 Complications with Current Practices in Post-Detonation Debris Analysis**

The glassy debris generated in a nuclear detonation contains constituents of interest to the forensic scientist. Within this debris, there exists a multitude of fission products (the elemental fragments of a nuclear fuel after undergoing fission), activation products (atoms exhibiting an activated state), and components of the weapon itself that can be identified and quantified to yield information of interest to the nuclear forensic analyst.<sup>8</sup> However, these constituents are difficult to extract from the vitreous state of the debris without extensive chemical manipulation.<sup>5</sup> Currently, the debris must be dissolved using established chemical dissolution processes, followed by liquid separation of select nuclides and quantitative analysis. The process is untimely and requires many steps to complete in a situation that intrinsically necessitates the most prompt analysis achievable. Improvements to reduce analysis time are critical areas of the present research.

### **1.6 Statement of the Problem**

Prompt and accurate analysis of nuclear melt glass is the primary essential component of the TNF contribution to the attribution cycle. Any improvement to timeliness adds critical utility during the technical analysis process. Consequently, a thorough reestablishment of elemental

separation criteria that increases both speed and accuracy toward quantitative nuclear forensic analysis could significantly contribute to a timely response following a nuclear terrorism event. This work aims to address the time component of forensic analysis by investigating the plausibility of gas-phase separations as an alternative to current liquid-phase separation techniques in a post-detonation forensic scenario.

### 1.7 Statement of the Question

The vital question considered in this dissertation is:

*To what extent can the optimization of a large-scale gas-phase fission product separation by measurement of selected lanthanide hexafluoroacetylacetone adsorptive thermodynamic parameters increase the timeliness and accuracy of post-detonation nuclear forensic analysis?*

In order to address this question, the entropy and enthalpy of adsorption ( $\Delta H_{\text{ads}}$  and  $\Delta S_{\text{ads}}$ ) of select fission product complexes are measured for the first time using an adapted thermochromatographic technique. The measured values are then used to model a large-scale gas-phase fission product separation under *isothermal* conditions in order to optimize the speed and efficiency of the process, if possible. The total time taken to synthesize, separate, and quantify the fission products is compared to the time taken for a similar liquid-phase procedure to ascertain the better method for speed and precision. To the best of the author's knowledge, no research has aimed to address isothermal chromatography as a viable option for post-detonation nuclear forensic analysis.

## 1.8 Objective of the Study

The objectives of this study are:

- 1) Prepare samples of fission product complexes that can be viably volatilized within the operating temperatures of standard gas chromatography instrumentation;
- 2) Develop methodology to properly adjust instrument parameters to yield timely eluent detection;
- 3) Measure  $\Delta H_{\text{ads}}$  and  $\Delta S_{\text{ads}}$  of the thirteen  $\text{NH}_4[\text{Ln}(\text{hfac})_4]$  complexes in question; and
- 4) Use the measured values to attempt to optimize a large-scale separation of these complexes

## 1.9 Dissertation Outline

This remainder of this dissertation is organized into the following chapters:

**Chapter 2: Literature Survey.** This chapter explores previously-conducted research used as a pedestal for the theories and calculations presented in this dissertation.

**Chapter 3: Experimental Development.** This chapter outlines the experimental setup of the research, including instrumentation, synthesis, characterization, and scope.

**Chapter 4: Methodology.** This chapter walks through the steps and calculations used to test the stated hypothesis.

**Chapter 5: Results and Discussion.** This chapter relates the results of the research conducted in the experimental and methodology sections.

**Chapter 6: Conclusion.**

## CHAPTER 2

### LITERATURE SURVEY

*Portions of this chapter are taken from my contributions to journal articles of which I am a co-author<sup>5,14,15</sup>*

#### 2.1 Essential Steps: Post-Detonation Nuclear Forensic Analysis

Post-detonation nuclear forensic analysis begins with the collection of materials produced in the extreme temperature and pressure where a nuclear weapon detonates. In the aftermath of a detonation, a specialized type of debris is formed that effectively encapsulates weapon components and fission products in a solidified glassy matrix.<sup>4</sup> This debris, or nuclear melt glass, is essential for nuclear forensic scientists to conclude weapon characteristics during post-detonation forensic analysis.<sup>5</sup> Analyzing the debris begins with non-destructive physical and radiological characterization and progresses toward dissolution and destructive analysis. Table 2.1 below shows typical analytical techniques for the characterization of pre-detonation nuclear materials; post-detonation materials, whose techniques are shown in Table 2.2, follow in a very similar manner, with radiochemical separations and radiological characterization having the largest contribution to subsequent attribution.

Nuclear forensic chemical separations are performed for a variety of reasons. In many cases, when using radiation detection to identify species within a sample, it is impossible to garnish an accurate understanding of the constituents given the variation in concentration of individual fission and activation products emitting radiative particles, which can range in concentration upwards of 15-20 orders of magnitude.<sup>8</sup> It is therefore necessary to isolate individual species and

count emissions in the near absence of other interfering elements. However, for the purposes of this research, separations are being performed

**Table 2.1** Characterization Techniques for Pre-Detonation Nuclear Materials (IAEA)<sup>16</sup>

Techniques/Methods	24 h	1 Week	2 Months
Radiological	Total Activity		
	Dose Rate ( $\alpha$ , $\beta$ , $\gamma$ , n)		
	Surface Contamination		
Physical	Visual Inspection	SEM/EDS	TEM (EDS)
	Radiography	XRD	
	Photography		
	Weight		
	Dimensions		
	Optical Microscopy		
	Density		
	Fingerprinting, Fibres		
Traditional Forensics			
Isotope Analysis	$\gamma$ spectroscopy	SIMS, TIMS, ICP-MS	Radiochemical Separation
	$\alpha$ spectroscopy		
Elemental/Chemical		ICP-MS	GC-MS
		XRF	
		Titration	
		IDMS	

in order to detect constituent species in a mass spectrometer (whether radioactive or not is immaterial). This allows full insight into the total concentration of a given charge-to-mass ratio. A major outcome of the instrumentation developed for this research, as discussed in Chapter 3, will overcome isobaric interferences (nuclides with identical charge-to-mass ratios).

## 2.2 Synthesizing Nuclear Debris Surrogates for Analytical Development

Rapid sample analysis is essential in a post-detonation environment for forensic attribution. While samples of nuclear melt glass (both surface and aerodynamic debris) are available to the

**Table 2.2** Characterization Techniques for Post-Detonation Nuclear Materials<sup>17</sup>

<b>Techniques/Methods</b>	<b>Instrumentation</b>	<b>Pre-Preparation</b>
Radiological	Alpha ( $\alpha$ ) spectroscopy	Remove stable element contamination
	Beta ( $\beta$ ) counting	Immerse in liquid scintillation fluid to determine gross count rate
	Gamma-ray ( $\gamma$ ) spectroscopy	No preparation needed other than similar counting geometry to standard counting source
Physical Characterization	Radiography	None
	Photography	None
	Weight	None
	Dimensions	None
	Optical Microscopy	None
Isotope Analysis	Density	None
	Gamma-ray ( $\gamma$ ) spectroscopy	No preparation needed other than similar counting geometry to standard counting source
	Alpha ( $\alpha$ ) spectroscopy	Remove stable element contamination
	Secondary Ion Mass Spectrometry (SIMS)	Dissolution to appropriate concentration, mitigation of isobaric interferences
	Thermal Ionization Mass Spectrometry (TIMS)	Dissolution to appropriate concentration, mitigation of isobaric interferences
	Inductively Coupled Plasma – Mass Spectrometry (ICP-MS)	Dissolution to appropriate concentration, mitigation of isobaric interferences
	Laser Ablation – ICP-MS	None
Elemental Analysis	Scanning Electron Microscopy/Energy Dispersive Spectroscopy (SEM/EDS)	Samples must be polished prior to analysis
	X-ray fluorescence (XRF)	None
	ICP-MS, SIMS	Dissolution to appropriate concentration, mitigation of isobaric interferences
	LA-ICP-MS	None
	X-ray absorption near edge structure (XANES)	Dissolution to appropriate concentration



academic community from the Trinity test (see Figure 2.1), many fission products have decayed and the Trinitite samples (see Figure 2.2) are only quasi-representative of the signatures that would be obtained from a newly acquired sample.



**Figure 2.1** Trinity Test near Alamogordo, NM<sup>18</sup>

As such, much work has been dedicated to creating realistic synthetic samples of nuclear melt glass for the experimental development of post-detonation analytical techniques.<sup>1,4,5,19–21</sup> Creation of these surrogates began as simple HEU-doped sol-gel glass as reported by Carney *et al.* in 2013.<sup>19</sup> The glass was impregnated with 93% HEU and neutron irradiated for 15 minutes in order to simulate, on a first-tier basis, the fission and activation products that would be found in nuclear debris.



**Figure 2.2** Trinitite Sample<sup>22</sup>

Many papers followed that advanced the elemental accuracy of synthetic nuclear debris. Trinitite, being the most accessible nuclear debris to the academic community, was first synthetically modeled by Molgaard in 2014<sup>23</sup> as seen in Figure 2.3 and the technique was subsequently published in 2015.<sup>4</sup> Studies ensued to determine the physical, chemical, and radiological accuracy of this synthetic debris as compared to actual Trinitite, and it was found that excellent correlation was achieved.<sup>4,21</sup>

The need for synthetic nuclear melt glass representative of an urban environment was the obvious next step toward developing analytical techniques for attribution purposes. Giminaro *et al.* recently addressed this need in a study detailing city-specific formulation techniques to identify the elemental composition of any given city using land use data.<sup>5</sup> Two representative

samples (Houson, TX and New York, NY) were modeled and synthesized in order to demonstrate the procedure, as shown in Figure 2.4 (the two beads on the lower left side of the figure).



**Figure 2.3** Synthetic Trinitite Sample<sup>4</sup>

The need for synthetic nuclear debris, both that which can be directly compared to actual debris and those that represent a hypothetical urban event, has clearly been largely addressed in recent years and efforts to improve the realism of the samples are ongoing. These samples provide a more credible baseline for developing post-detonation forensic techniques for real debris.<sup>20</sup>



**Figure 2.4** Synthetic Urban Nuclear Melt Glass

### **2.3 Synthesis and Characterization of $\text{Ln}[\text{hfac}]_4$ Complexes**

Identifying and quantifying constituents within the melt glass itself is a crucial component of post-detonation forensic analysis. Luckily, analytical separation science is a field that has been around for decades and has much to offer the forensic analyst interested in melt glass analysis. The fission and activation products generated in a nuclear detonation are impregnated into the melt glass debris and can yield useful insight into the characteristics of the weapon. Figure 2.5 shows common fission products produced in common isotopes of uranium and plutonium.<sup>24</sup>

It can be seen that a large portion of the fission products fall into the RE category, also known as lanthanides (Ln), as shown in Figure 2.6, and are a subsequently useful class of elements for forensic scientists.

The synthesis of RE hexafluoroacetylacetonate complexes (hereafter referred to as  $\text{Ln}[\text{hfac}]_x$  complexes) was first performed several decades ago and has continued largely procedurally unchanged.<sup>25</sup> However, exhaustive characterization has only recently been detailed on certain hfac complexes in order to confirm the integrity of the molecules being synthesized.<sup>15</sup> Shahbazi *et al.* have shown complete characterization of four of the  $\text{Ln}[\text{hfac}]_4$  complexes being studied in this work:  $\text{Sm}[\text{hfac}]_4$  (**1**),  $\text{Gd}[\text{hfac}]_4$  (**2**),  $\text{Dy}[\text{hfac}]_4$  (**3**), and  $\text{Tm}[\text{hfac}]_4$  (**4**), and the results show that the integrity of these molecules is expected to be intact.<sup>15</sup> Complete characterization of the molecules can be found in Appendix A.

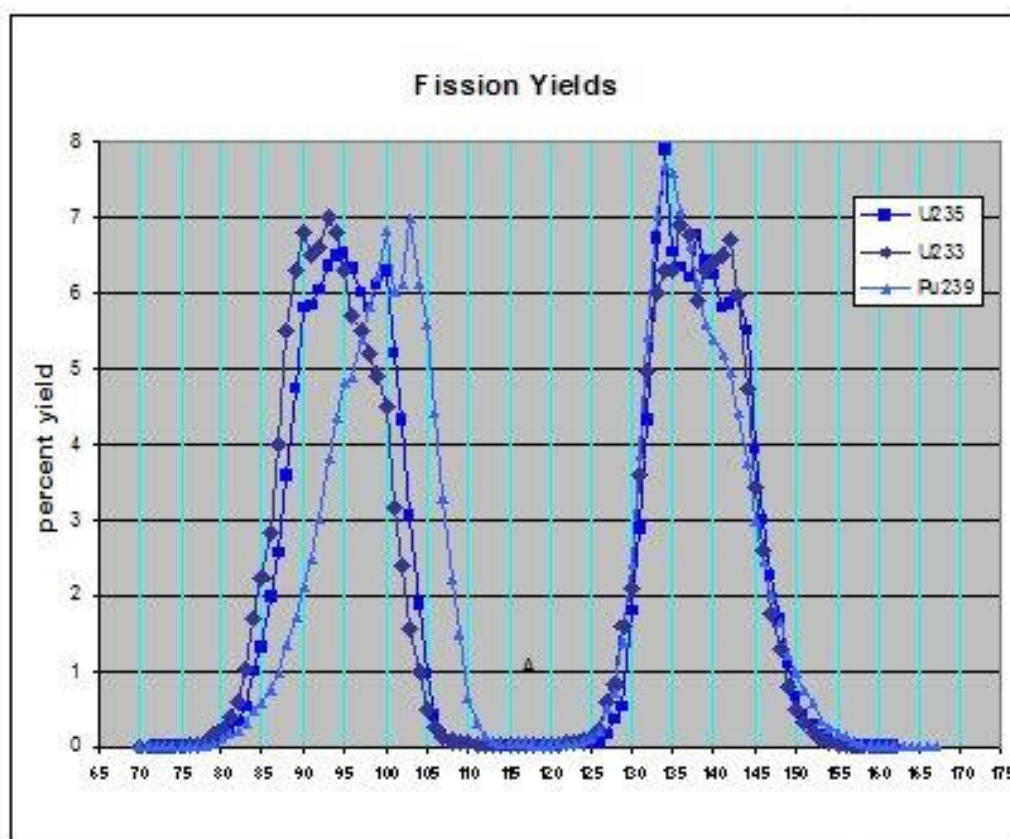


**Figure 2.5** Fission Product Spectrum<sup>24</sup>

## 2.4 Modern Rare Earth Separations

RE metals are incredibly important for many electronic applications and are thus currently isolated for such uses.<sup>10,11</sup> Modern techniques, however, are costly and inefficient when performed in a liquid separation environment when compared to similar separations that are

1 18

1 H 2 He

2 Li Be 13 B 14 C 15 N 16 O 17 F Ne

3 Na Mg 3 4 5 6 7 8 9 10 11 12 Al Si P S Cl Ar

4 K Ca Sc Ti V Cr Mn Fe Co Ni Cu Zn Ga Ge As Se Br Kr

5 Rb Sr Y Zr Nb Mo Tc Ru Rh Pd Ag Cd In Sn Sb Te I Xe

6 Cs Ba Hf Ta W Re Os Ir Pt Au Hg Tl Pb Bi Po At Rn

7 Fr Ra Rf Db Sg Bh Hs Mt

Inner Transition Elements  
f-block

La Ce Pr Nd Pm Sm Eu Gd Tb Dy Ho Er Tm Yb Lu

Ac Th Pa U Np Pu Am Cm Bk Cf Es Fm Md No Lr

Lanthanides

**Figure 2.6 Rare Earth Elements**<sup>26</sup>

theoretically possible in the gas phase. Since the 1970's, RE industrial separations have been performed *en masse* using the theory of countercurrent extraction,<sup>11</sup> particularly in China, the world's largest producer of RE metals, as is shown in Figure 2.9.<sup>10</sup> In this procedure, protons are carried by a reagent from the aqueous phase (top layer) to the organic phase (lower layer) when a specified concentration is reached. A homogenous-like reaction occurs followed by scrubbing, stripping, and ionic adsorption to purify the metals.<sup>11</sup> On-line extraction of the countercurrent method is currently practiced, with little technological improvement over the last several decades. Large-scale ion chromatography practices are also in use, as shown in Figure 2.7.



At smaller scales, principally research separations and extractions, several techniques have been investigated and successfully employed, though nearly all non-volatile separations involve exchange columns or liquid-liquid extraction.<sup>27–29</sup> One of the most common methods, as presented by Tompkins and Mayer,<sup>27</sup> Street and Seaborg,<sup>28</sup> Pin *et al.*,<sup>29</sup> and many others, demonstrates separation of RE elements from actinides using cation exchange columns to

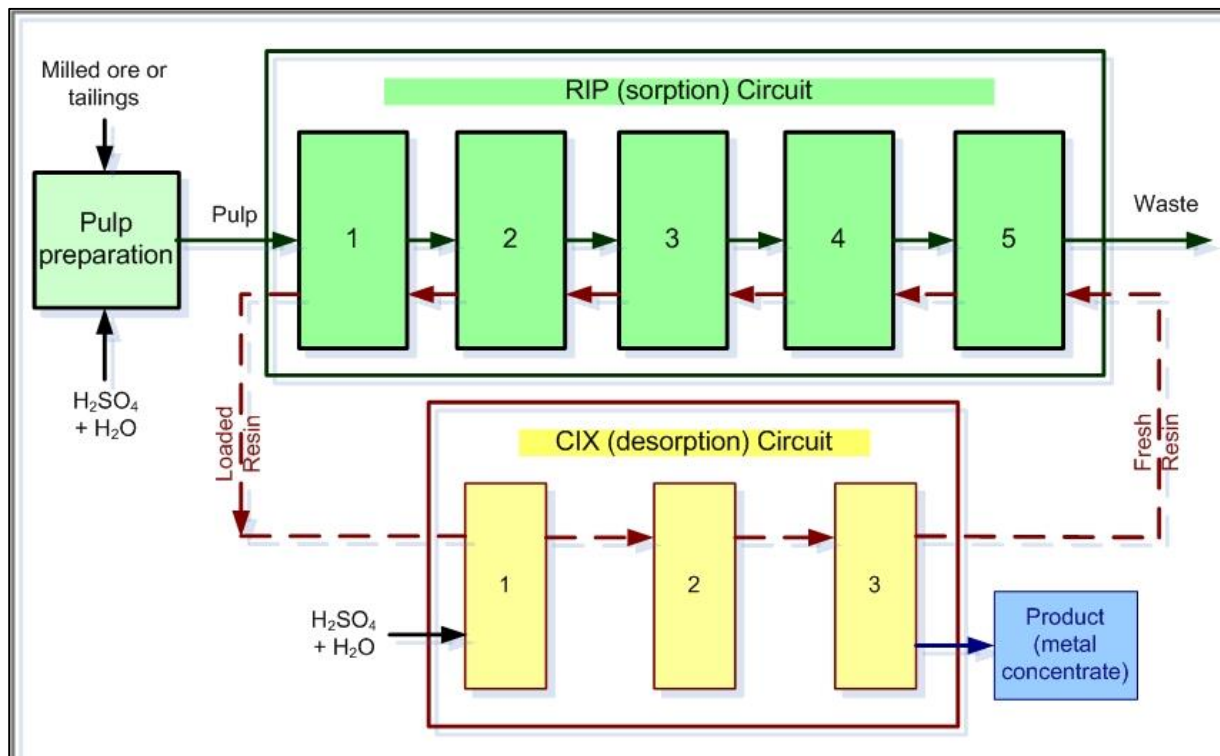


**Figure 2.7** Large-Scale Ion Exchange Chromatography<sup>30</sup>

capitalize on the differences in chemical properties between the individual elements, a detailed process of which is shown in Figure 2.8.<sup>29</sup> This has many uses in nuclear security, particularly in forensic investigations and attribution of weapon materials. Nearly all nuclear forensic research

separations are performed in the liquid phase due to the thermal properties gas chromatography necessitates and therefore take longer to complete, but good resolution is usually observed.<sup>15</sup>

Though gas-phase separations have been explored for a number of materials, they predominantly involve specialized polymer or ionic liquid membranes that cater to specific elements or molecules. Baltus *et al.* have explored the viability of such separations performed on greenhouse

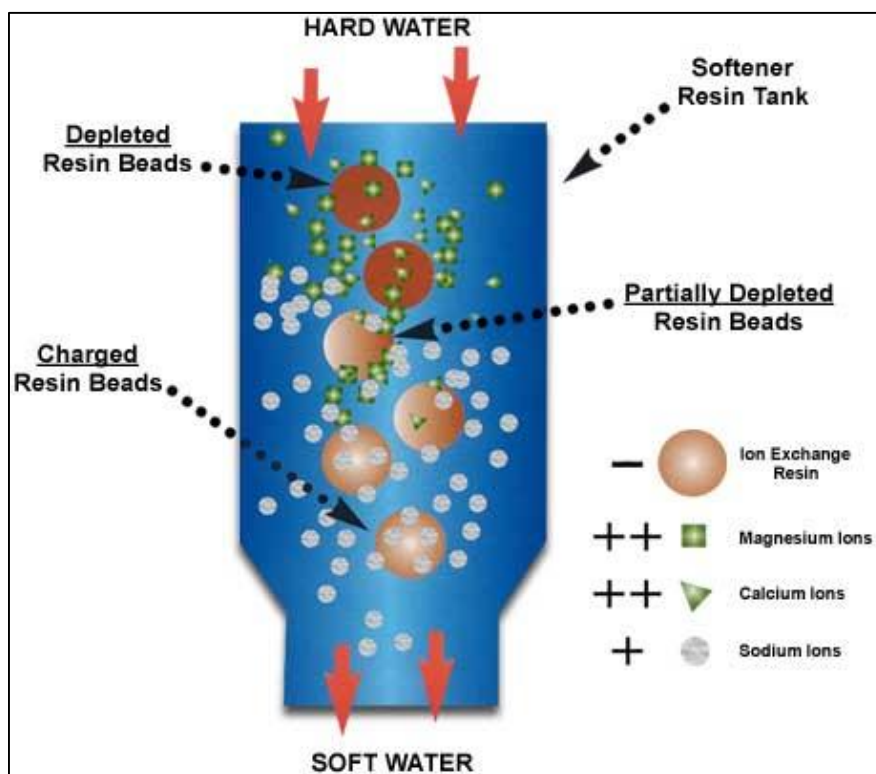


**Figure 2.8** Cation Exchange Procedure<sup>31</sup>

gases such as carbon dioxide and methane in factories emitting such pollutants. Results showed viability, though with the caveat of permeation of other undesirable chemicals along with the targeted gas.<sup>32</sup> Such detection methods do not normally aim to quantify separated products, particularly on the isotopic scale needed here.



Many volatile chemicals are separated in the gas phase, particularly organics (such as aromatics), but constituents of nuclear melt glass of importance to the forensic scientist are necessarily non-volatile (any volatiles would have escaped during the formation process unless trapped in a pocket). Further, the majority of the complexes found in nuclear melt glass are inorganic molecules that do readily separate in the gas phase.<sup>15</sup>



**Figure 2.9** Tiered Industrial Rare Earth Separation<sup>33</sup>

## **2.5 Superheavy Element Thermochromatography**

A leading area of rapid gas phase experimentation has been pioneered by groups for superheavy element discovery<sup>34</sup> and analysis<sup>35</sup> as described by Shaughnessy *et al.*,<sup>36</sup> Zvára *et al.*,<sup>37</sup> and Even *et al.*<sup>38</sup> Superheavy elements are elements with an atomic number greater than or equal to 112.<sup>39</sup> Many of these transactinide elements have exceedingly short half-lives and have been

successfully detected using thermochromatography.<sup>40</sup> Transition metal halides were first successfully separated in the 1960s using gas-solid chromatography; their volatility and ability to separate in the gas phase can be largely attributed both their 3+ oxidation and coordination number that give the molecules symmetry.<sup>37</sup> This property was soon exploited to produce and detect the first transactinide elements.<sup>37</sup> Producing these elements necessitated rapid procedures given their extremely short half-lives, and thermochromatography (a gas-phase separation technique using temperature programming to solve the general elution problem of gas mixtures) was the method of choice for such rapid separation.<sup>41</sup>

As a cursory example, element 106 (seaborgium, Sg) was produced by bombarding a curium target with a neon beam at a rate of several atoms per week.<sup>42</sup> With this production rate and the intrinsically short half-life of Sg, rapid detection of the atoms before their decay was essential. After the atoms were created, they were deposited onto aerosolized particles and transported through the thermochromatographic column to a rotating step-motor alpha detector wheel,<sup>42</sup> as shown in Figure 2.10.

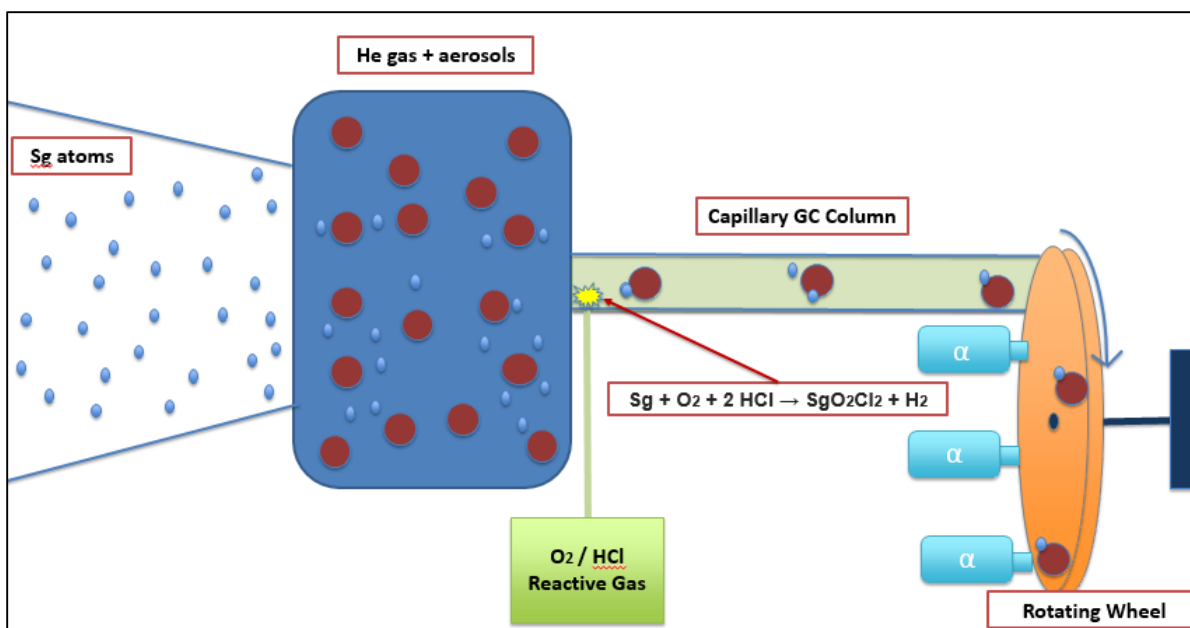


**Figure 2.10** Author's Rendition of Sg Separation Procedure

This technique allowed for the alpha decay particles from the parent Sg atom and its daughters to be detected within the time span of seaborgium's half-life.

However, thermochromatographic procedures as applied to superheavy element discovery have not been investigated for use in volatilized rare earth complexes for rapid separation purposes until recent investigations by Hanson *et al.*<sup>13</sup> The experimental parameters and principles of adsorption give every indication that RE separations are feasible in the gas phase as long as the values for entropy and enthalpy of adsorption are sufficiently varied for the volatilized complexes. Modeling by Garrison *et al.* was performed on gas-phase RE chlorides at high temperatures ( $> 600\text{C}$ ),<sup>12</sup> but this work aims to employ rapid separations at low temperatures ( $< 300\text{C}$ ) in order to operate within the confines of gas chromatography.

## 2.6 Separation Viability

Performing separations of RE's in this manner requires chemical manipulation, or more specifically, the attachment of a volatile ligand to the metal complex in order to operate and separate at low temperatures.<sup>43</sup> Greulich *et al.* have already exploited this reasoning in the gas phase for individual elements, though the samples were necessarily radioactive (neutron-activated) and detection of the products was limited to  $\gamma$  and  $\beta^-$  emission counting.<sup>44</sup> Other separations of note utilizing ligand-metal complexes are predominantly reliant on radiation,<sup>45</sup> including those methods implemented in the heavy element community,<sup>34,35,37,38,40,42,46</sup> whereas a robust detection method of both stable and unstable isotopes is essential in the proposed research presented here for accurate and reliable forensic attribution.<sup>8</sup>

## 2.7 Legal Requirements of TNF Data

The data produced in a nuclear forensic investigation, given its implications, may necessitate meeting certain legal benchmarks in order to be considered a viable component of the attribution process. The following is an excerpt from a co-authored paper between S. A. Stratz, J. A. Gill, J. D. Auxier II, and H. L. Hall entitled “Modern Advancements in Post-Detonation Nuclear Forensic Analysis” that outlines the importance of meeting legal specifications during any nuclear forensic investigation:<sup>14</sup>

*As with any forensic endeavor, data supporting the forensic analysis process may eventually reach review by a judicial body. Any country wishing to attribute a nuclear incident to another sovereign nation or subnational entity will face intense scrutiny, and as such, must have a high standard of legally defensible forensic methodology. The NFAA does not contain language*

*specifically referring to a defined standard; however, it does recommend international cooperation and designates investigative agencies that are bound by legal standards. The most relevant to nuclear forensic methods is the Daubert standard as it applies to Federal Rules of Evidence, Article 7, Rule 702.<sup>47-49</sup> Based on the Daubert standard, judges are given means by which they can assess an expert's scientific testimony on the grounds of reasoning or methodology. Under this standard, five factors are used to assess the validity of a method:<sup>48</sup>*

- 1) whether the theory or technique in question can be and has been tested;*
- 2) whether it has been subjected to peer review and publication;*
- 3) its known or potential error rate;*
- 4) the existence and maintenance of standards controlling its operation; and*
- 5) whether it has attracted widespread acceptance within a relevant scientific community.*

*For the United States, any research effort seeking board acceptance and government support must meet this standard.*

*Application of this standard to forensics has rightly received rigorous attention in the scientific community.<sup>47,50-53</sup> Understanding the law through precedence is one of the only reliable means of interpreting law. In addition, efforts are being made to establish certified reference materials (CRMs) and recognized databases of nuclear information that may act as a known standard for other nuclear materials.<sup>54</sup> Both of these standards generally agree with the requirements for competence outlined in International Organization for Standardization (IOS) code 17025. It is clear that legal nuclear forensic investigations necessitate high-quality data with both precision and accuracy in order to be upheld by a legislative body.*

## 2.8 Experimental Evaluation of Enthalpy and Entropy of Adsorption

Many equations have been derived over the years to cultivate thermodynamic characteristics from experimental gas chromatography data. Perhaps one of the foremost pioneers in the area of thermochromatographic extrapolations of thermodynamic data is Zvara, who eventually wrote an entire text on the inorganic radiochemistry of heavy elements.<sup>37</sup> The derivations and subsequent equations presented in his earlier work have been used over the years to obtain adsorption properties of complexes in the gas phase. *Eichler et al.* produced several models from chromatographic fundamentals including the material transport model, standard adsorption entropy model, localized adsorption model, and a quasi-third-law method.<sup>55</sup> *Rudolph et al.* extrapolated a very useful set of equations to determine the entropy and enthalpy of adsorption of gas-phase complexes using a temperature programming technique.<sup>56</sup> They have also introduced more accurate techniques for measuring these quantities using isothermal chromatography. Most pertinent to this work is a set of equations derived by *Steffen et al.* that helps determine the enthalpy and entropy of adsorption of gaseous complexes using an on-column temperature gradient.<sup>57</sup> The derivations presented in this work were ultimately used in the author's calculations presented in Chapter 4.

## **CHAPTER 3**

### **EXPERIMENTAL DEVELOPMENT**

#### **3.1 Scope**

There are four major thrust areas that fall under the purview of this research. Characterizing the thermodynamic properties of the volatile organometallic complexes is the primary desired outcome of this effort, but three pertinent milestones are required to arrive at the technological capability to measure these properties.

First, a functional instrument to accurately, repeatedly, and reliably produce consistent complex elution times at a variety of isothermal temperatures is essential. Any fluctuations in these retention times without probable cause or manual changing of operating conditions is not adequate for the requisite precision of this characterization process. Developing a continuous and reliable instrument setup is the first stage of this effort and is expected to take the longest time to complete. However, since the adsorptive thermodynamic characteristics of the complexes under consideration for separation are not yet known, it is possible that the absence of a sufficiently large difference in the entropy and enthalpy of adsorption of these complexes could prevent the necessary level of separation required for isothermal chromatography.

Second, after developing functional instrumentation, the instrument must detect, at the mass spectrometer end, an aliquot of injected sample from the gas chromatography end. The first successful detection of an injected sample proves continuity of the instrument and sufficiently constrained operating conditions. Successful detection should show a peak of the injected metal while simultaneously showing absences of peaks of elements that are not present in the injected sample.

Third, a multiple-complex sample of a mixture of several different organometallic fission products should be injected and successfully detected. Optimally, these complexes would elute with a small amount of separation time between them, but even if this does not occur, detecting all injected metals in the mixed sample while not showing detection of non-present elements is the key to this milestone. At the time of this writing, it is not yet known whether or not this method will result in the separation of the injected samples.

Finally, the retention times of these complexes will be tested at varying operating temperatures, and should decrease as the temperature is increased. If this does not occur, it is not certain whether or not the selected ligand (hfac) has the proper selectivity between the lanthanide metals to result in adsorption to the uncoated silicon column. A lack of adsorption results in a lack of ability to measure the adsorptive thermodynamic properties. Successfully measuring varying retention times at fixed temperature differences will allow for the characterization of the enthalpy and entropy of adsorption of these complexes, which is ultimately the desired outcome of this research.

### **3.2 Synthesis and Characterization**

Much work has been performed to confirm the molecular integrity and purity of the fission product complexes used in this research<sup>15</sup> (see Appendix A). The complexes are composed of a fission product, in this case a RE metal, attached to a volatile ligand, in this case 1,1,1,5,5,5-hexafluoroacetylacetone. These compounds are not commercially available, and as such, are synthesized in-house. The synthesis method follows, but will not be further detailed, as it is not the focus of this research, but rather a necessary step to begin thermodynamic measurements.



A series of  $\text{Ln}[\text{hfac}]_x$  complexes were synthesized from high-purity materials. The RE oxides (Sigma Aldrich, 99.99%) were combined with hot, concentrated HCl (Fisher, ACS Reagent Grade) to yield the chloride salt in an acid solution. The solution was allowed to cool. 1,1,1,5,5,5-hexafluoroacetylacetone (hfac, Acros, 99.9%) was obtained and combined with equimolar amounts of concentrated  $\text{NH}_4\text{OH}$  (Fisher, ACS Reagent Grade) at  $0^\circ\text{C}$ . The two liquids reacted vigorously producing a white solid ( $\text{NH}_4[\text{hfac}]$ ) that was stirred to fully react the reagents. The solid was then placed in a desiccator for storage. The  $\text{NH}_4[\text{hfac}]$  was dissolved in 5 mL of diethyl ether (ACS Reagent Grade, Fisher) to which the aqueous rare earth chloride was added in a ratio of 4:1. The mixture was shaken vigorously for 30 seconds, and then set for 5 minutes, repeating 3 times. At the conclusion of the last separation, the organic phase was drawn off and placed in a vacuum desiccator to dry the sample and remove the ether. The resulting compounds are shown in Figure 3.1 and are of the form  $\text{Ln}[\text{hfac}]_4$ . Subsequent characterization of the complexes was performed using Fourier-Transform Infrared Spectroscopy (FTIR), Nuclear Magnetic Resonance (NMR), Thermogravimetric Analysis (TGA), Single Crystal X-ray Diffraction (SC-XRD), and Elemental Analysis. These resulting characterization concluded that these compounds are indeed of the expected molecular structure and composition.

The integrity of the samples, particularly their trace lanthanide metal content, is essential information due to the extreme sensitivity - on the order of parts per trillion (ppt) - of the mass spectrometer. The samples used for GC injections were directly dissolved in ultrapure water and diluted as appropriate for ICP-MS analysis. Though several of the samples demonstrated trace levels of contamination, as shown in Table 3.1, no contaminants were sufficiently concentrated to cause issues during testing. Knowing the level of contamination at the ppt level allows for

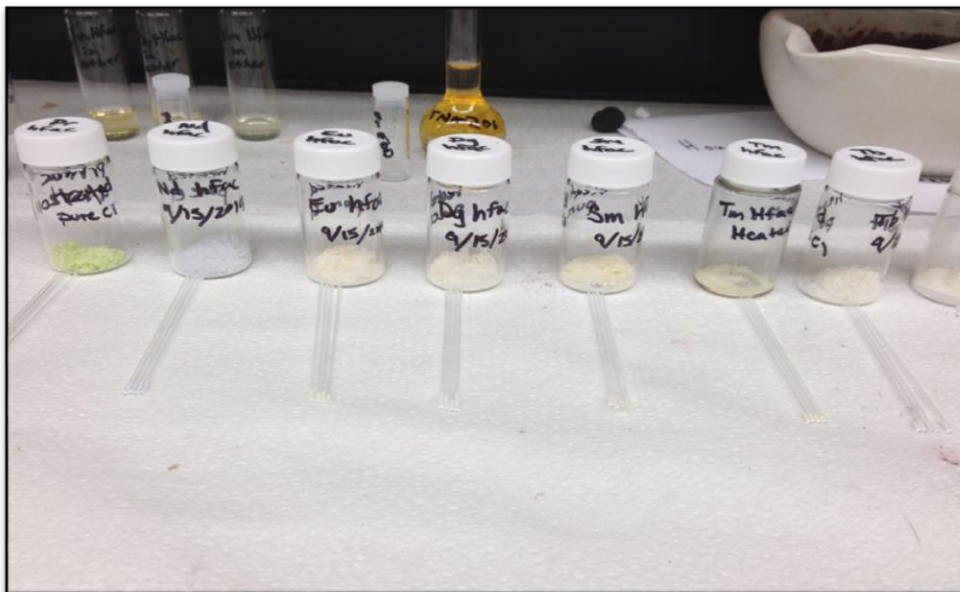


**Figure 3.1** Fully Synthesized RE Hfac Complexes

accurate error analysis and the ability to attribute known contaminants in resulting test data. Results from ICP-MS sample integrity tests are shown in Appendix B.

### 3.3 Separation Chemistry

The  $\text{NH}_4[\text{Ln}(\text{hfac})_4]$  fission product complexes, in order to exhibit viability for isothermal chromatographic separations, were tested for volatility and feasibility of separation in an open tubular gas chromatography (OTGC) system. The dependence of retention volume on temperature is requisite knowledge to calculate complex volatility when introduced into a solvent. Because the determination of  $\Delta H_{\text{ads}}$  and  $\Delta S_{\text{ads}}$  requires running the samples at various temperature profiles in the OTGC system, it is also of interest to know the retention volume half-value as it correlates to temperature. In other words, it is useful to know what change in

**Table 3.1** Sample Contaminants

Sample	Contaminant
La	-
Pr	<sup>138</sup> Ba
Nd	-
Sm	-
Eu	-
Gd	<sup>138</sup> Ba
Tb	-
Dy	-
Ho	-
Er	<sup>138</sup> Ba
Tm	-
Yb	-
Lu	<sup>139</sup> La

temperature will reduce the retention volume in half in order to produce a useful temperature range at which to test the samples. The concepts and equations outlined in “Chromatography: concepts and contrasts” notes that this relationship requires:<sup>41</sup>

$$\frac{K_2}{K_1} = \frac{1}{2}$$

**Equation 3.1**

Expanding the definition of the partition coefficients yields:

$$\frac{K_1}{K_2} = 2 = \frac{\exp(-\Delta \frac{\mathcal{H}}{\mathfrak{R}T_1})}{\exp(-\Delta \frac{\mathcal{H}}{\mathfrak{R}T_2})} = \exp[\frac{\Delta \mathcal{H}}{\mathfrak{R}T} \left( \frac{\Delta T}{\bar{T}} \right)]$$

**Equation 3.2**

Where  $\Delta T$  is the desired temperature difference to produce a halving in the retention volume and  $\bar{T}$  is the average of the two temperatures. Taking the log:

$$\Delta T = \frac{0.693 \mathfrak{R} T^2}{\Delta \mathcal{H}}$$

**Equation 3.3**

Using Trouton's rule where  $\Delta H/T_b = 21$  and the values found in Table A.1 converted to Kelvin. These values are of high utility when designing the temperature profile of the thermochromatographic samples.

### 3.4 Instrumentation

Several instrument components are needed in order to volatilize and detect powdered organometallic complexes under isothermal conditions. Many off-the-shelf GCMS units are available for purchase that operate within the sublimation temperatures of the complexes used in

**Table 3.2** Temperature Retention Volume Half-Values

Hfac Complex	Half-Value ( C )
Lanthanum (La)	27.5
Praseodymium (Pr)	30.0
Neodymium (Nd)	29.4
Samarium (Sm)	30.8
Europium (Eu)	29.9
Gadolinium (Gd)	30.1
Terbium (Tb)	31.1
Dysprosium (Dy)	31.7
Holmium (Ho)	32.6
Erbium (Er)	32.7
Thulium (Tm )	31.7
Ytterbium (Yb)	32.3
Lutetium (Lu)	32.5
Ammonium (NH <sub>4</sub> )	23.9

this research. However, a very specific type of mass spectrometer is required to perform the type of isotopic identification and quantification needed for elements that inherently exhibit isobaric interferences. Unfortunately, the lanthanide series contains many elements with overlapping isotopes that cannot be differentiated within a mass spectrometer detector. It is therefore necessary for the elements themselves to be separated *before* reaching the mass spectrometer so that isobaric interferences can be overcome. Additionally, the mass spectrometer must have the capability of completely deconstructing the incoming complexes into their elemental components for individual isotopes to be detected and displayed to the operator. For these reasons, an instrument had to be built in-house to overcome all of these obstacles since no off-the-shelf GCMS (as of the time of this writing) has the capability of deconstructing complexes into individual elemental components.

The gas chromatography instrument chosen for this setup is a Hewlett-Packard 5890A with customizable temperature settings between room temperature and 400 °C with argon carrier gas flowing at approximately 7 mL/min through a 7-m uncoated 0.53 mm I.D. Agilent quartz column. The column, in order to reach the plasma torch of the mass spectrometer without experiencing temperature fluctuations, is enveloped in steel tubing with intermittent heating collars along the length of the tube. The temperature programming unit is an Omega CN1504 multi-zone controller with four heating control zones. The nebulizer flow carrying the sample from the end of the quartz column to the plasma torch in the ICP-TOF-MS is also heated using one of the four control zones and a custom quartz heating coil. Mass spectra were recorded using a GBC Optimass 9500 ICP-TOF-MS with 1200 W plasma power and a 0.950 L/min nebulizer flow. A schematic of the instrument is shown in Figure 3.2. An image of the entire coupled system is shown in Figure 3.3 with a profile image shown in Figure 3.4.

Unfortunately, this system caused a large number of issues with complex flow continuity due to the non-uniform manner in which the heating collars were placed. Sections of the steel connection tubing under the heating collars exhibited intensely hot temperatures that both degraded the column coating, making it brittle, and likely degraded the complexes themselves within the system. Additionally, the lengths of column between the heating collars became too cold for the volatilized complexes to remain in a gaseous state and caused considerable condensation. The condensation appeared to block the flow of the complex through the system and completely inhibited reliable, repeatable detection in the mass spectrometer.

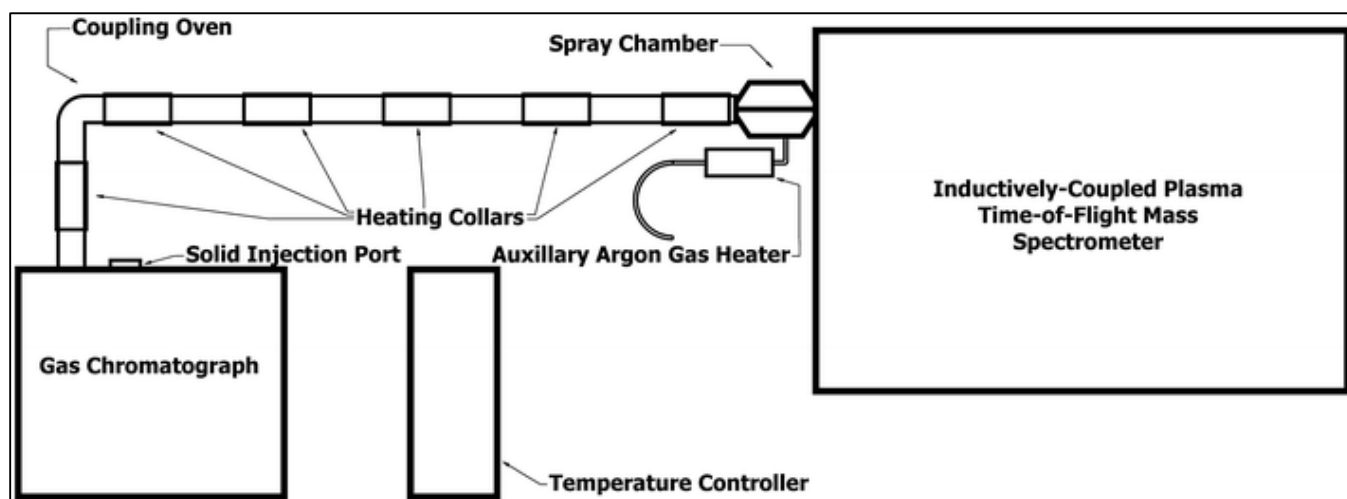


**Figure 3.2** GC-ICP-TOF-MS Schematic (Version 1)

To address this issue, a new connection was designed to replace the stainless steel heating tube connecting the GC and the ICP-TOF-MS. A much smaller (and shorter) 0.25" flexible metal pipe with spiral grooving along its length was chosen to replace the cumbersome stainless steel tube

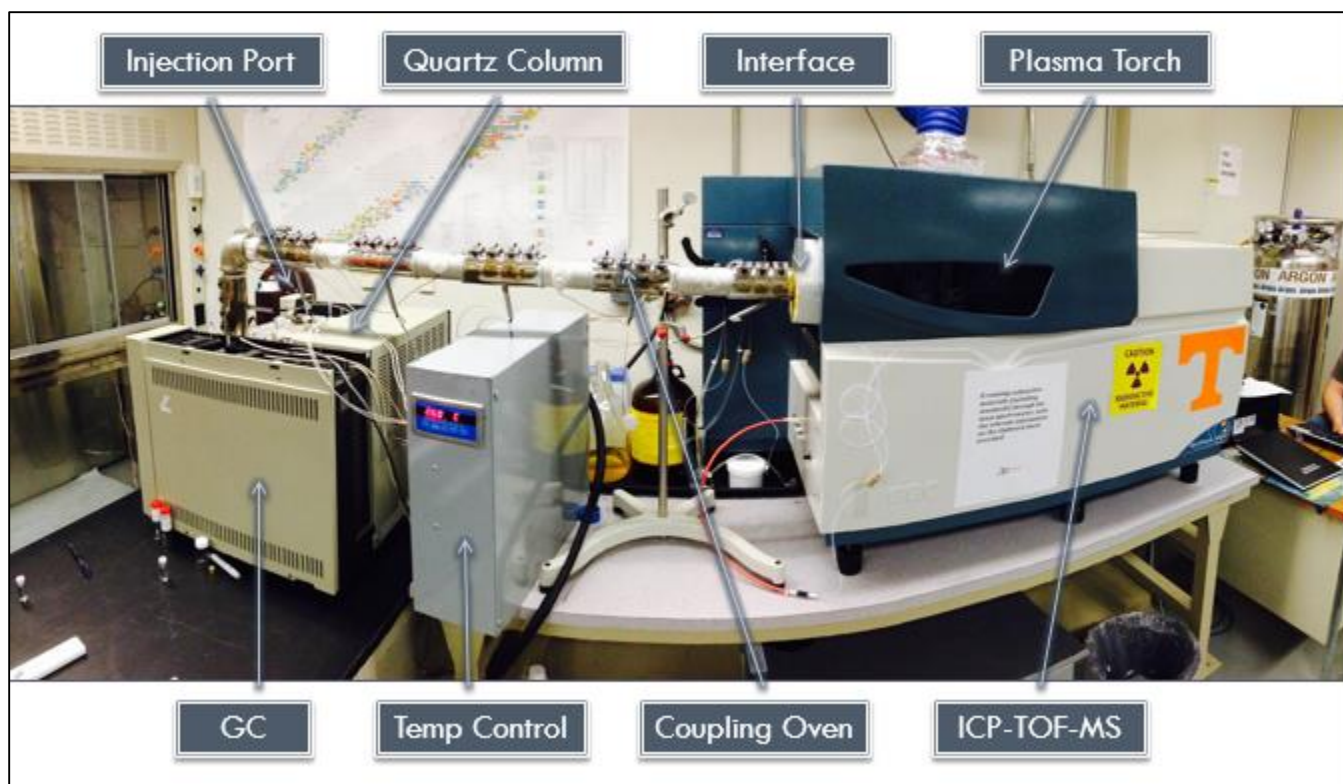


**Figure 3.3** GC-ICP-TOF-MS Front View (Version 1)

connection. In place of heating collars, insulated nichrome wire was laid into the spiral grooving along the length of the pipe segment to provide reliably even heating. A hold was drilled in the middle of the pipe to accommodate a thermocouple that is connected to the original temperature controller. The entire connection is covered in fitted insulation to produce a very consistent internal temperature. Switching to this connection vastly improved the operation of the system and prevented a number of column temperature issues. A rendering of the new coupling oven is shown in Figure 3.5, where the steel tube, fitted orange insulation, nichrome wire, and thermocouple can be seen, and the newly assembled system (denoted as “version 2”) is shown in Figure 3.6. The internal configuration of the ICP-TOF-MS is shown in Figure 3.7.





**Figure 3.4** GC-ICP-TOF-MS Profile (Version 1)

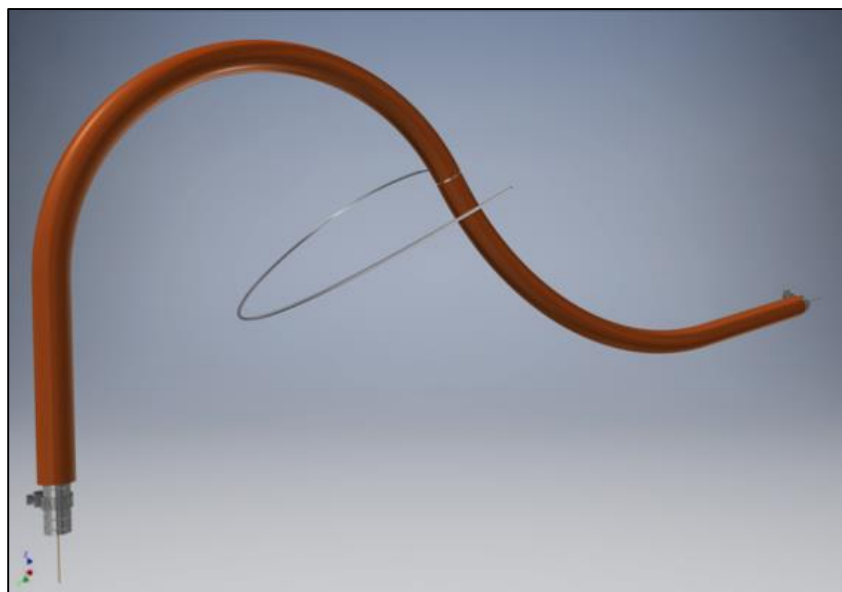


**Figure 3.5** Coupling Oven (Version 2)

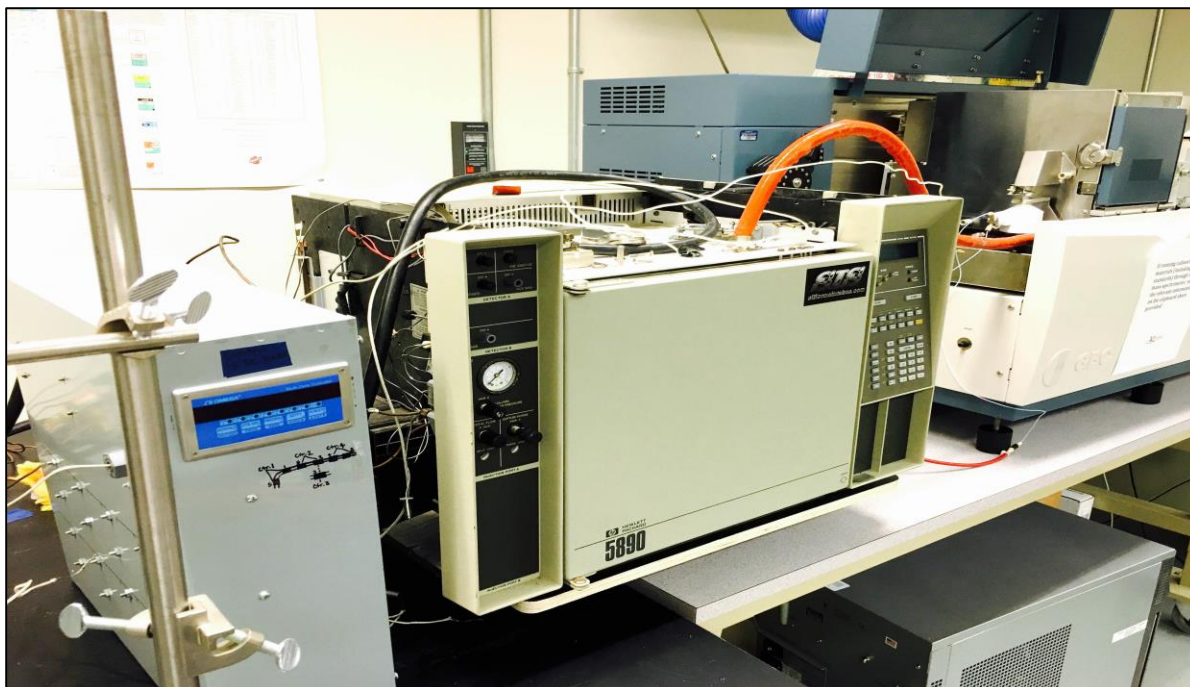


**Figure 3.6** Assembled GC-ICP-TOF-MS (Version 2)

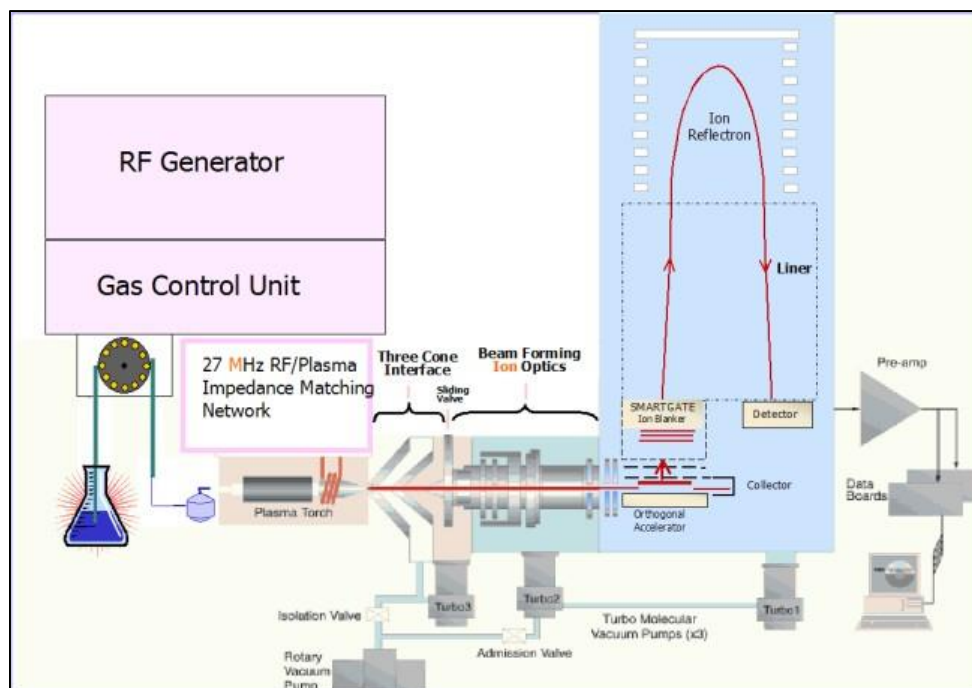


**Figure 3.7** ICP-TOF-MS Process<sup>58</sup>

It is clear from a comparison the two instrument versions that the second version is much less cumbersome and inherently more efficient than the first version. Resulting injection/detection experiments were significantly improved after switching to the new coupling oven.

## **CHAPTER 4**

### **METHODOLOGY**

#### **4.1 Engineering: Developing a Functional Coupling System**

The first stage of the proposed research was to establish successful, repeatable co-operation of the GC and ICP-TOF-MS. After physical coupling and initial beta runs, very few of the injected samples into the GC port were detected by the ICP-TOF-MS. Even those samples that were detected were not repeatable using the same method in succession. As such, it was obvious that there was a loss of continuity between the two instruments, even considering their mechanical connection. It was discovered that the plumbing in the GC was incorrectly attached; subsequent disassembly and reconnection of the flow valves, piping, and discharge valves yielded reliable gas flow operation of the GC system. Additionally, it was discovered that the GC injection port was malfunctioning - the rubber septum and a new splitless inlet were replaced and the injection issues were largely resolved. The system can run in both “split” mode – meaning only a small portion of the sample injected is taken into the machine – and “splitless” mode, where the entire sample is injected into the machine. The major benefit of the former is peak resolution on the ICP-TOF-MS side of the apparatus, while the benefit of the latter is quantitative analysis. Both split and splitless injection methods were attempted; splitless yielded more accurate sample detection and was therefore used for all experimental runs.

## 4.2 Injection Methodology

Samples of  $\text{Ln}[\text{hfac}]_x$  were injected into the GC injection port for column separation and ultimate detection in the ICP-TOF-MS. Initial injections involved a 1 microliter  $\text{Ln}[\text{hfac}]_x$  sample dissolved at a 0.1 mg/ml concentration in pure anhydrous ethyl ether. The injection port, GC oven, coupling oven, and quartz spiral were heated to the same temperature (varying from 130-170°C). The flow rate through the column was set to 0.85 ml/min with a splitless injection and negligible purge flow. In this arrangement, all species introduced into the GC flowed only through the heated column for detection in the ICP-TOF-MS. An early injection is shown in Figure 4.1.

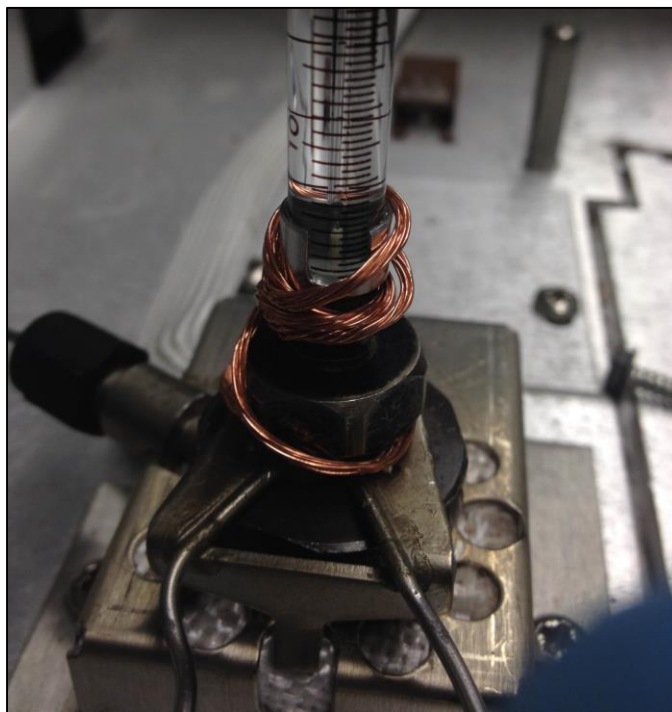


**Figure 4.1** Solid Injection of  $\text{Pr}[\text{hfac}]_4$

### 4.3 Proof of Concept: Separation Viability

Initial beta-testing procedures and proof-of-concept fission product separations were performed on a Hewlett-Packard gas chromatography mass spectrometer instrument using an Agilent 6890 column and a 5973 mass selective detector. Experimental adjustments were made until the samples eluted from the column in a reasonable timeframe. Helium was used as a carrier gas with a flow rate of 0.8 mL/min on a 30 m column. The injection inlet was heated to 250 °C to volatilize the samples. The oven temperature was set to 70°C, with a 0.00 min hold time. The oven was then heated at a rate of 25.0°C/min to a set point 150°C and held for 5.00 min. Figure 4.2 below shows the resulting separation, after months of experimental optimization, using Sm, Dy, and Tm.

However, this instrument, while demonstrating an ability to separate the complexes, is an aging piece of equipment and does not have the resolution for extremely accurate isotopic identification. Additionally, this instrument measures complex fragmentation and is not a reliable source of isotopic identification. It is therefore prudent to gather accurate data on an instrument with much more precision and an ability to isolate individual isotopes for rapid identification. It was also found at a later time that the initial tests in this instrument were likely misinterpreted due to contamination of the column; installing a new column and repeating the tests yielded non-similar results. It is thought that the complexes did in fact elute from the column, but they eluted in heavy fragments that were not being recorded at the time of beta testing. The fragmentation of these species into such large complexes could be prevented if the detector were to completely disassemble the species, such as in an inductively-coupled plasma detector.

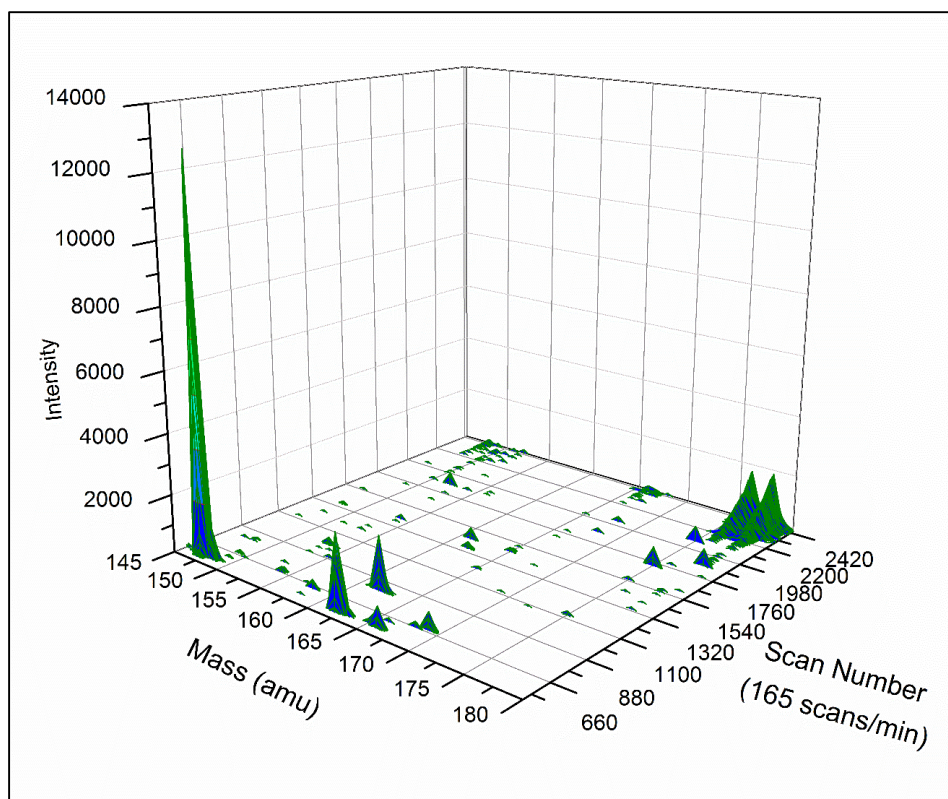


**Figure 4.2** 3D plot of GC-MS data from a sample injection of Sm, Dy, and Tm hfac

It was decided to use a gas chromatography unit with an attached inductively-coupled plasma time-of-flight mass spectrometer (ICP-TOF-MS) for an accurate spectrum of sample species. This instrument, unfortunately, is not commercially available as are its liquid-injection counterparts. As was outlined in Chapter 3, it was therefore necessary to build the instrument in-house by coupling a gas chromatography instrument to an ICP-TOF-MS. Mass spectra were recorded using a GBC 9000 Opti-mass ICP-TOF-MS. A custom-designed quartz coil was installed to heat the argon nebulizer flow surrounding the plasma torch where the GC column enters the ICP-TOF-MS, as shown in Figure 4.3 and Figure 4.4.



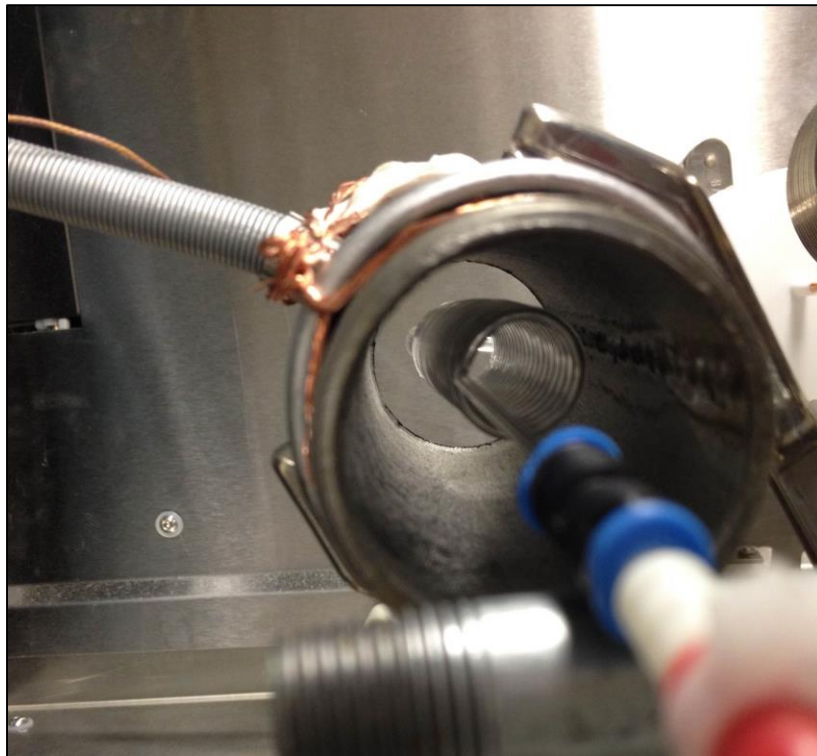


**Figure 4.3** Custom Quartz Argon Heating Column

The gas chromatography instrument is a Hewlett-Packard 5890A with a 30 m uncoated 0.53 mm I.D. Agilent quartz column. The temperature programming unit is an Omega CN1504 multi-zone controller with four heating control zones. Seven individual thermocouples are attached to the control box to heat a 1.5" I.D. stainless steel tube that connects the GC to the ICP-TOF-MS, as shown in Figure 4.5.



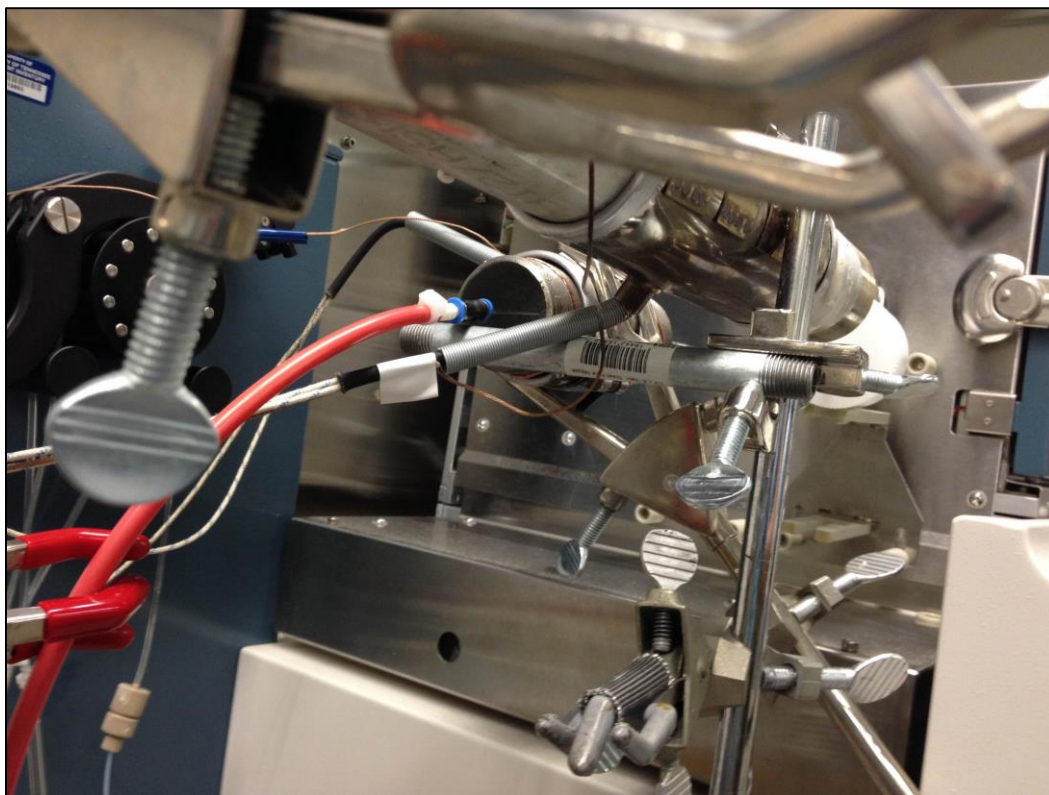


**Figure 4.4** Quartz Argon Heating Coil Positioning



**Figure 4.5** Stainless Steel Tube Oven Connection

The plasma torch obliterates molecules emitted from the end of the quartz column for subsequent detection in the TOF section of the MS. As discussed in Chapter 3, the coupling oven was replaced by a much smaller and more efficient coupling piece.

#### **4.4 Thermodynamic Measurements**

In order to obtain the entropy and enthalpy of adsorption of the introduced samples, which is necessary for separation optimization, several injections of the same species at varying temperatures must be carried out.<sup>13</sup> Originally, the intention was to introduce injections at five separate temperatures – 130, 140, 150, 160, 170 °C - per sample, and five runs performed at each temperature to ensure statistically meaningful results. In total, approximately 400 runs were necessary (five runs at five temperatures for each of the RE complexes) to accrue the necessary data for optimization. Unfortunately, after several months of injections involving every lanthanide sample at a range of temperatures and operating conditions, separations between the elements were never achieved. Instrument continuity was no longer an issue – almost every injection was associated with a mass spec peak – but the complexes were invariably eluted at the same time in every experiment. Several of these tests are shown below in Figures 4.6 - 4.8. Detection speed was usually on the order of 30-500 seconds depending on the operating conditions. It is important to note that injections in the following figures are not associated with time zero, but rather were injected throughout the recorded time during on-line experimentation. The lack of separation in these (and many other) experiments was not completely unexpected; the fact that the thermodynamic properties are likely to be similar and are, as of yet, unknown, has always indicated the possibility that the hexafluoroacetylacetone ligand may not allow for chromatographic separations of these complexes in these conditions.

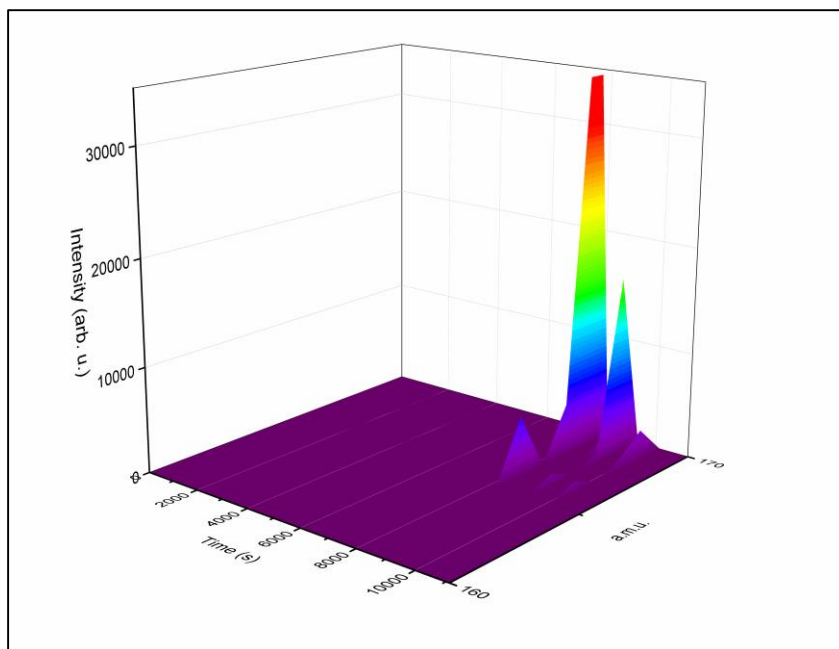


**Figure 4.6** Tm/Er Mixture Detection

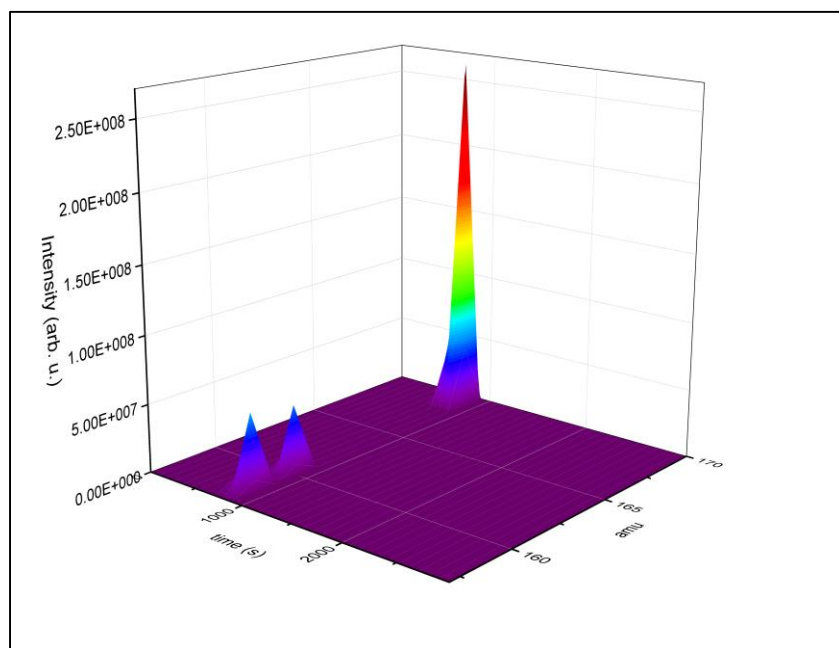


**Figure 4.7** Tm/Gd Mixture Detection

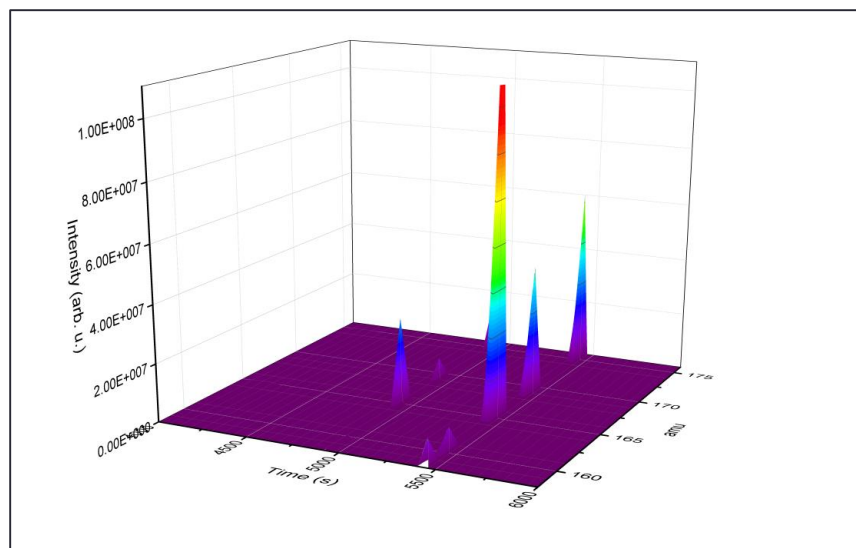


**Figure 4.8** Gd/Ho/Tm/Lu Mixture Detection

The accepted theory by the author and several other researchers contributing to this project is that the detected eluents are, in fact, “blowthrough” complexes that never interacted with the column surface in the first place. When a sample is injected, a small amount of air within the syringe plunger is injected alongside the sample (on the order of 0.5 ml) to ensure that the sample exits the needle and enters the injection port. It is possible that a small amount of the sample rides the air front along the length of the column and has limited interaction with the column. This could cause the simultaneous detection of the species within the injected sample. If this is in fact occurring, it means that the remainder of the sample remains permanently within the system. Microscopic analysis of the quartz column indicates that deposits are indeed occurring at various points along the column.

However, further experiments indicate that the majority of the injected sample does, in fact, traverse the length of the column unaffected and should be detected in the mass spectrometer.

This would imply that there is a continuity issue in the interface between the coupling oven and the plasma torch.

Early experiments with this instrumentation were performed with the quartz column pushed all the way to the edge of the plasma within the mass spectrometer. Though this is intuitively the most effective way of introducing the sample into the MS, a multitude of issues occurred with that setup. Such large sample volumes, particularly those not introduced as liquids, cause intense plasma disruptions that many times concluded with unintended automatic instrument shutdown. Issues also developed with the end of the column that was in contact with the edge of the plasma boundary.

Due to these issues, it was decided to retract the end of the quartz column into the spray chamber where it would be directly carried into the plasma torch by the nebulizer flow. The problem with this setup is the inherent cooling associated with a large change in carrier gas flow rate. Instead of carrying the sample in a gaseous state directly to the plasma torch, this setup assumes that the complexes will condense immediately upon introduction to the spray chamber. The volumetric nebulizer flow in the spray chamber consistently flows approximately three orders of magnitude faster than the column carrier gas, and is assumed to cause the re-condensed complex particles to form aerosols within the spray chamber that can be transported to the plasma torch within the nebulizer air stream. This assumption is confirmed by the fact that complexes are regularly detected within the mass spectrometer after switching to this setup.

Though the change in column introduction setup precluded many of the plasma issues that were previously encountered, no change was seen as far as separation of the injected complexes. Samples invariably eluted simultaneously with both setups, and the inability to calculate

adsorption properties of these complexes without clear separation between the elements lead to a requisite change in the methodology used to collect thermodynamic values of the complexes.

#### 4.5 Separation Optimization

Plotting resulting retention times of the complexes as a function of temperature yields a lognormal distribution as defined by Equation 1 below.

$$RT \ln \left[ \frac{D}{4} \left( \frac{retention_{compound}}{retention_{carrier}} - 1 \right) \right] = T \Delta S_{adsorption}^0 - \Delta H_{adsorption}^0$$

**Equation 4.1**

Churburkev *et al.* originally derived this equation in order to express a linear relationship between temperature and enthalpy/entropy of adsorption using the foundational mathematics of chromatography, where  $R$  is the ideal gas constant,  $T$  is the temperature, and  $D$  is the inner column diameter.<sup>59</sup> This equation was derived using two main assumptions: 1) an uncoated/unpacked GC column and 2) isothermal conditions. The column applied in this work is therefore a 30m unpacked, uncoated quartz column with a 0.53 mm I.D. All experimental runs applied isothermal conditions. Plotting the resulting retention times on a graph correlating the logarithmic term to the inverse temperature of the experiment yields a linear relationship from which the enthalpy and entropy of adsorption could be measured directly. However, the fact that the complexes did not elute under the same operational conditions indicates that this approach cannot be used to determine the enthalpy and entropy of adsorption. It is known that the

$\text{Ln[hfac]}_4$  complexes sublime at a range of temperatures, and thus, separation between the metal complexes should be observed. This fact gives credence to the theory of air peak blowthrough outlined in the previous section. Fortunately, because the complexes have demonstrated a difference in sublimation temperatures, an alternate approach can be used to determine their enthalpies and entropies of adsorption using thermochromatography.

If a suite of complexes, in this case the  $\text{Ln[hfac]}_4$  complexes, demonstrate variation in volatilization temperatures, a temperature gradient can be used to experimentally determine adsorptive thermodynamic characteristics. Each complex will deposit along the column at a characteristic temperature called the “deposition temperature”. This temperature can be used in conjunction with the experimental operating conditions to converge the enthalpy and entropy of adsorption of the deposited complexes.

Steffen and Bachmann<sup>57</sup> have outlined a derivation used to calculate the entropy and enthalpy of adsorption from deposition patterns within a temperature gradient. From linear ideal gas chromatography:

$$\frac{dl}{dt} = \frac{u_r}{K_i + 1}$$

#### **Equation 4.2**

For the migration of the complex in a thermochromatographic column, this must be expressed as a function of temperature:

$$u_T = u_0 \left( \frac{T}{T_0} \right)$$

**Equation 4.3**

Where  $u_0$  is the carrier gas velocity at temperature  $T_0$ . The temperature gradient can be expressed as:

$$\frac{dT}{dl} = -a$$

**Equation 4.4**

Where  $a$  is the temperature gradient. Expressing  $K_i$  in terms of  $K_c$ :

$$K_i = K_c \left( \frac{s}{V_g} \right)$$

**Equation 4.5**

Where  $s$  is the surface area of the quartz column in contact with the sample (per unit length) and  $V_g$  is the dead volume in the column per unit length.  $K_p$  can be expressed in terms of  $K_c$ :

$$K_p = K_c (RT)^{\Delta v}$$

**Equation 4.6**



Where  $\Delta v$  is the change of the number of moles in the gas phase by adsorption onto a solid phase, which is assumed to be equal to -1. From these equations, the following is known:

$$K_i = \left(\frac{s}{V_g}\right) RT \exp\left(\frac{-\Delta H^\circ}{RT} + \frac{\Delta S^\circ}{R}\right)$$

**Equation 4.7**

Where  $-\Delta H^\circ$  and  $\Delta S^\circ$  are the standard enthalpy and entropy of adsorption, respectively. It follows that:

$$dt = \frac{T_0}{u_0 a T} \left[1 + \frac{s}{V_g} RT \exp\left(\frac{-\Delta H^\circ}{RT} + \frac{\Delta S^\circ}{R}\right)\right] dT$$

**Equation 4.8**

For the movement of the compound within the negative temperature gradient:

$$\int_0^{t_a} dt = \frac{T_0}{-a u_0} \int_{T_s}^{T_a} \left[\frac{1}{T} + \frac{s}{V_g} R \exp\left(\frac{-\Delta H^\circ}{RT} + \frac{\Delta S^\circ}{R}\right)\right] dT$$

**Equation 4.9**

And therefore:

$$t_a = \frac{T_0}{-au_0} \left[ \ln \frac{T_s}{T_a} + \frac{s}{V_g} R \exp\left(\frac{\Delta S^\circ}{R}\right) \int_{T_a}^{T_s} \exp\left(\frac{-\Delta H^\circ}{RT}\right) dT \right]$$

**Equation 4.10**

From these relationships, the following can be derived:

$$\frac{au_0 t_a}{T_0} = \ln \frac{T_s}{T_a} + \frac{s}{V_g} R \exp\left(\frac{\Delta S^\circ}{R}\right) \exp\left(\frac{-\Delta H^\circ}{RT_a}\right)$$

**Equation 4.11**

When  $T_s/T_a$  is neglected:

$$\ln Z = \ln \frac{at_a u_0 V_g}{R s T_0} - \frac{\Delta S^\circ}{R}$$

**Equation 4.12**

Which can be solved for  $t_a$ :

$$\ln t_a = \ln Z + \frac{\Delta S^\circ}{R} + \ln \frac{R s t_0}{a u_0 V_g}$$

**Equation 4.13**

And therefore:

$$\log t_a = \frac{-\Delta H^\circ}{2.3RT_a} + \frac{\Delta S^\circ}{2.3R} + \log \frac{Rst_0}{au_0V_g}$$

**Equation 4.14**

is obtained. When several experiments are performed at various operating conditions (changing, for example, the linear gas velocity  $u_0$ ), and the resulting lines are plotted on a graph of enthalpy of adsorption versus entropy of adsorption, the intersection of the lines yields the resulting enthalpy and entropy of adsorption of the complex under interrogation.

In lieu of a temperature gradient, a procedure using cold column complex deposition and temperature ramping was used to mimic a temperature gradient (attempts to create a temperature gradient necessary for these complexes were unsuccessful). One end of the quartz column was introduced to room temperature while the other end remained connected to the injection port. The majority of the column was within the GC oven where the temperature could be finely controlled with only the last 5-6 cm of column remaining in room temperature conditions. A complex was injected at a sufficiently high temperature such that it traversed the length of the column and deposited on the last 5-6 cm where it was exposed to a sudden temperature shock. The end with the complex deposit was then put back into the GC with the remainder of the column and subject to a gradual temperature increase. Each temperature was held for 10 minutes, after which the column was inspected for remaining deposition. The temperature was increased until the deposit eluted within the 10-minute timeframe. Using this method, we were able to confine a 5-degree window in which the complex would elute; this temperature is the temperature at which the complex becomes a gas and elutes at the given operational conditions,

and conversely, the deposition temperature at which the complex condenses from a gas to a solid within the column.

With a deposition temperature range, a known carrier gas flow rate, and a known ramp rate, all necessary variables can be substituted into the derived equation and plotted to yield linear equations. Performing the same experiment with the same complex, but varying the carrier gas flow rate, produces a line with a slightly different slope that intersects the first line under the original operating conditions. This intersection yields the enthalpy and entropy of adsorption values. It is obvious that the more lines plotted for a given complex, the more the error can be converged and minimized.

#### **4.6 Expected Results**

The enthalpy and entropy of adsorption of the  $\text{Ln}[\text{hfac}]_x$  complexes are the primary novel parameters being measured in this work in support of separation optimization. However, that does not preclude approximations of these parameters, especially considering related experiments such as Thermogravimetric Analysis (TGA) and Differential Thermogravimetric Analysis (DTA). These experiments measure the mass difference of a solid sample after prolonged heat exposure. Through mathematical manipulation, measurements made in these experiments can yield approximations to the entropy and enthalpy of adsorption. The expected measured results from this work indeed fell within range of these values. Appendix E details the entropy and enthalpy of adsorption as estimated from TGA and DTA analysis (this source of estimation involves equations used primarily in super heavy element synthesis and is based on very few data points. There are large error bars on each result, as shown in Appendix E).

## **CHAPTER 5**

### **RESULTS AND DISCUSSION**

#### **5.1 Deposition Temperature Ranges of Individual Ln[hfac]<sub>4</sub> Complexes**

Samples of individual Ln[hfac]<sub>4</sub> complexes, aside from La[hfac]<sub>4</sub>, Ce[hfac]<sub>4</sub>, and Pm[hfac]<sub>4</sub>, were injected according to the methodology outlined in the previous chapter to observe and isolate deposition temperature ranges along the column. Four pressure values were initially used to discern temperature variances as they related to column pressure; however, after injecting several samples at the highest pressure value of 42 psi, it was observed that the adsorption properties of the complexes were completely overridden by the high pressure within the column. A minimum tank pressure of 10 psi (physical limitation) and maximum pressure of 42 psi (thermodynamic limitation) left an acceptable range of three individual pressures: 12 psi, 22 psi, and 33 psi, to be used. Adding more pressure values within this range did not allow for sufficient discernment of deposition temperature ranges between the pressure values, so in the end, only these three pressure values were used to measure the adsorption properties of the complexes. Resulting deposition temperature ranges are shown in Table 5.1.

#### **5.2 Adsorption Plots**

The temperature deposition profiles of each element were used to model adsorption behavior using the equation outlined in the previous chapter. In conjunction with pressure, temperature ramp rate, flow rate, and other operating conditions, adsorption enthalpy and entropy values could be plotted at each temperature value and graphed concurrently. The three points of

intersection of these lines (produced from the three pressure values used during experimentation and subsequent variations in deposition temperature) relay three converged entropy and enthalpy values for each complex. Under ideal conditions, these points would all overlap and convey a single value for enthalpy and entropy of adsorption. However, due to experimental error, the three points of intersection must be averaged. Figures 5.1 – 5.12 show the plots resulting from the data obtained in Table 5.1.

**Table 5.1** Pressure-Dependent Deposition Temperatures of Ln[hfac]4 Complexes, °C

	<b>12 psi</b>	<b>22 psi</b>	<b>33 psi</b>	<b>42 psi</b>
<b>Pr</b>	140-145	135-140	130-135	115-120
<b>Nd</b>	140-145	135-138	130-135	111-117
<b>Sm</b>	150-155	142-148	130-135	104-109
<b>Eu</b>	155-160	143-148	113-118	113-116
<b>Gd</b>	150-155	125-130	110-112	105-110
<b>Tb</b>	110-115	96-100	92-96	x
<b>Dy</b>	126-130	120-125	115-120	x
<b>Ho</b>	122-127	117-122	110-115	x
<b>Er</b>	145-150	120-125	107-112	x
<b>Tm</b>	140-145	131-136	110-115	x
<b>Yb</b>	155-160	129-134	110-115	x
<b>Lu</b>	145-150	130-135	105-110	x
<b>Flow rate (ml/min)</b>	2.25	3.70	6.00	7.38

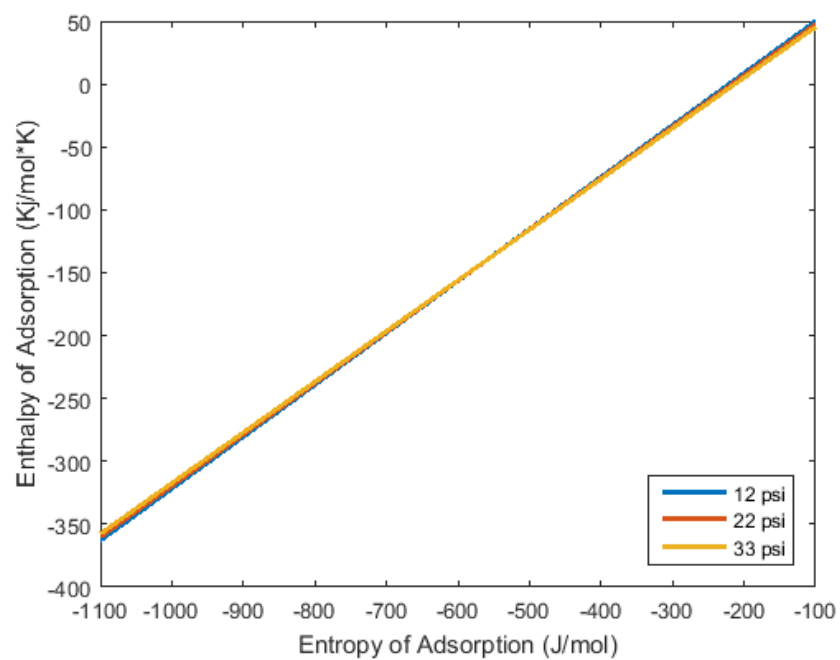


**Figure 5.1** Pr[hfac]<sub>4</sub> Adsorption Convergence Plot

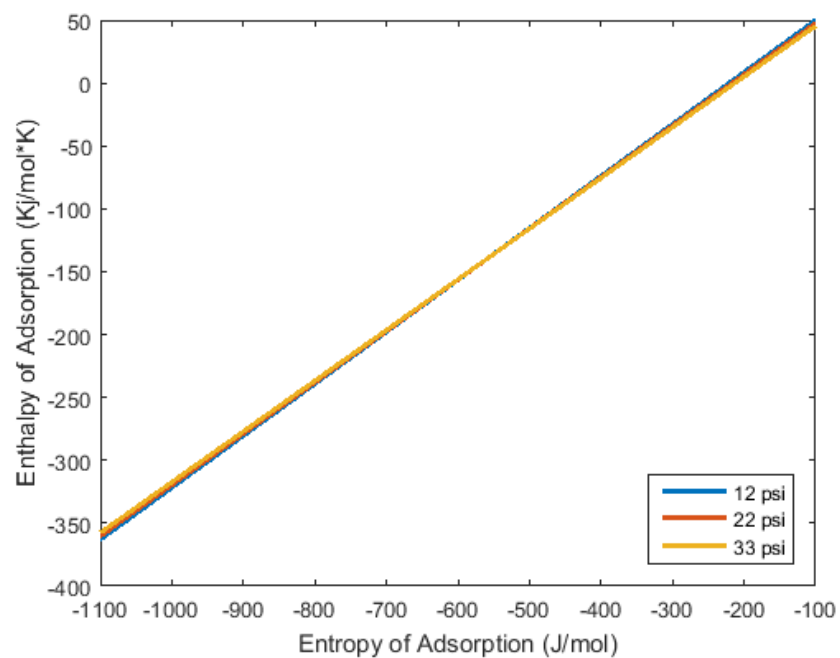


**Figure 5.2** Nd[hfac]<sub>4</sub> Adsorption Convergence Plot

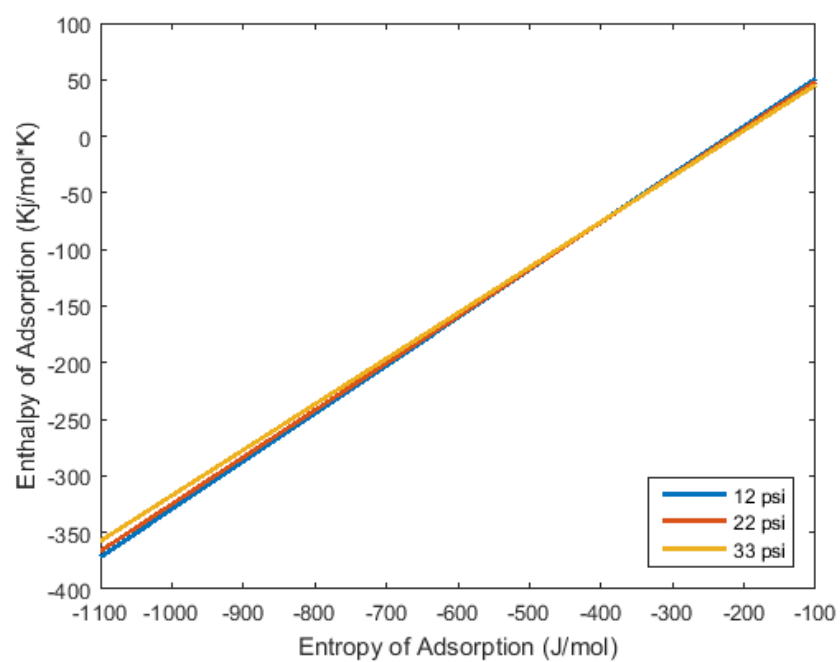


**Figure 5.3** Sm[hfac]<sub>4</sub> Adsorption Convergence Plot

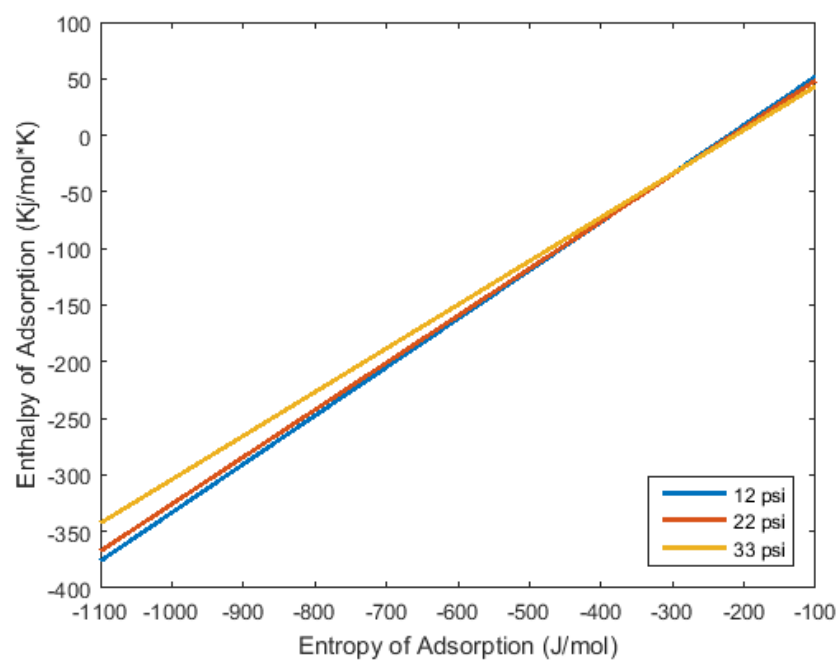


**Figure 5.4** Eu[hfac]<sub>4</sub> Adsorption Convergence Plot



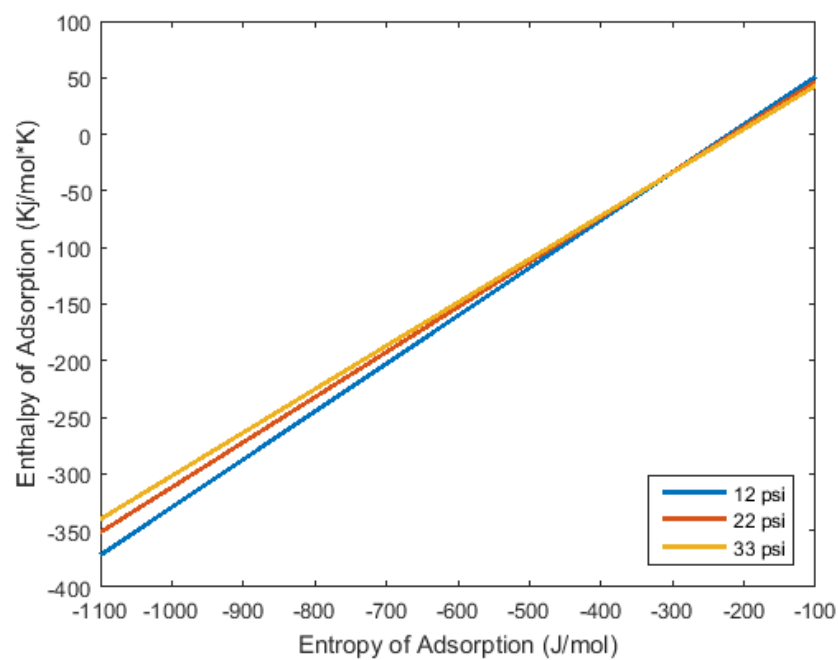


**Figure 5.5** Gd[hfac]<sub>4</sub> Adsorption Convergence Plot

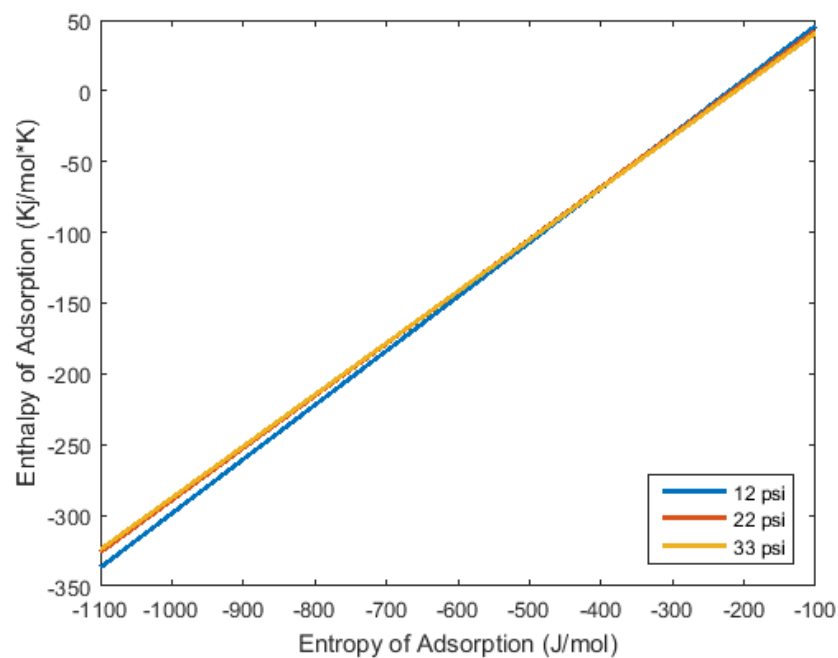


**Figure 5.6** Tb[hfac]<sub>4</sub> Adsorption Convergence Plot

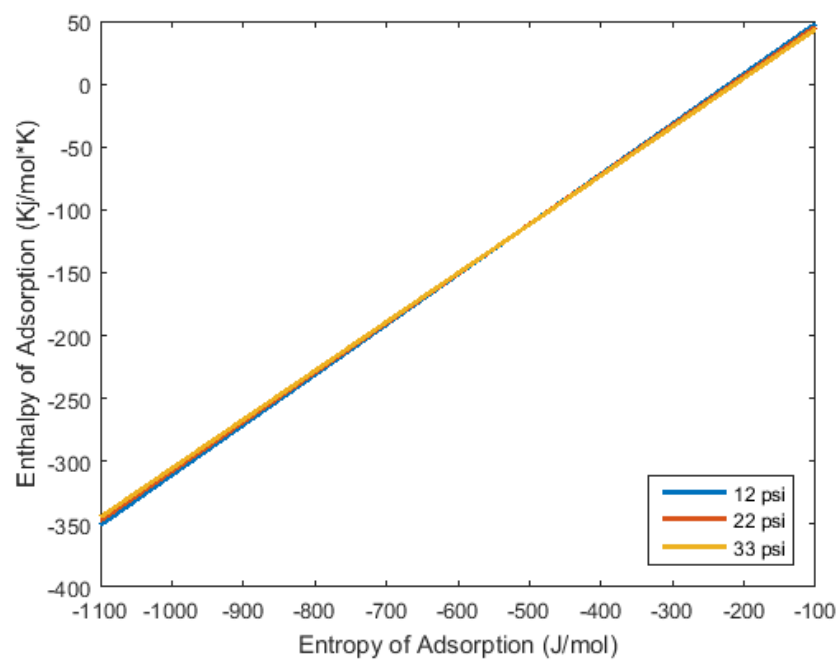


**Figure 5.7** Dy[hfac]<sub>4</sub> Adsorption Convergence Plot

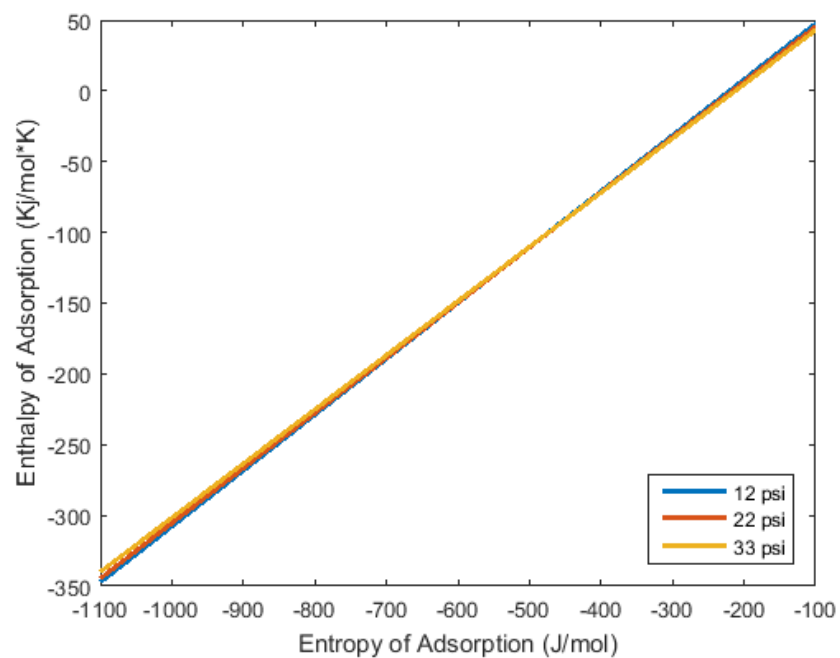


**Figure 5.8** Ho[hfac]<sub>4</sub> Adsorption Convergence Plot

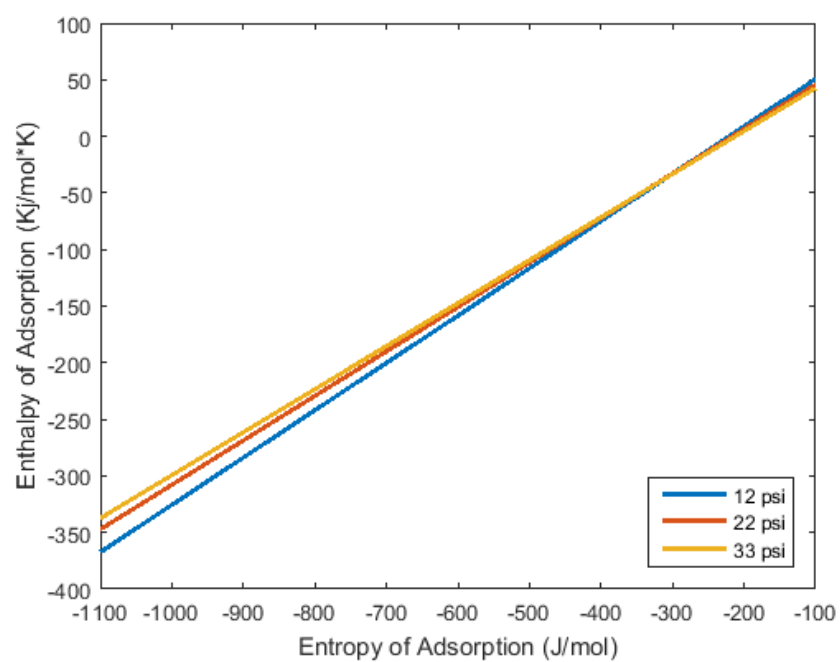


**Figure 5.9** Er[hfac]<sub>4</sub> Adsorption Convergence Plot

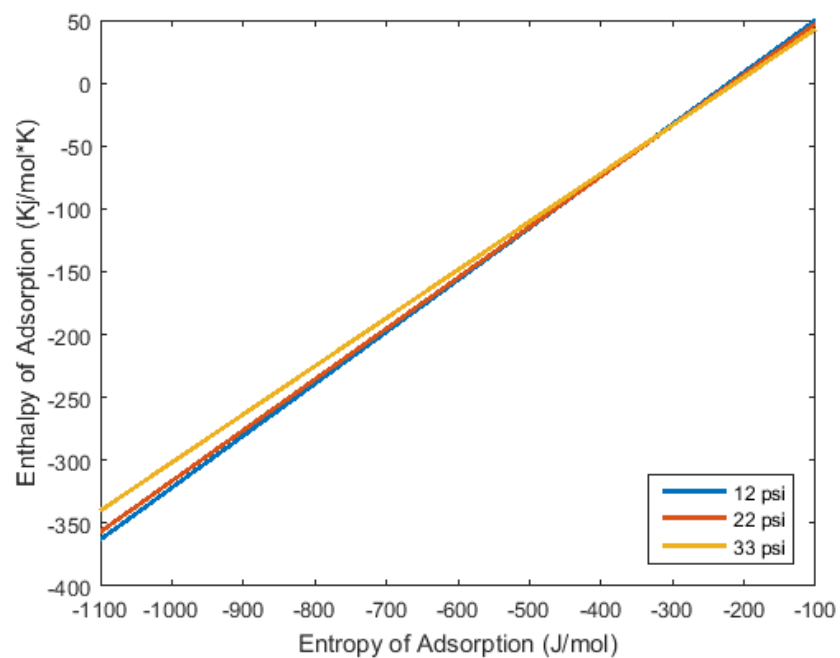


**Figure 5.10** Tm[hfac]<sub>4</sub> Adsorption Convergence Plot

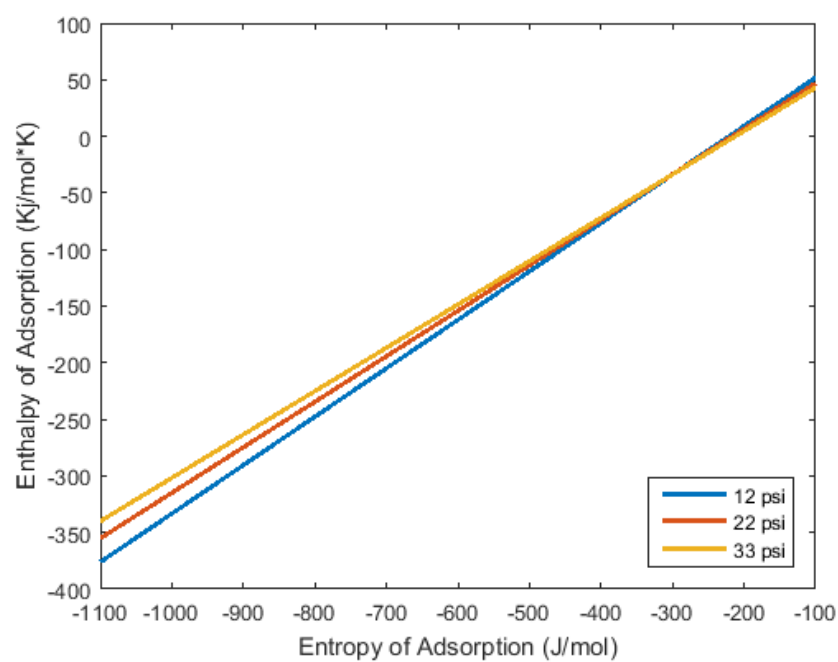


**Figure 5.11** Yb[hfac]<sub>4</sub> Adsorption Convergence Plot

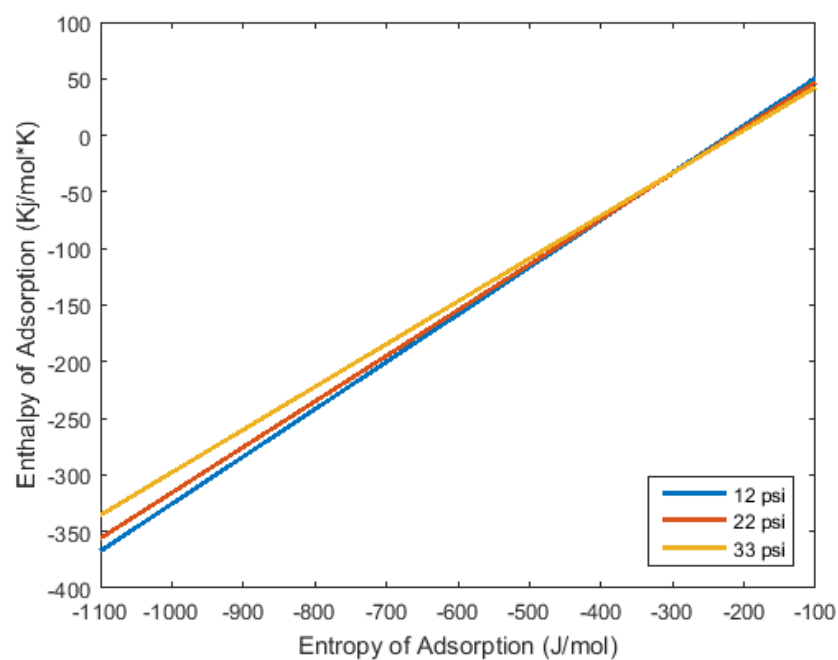


**Figure 5.12** Lu[hfac]<sub>4</sub> Adsorption Convergence Plot

### 5.3 Enthalpy and Entropy of Adsorption of Ln[hfac]<sub>4</sub> Complexes

The points of intersection of the lines outlined in section 5.2 are shown in Table 5.2, along with the standard deviation from both experimental and theoretical error. Experimental error was largely due to the visual approach used to inspect the column for complex elution (e.g., at what temperature is the complex completely gone?), and theoretical error can be attributed to the difference in intersection points of the plots shown in Figures 5.1 – 5.12. Experimental error was small compared to theoretical error.

**Table 5.2** Enthalpy and Entropy of Adsorption Values of Ln[hfac]<sub>4</sub> Complexes

	$-\Delta H_{\text{ads}} \text{ (-KJ/mol}\cdot\text{K)}$	$-\Delta S_{\text{ads}} \text{ (-J/mol)}$
<b>Pr</b>	$139 \pm 4$	$557 \pm 19$
<b>Nd</b>	$139 \pm 5$	$557 \pm 22$
<b>Sm</b>	$76 \pm 17$	$398 \pm 51$
<b>Eu</b>	$42 \pm 21$	$317 \pm 59$
<b>Gd</b>	$38 \pm 7$	$310 \pm 27$
<b>Tb</b>	$83 \pm 49$	$440 \pm 143$
<b>Dy</b>	$118 \pm 8$	$516 \pm 29$
<b>Ho</b>	$109 \pm 21$	$493 \pm 66$
<b>Er</b>	$39 \pm 10$	$315 \pm 34$
<b>Tm</b>	$53 \pm 25$	$348 \pm 70$
<b>Yb</b>	$33 \pm 3$	$299 \pm 17$
<b>Lu</b>	$38 \pm 11$	$310 \pm 38$

The newly-obtained enthalpy of adsorption values can now be compared to previously-known sublimation enthalpy values calculated by Shayan Shahbazi<sup>60</sup> to obtain a linear relationship, as shown in Figure 5.15 and Figure 5.16.

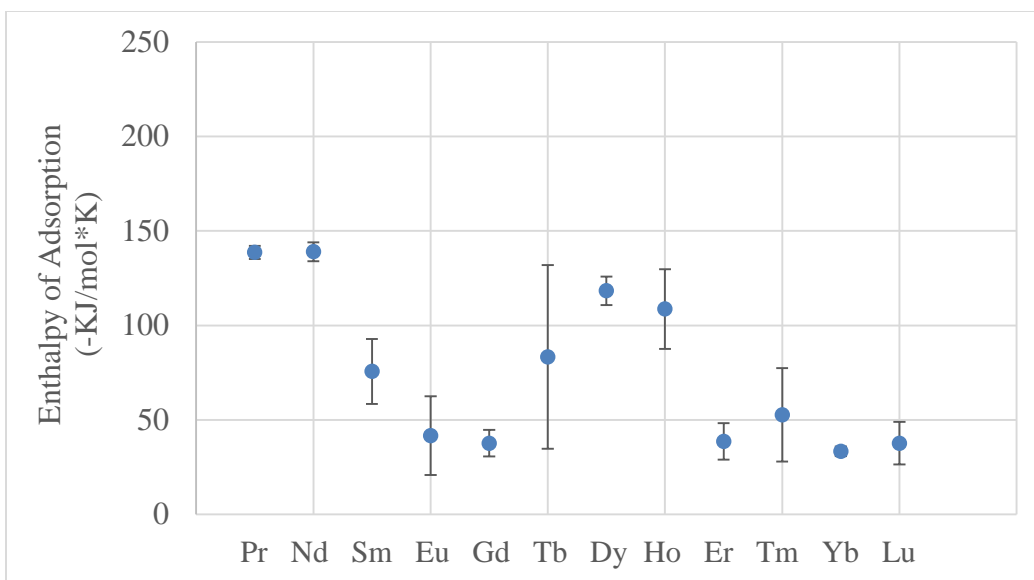


**Figure 5.13** Enthalpy of Adsorption of  $\text{Ln}[\text{hfac}]_4$  Complexes

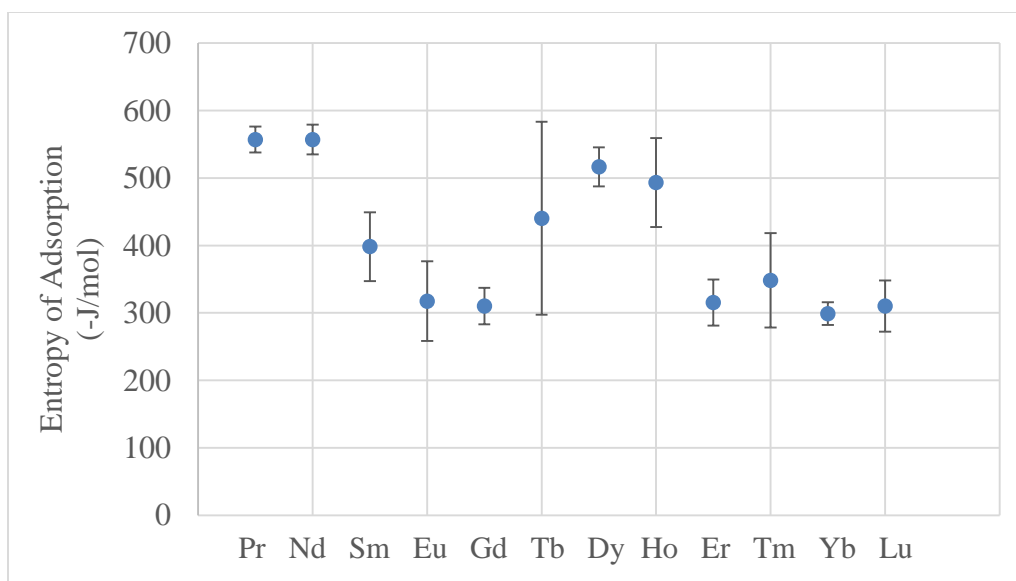


**Figure 5.14** Entropy of Adsorption of  $\text{Ln}[\text{hfac}]_4$  Complexes

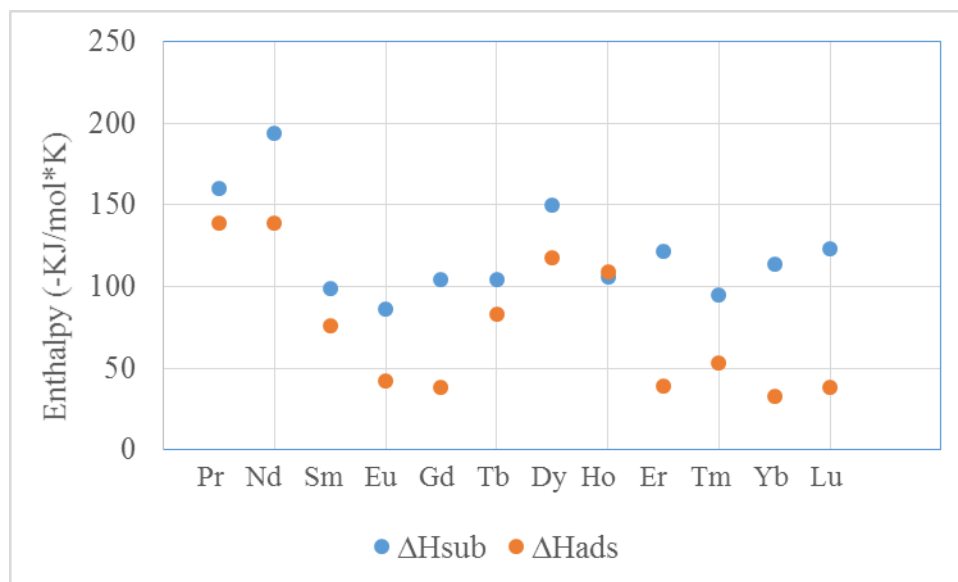


**Figure 5.15** Enthalpy of Adsorption vs. Enthalpy of Sublimation for Ln[hfac]<sub>4</sub> Complexes

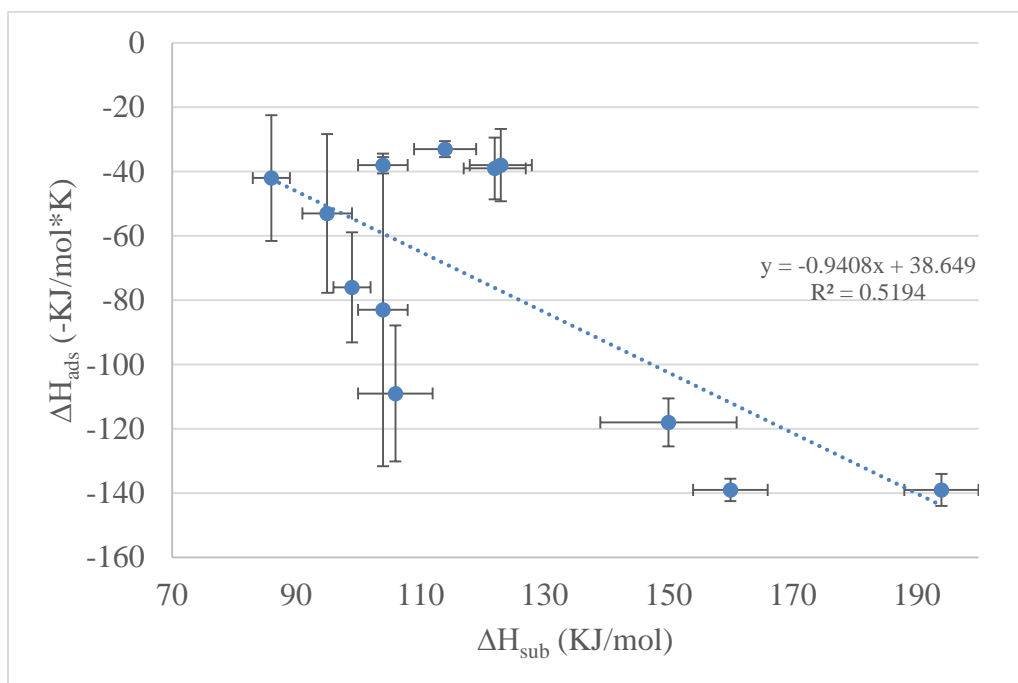


**Figure 5.16** Adsorption Enthalpy vs. Sublimation Enthalpy

Ninety percent of these values fit into a relationship defined by Equation 5.1, relating the *average* enthalpy of adsorption to the *average* enthalpy of sublimation of  $\text{Ln[hfac]}_4$  complexes (omitting source value standard deviation). The 10% excluded from this relationship were those complexes that were difficult to experimentally determine the deposition temperature, and the uncertainty in these measurements did not lend itself well to discerning a trend from the complexes that were more accurately experimentally determined. More extensive testing of these complexes would hopefully yield data that is accurate to a degree that allows for trend identification, but at the time of writing, this additional experimentation has not yet been performed and the outliers were not considered appropriate for trend calculations.

$$\Delta\bar{H}_{ads} = (-0.94)\Delta\bar{H}_{sub} + (38.65 \pm 40.5)$$

### Equation 5.1

Though the error in this equation is large, it is the first published trend relating the enthalpy and entropy of adsorption of these complexes and can be used as a first-order approximation to find the general relationship between these two values. Future work using isothermal chromatography can more accurately predict the adsorption enthalpy to yield a better approximation, but experimental issues with the coupling device between the mass spectrometer and gas chromatography instrument during isothermal experimentation did not allow for these experiments to proceed in the time allotted for these calculations.

However, if the data points with greater than 10% standard error are removed from the series, the remaining seven data points can be plotted with a much more observable trend, as shown in

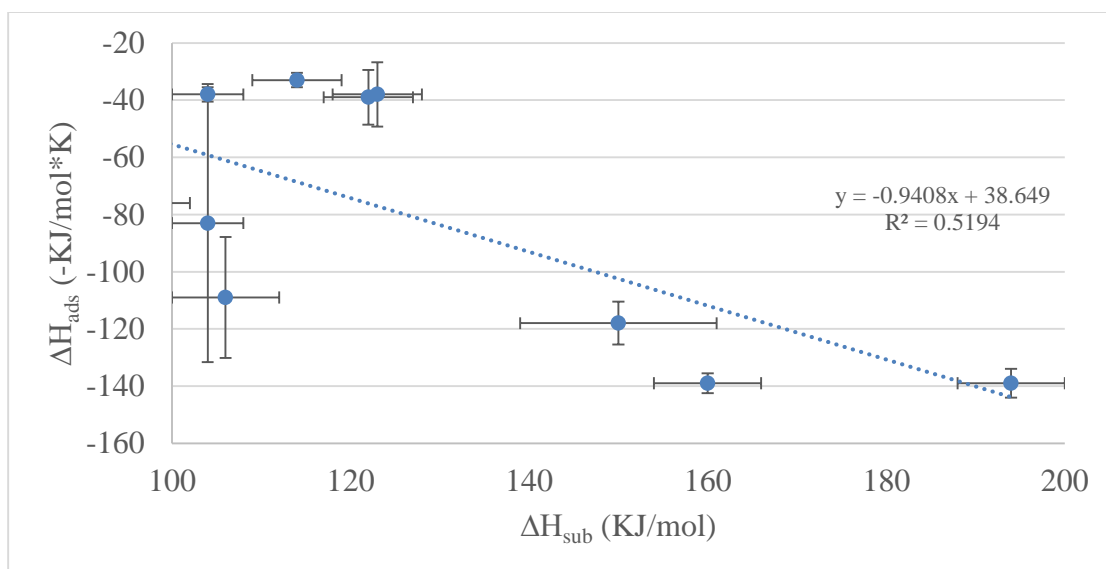


Figure 5.17. Using this data to formulate a new equation relating adsorption enthalpy and sublimation enthalpy, Equation 5.2, hereafter referred to as the Stratz-Shahbazi Relationship, is observed:

$$\Delta\bar{H}_{ads} = (-1.49)\Delta\bar{H}_{sub} + (128.04 \pm 30.5)$$

### Equation 5.2

This equation can be used to predict, on a first-tier basis, the relationship between the enthalpy of adsorption and enthalpy of sublimation of lanthanide hexafluoroacetylacetonates.



**Figure 5.17** Selected Adsorption Enthalpy vs. Sublimation Enthalpy

### 5.4 Monte Carlo Modeling using Adsorption Enthalpy Values

A Monte Carlo model, first written by John Garrison for lanthanide chloride thermochromatography and adapted to the present research by Shayan Shahbazi, uses the newly-

calculated adsorption enthalpy values obtained in this research to calculate retention time along a quartz column at a set of specified operating conditions. This model assumes a 26-meter uncoated quartz column with an inner diameter of 0.53 mm, argon carrier gas, and lanthanide hexafluoroacetylacetonate sample injections. All of the samples exhibited volatility within these conditions at a temperature of 130°C during deposition testing, and therefore, the model was tested at this temperature to discern retention times. Table 5.3 shows the results of the model at these conditions.

**Table 5.3** Simulated Monte Carlo Retention Times of Ln[hfac]<sub>4</sub> Complexes at 130°C

	<b>time_min (s)</b>	<b>time_avg (s)</b>	<b>time_max (s)</b>
<b>Pr</b>	1.80E+12	5.94E+12	1.96E+13
<b>Nd</b>	1.33E+12	5.92E+12	2.63E+13
<b>Sm</b>	583.78	41122.41	6467867.88
<b>Eu</b>	328.72	330.87	1168.99
<b>Gd</b>	328.76	328.81	329.07
<b>Tb</b>	328.86	3.26E+05	7.28E+11
<b>Dy</b>	1.03E+09	1.12E+10	1.21E+11
<b>Ho</b>	1.45E+06	7.61E+08	4.00E+11
<b>Er</b>	328.74	329.36	341.49
<b>Tm</b>	328.73	370.91	73412.69
<b>Yb</b>	328.76	328.82	328.97
<b>Lu</b>	328.73	329.19	341.47

**Table 5.4** Simulated Monte Carlo Retention Times of Ln[hfac]<sub>4</sub> Complexes at 193°C

	<b>time_min (s)</b>	<b>time_max (s)</b>
<b>Pr</b>	7.25E+09	5.71E+10
<b>Nd</b>	5.61E+09	7.38E+10
<b>Sm</b>	306.87	142717.27
<b>Eu</b>	284.89	346.77
<b>Gd</b>	284.90	284.96
<b>Tb</b>	284.92	3.31E+09
<b>Dy</b>	1.13E+07	7.04E+08
<b>Ho</b>	3.90E+04	1.97E+09
<b>Er</b>	284.90	286.54
<b>Tm</b>	284.89	3209.46
<b>Yb</b>	284.90	284.95
<b>Lu</b>	284.90	286.54

Though the retention times of these complexes vary significantly, even considering their relative proximity in adsorption enthalpy, molecular weight, and density, the indication that there is a possibility of little to no separation of the complexes appears to be in line with the general trend observed during isothermal chromatography experiments. During experimentation using samples of mixed Ln[hfac]<sub>4</sub> complexes, resulting peaks would either elute simultaneously or not at all. Much time was dedicated to understanding the reason for these complexes eluting simultaneously when their adsorption enthalpies were not predicted to significantly overlap. In fact, this repeated observance lead to the new temperature ramping method being implemented to overcome the simultaneous elutions. Until the thermodynamic properties were measured and implemented in the Monte Carlo simulation, the data was thought to be a product of a fault in instrumentation engineering or device coupling. However, observed trends indicating concurrent elutions of several complexes (and no elution whatsoever of other complexes during the same experimental period) seem to validate the retention separation trend (if not the magnitude of the retention time) seen in Monte Carlo simulations, as shown in Figure 5.18.

It is important to note that these experiments are conducted on-line and injections are executed throughout the duration of the timescan, not at time zero. Four of the complexes, Pr{hfac}<sub>4</sub>, Nd{hfac}<sub>4</sub>, Dy{hfac}<sub>4</sub>, and Ho{hfac}<sub>4</sub>, are not predicted to elute from the system at all in the Monte Carlo simulations, even when the model is implemented at their respective degradation temperatures (in other words, the highest temperature at which the individual complexes can be tested before degradation onset). This is in direct contradiction to the many experiments in which these complexes were detected along with the complexes that are predicted to elute. The hypothesis for these occurrences is that either the MC model is incorrect when it pertains to these

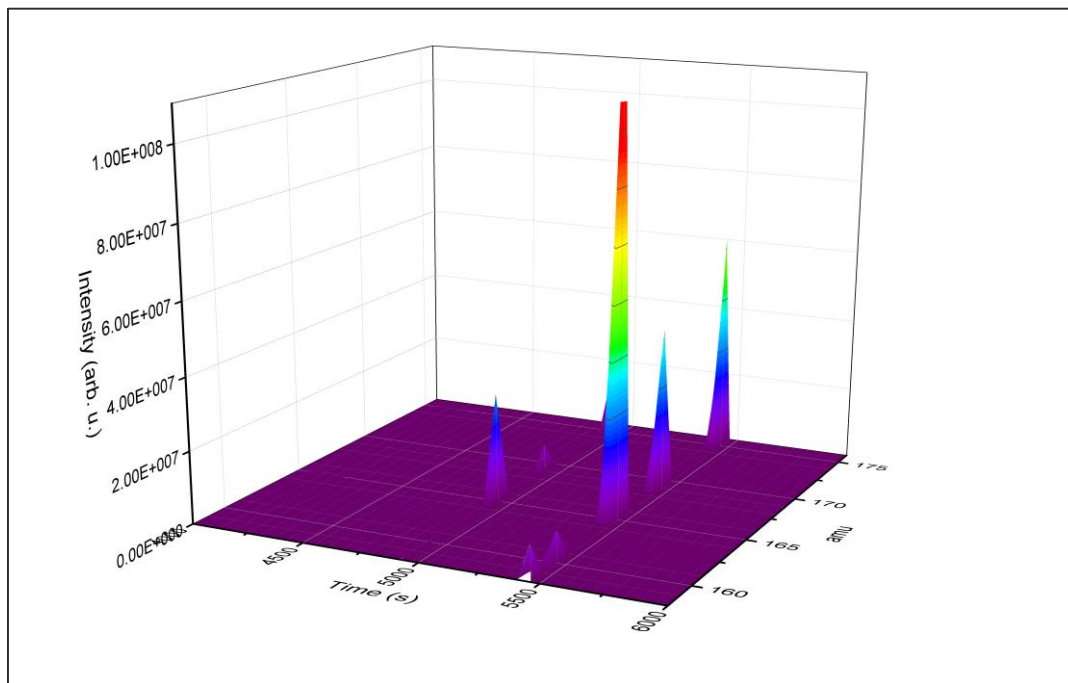


**Figure 5.18** Gd{hfac}<sub>4</sub>, Ho{hfac}<sub>4</sub>, Tm{hfac}<sub>4</sub>, Lu{hfac}<sub>4</sub> Injections

complexes, or that their detection is an artifact of “blowthrough”, or sample that is carried along the initial air pressure peak all the way to the plasma torch without any column interaction. This

would explain why complexes which are not predicted to arrive at the mass spectrometer within a timely manner are detected within a very short time period after injection. The relatively large peaks that elute could be due to the lack of sublimation of these complexes and subsequent air peak fronting in an unaltered powdered form. Though other thermodynamic, physical, or chemical processes may be governing this contradiction between experimental and theoretical results, the blowthrough theory appears to hold the most promise.

### **5.5 Thermodynamic Model**

A simple thermodynamic model predicated on superheavy element chromatography was developed to predict retention times of the  $\text{Ln}[\text{hfac}]_4$  complexes in an isothermal system based on measured adsorption enthalpy and entropy values. The model assumes a 26-meter uncoated 0.53 mm quartz column, both of which were used for the experimental setup described in Chapter 3. The column length was originally 30 meters, but several sections were broken off for analysis purposes before the data was collected. To compare this model directly to the Monte Carlo simulation results demonstrated in section 5.4, iterations of the model were executed at 130°C and 193°C (corresponding to the lowest temperature at which all complexes were volatile within the system and the highest temperature at which no complexes are expected to thermally degrade, respectively) and at the same carrier gas flow rate of 1.2 ml/min. Resulting retention times, both maximum and minimum, based on the standard deviation of the enthalpy and entropy of adsorption values, are tabulated in Tables 5.5 and 5.6.

**Table 5.5** Thermodynamic Model Retention Time of Ln[hfac]<sub>4</sub> Complexes at 130°C

	time_min (s)	time_max (s)
<b>Pr</b>	48.09	48.09
<b>Nd</b>	48.09	48.09
<b>Sm</b>	48.09	48.11
<b>Eu</b>	48.09	48.14
<b>Gd</b>	48.09	48.09
<b>Tb</b>	48.09	825436.76
<b>Dy</b>	48.09	48.09
<b>Ho</b>	48.09	48.15
<b>Er</b>	48.09	48.09
<b>Tm</b>	48.09	49.12
<b>Yb</b>	48.09	48.09
<b>Lu</b>	48.09	48.09

**Table 5.6** Thermodynamic Model Retention Time of Ln[hfac]<sub>4</sub> Complexes at 193°C

	time_min (s)	time_max (s)
<b>Pr</b>	41.59	41.59
<b>Nd</b>	41.59	41.59
<b>Sm</b>	41.59	41.59
<b>Eu</b>	41.59	41.59
<b>Gd</b>	41.59	41.59
<b>Tb</b>	41.59	3512.63
<b>Dy</b>	41.59	41.59
<b>Ho</b>	41.59	41.59
<b>Er</b>	41.59	41.59
<b>Tm</b>	41.59	41.63
<b>Yb</b>	41.59	41.59
<b>Lu</b>	41.59	41.59

These values are approximately an order of magnitude lower than the MC simulations and do not demonstrate the significant increase in retention time seen in Pr, Nd, Dy, and Ho as were observed in the MC simulations. Additionally, aside from Tb (undoubtedly due to its large experimental error), there is almost no difference in retention time between the complexes, which is in line with both the minimum retention time values from the MC simulations and the experimental data obtained during isothermal experiments. Figure 5.19 demonstrates the theoretical (both MC and thermodynamic models) versus experimental data for isothermal Gd[hfac]<sub>4</sub> injections at 150°C, 170°C, and 190°C at a 0.8 ml/min carrier gas flow rate, and it can be seen that the thermodynamic model is much closer to the experimental retention times than that of the MC model.

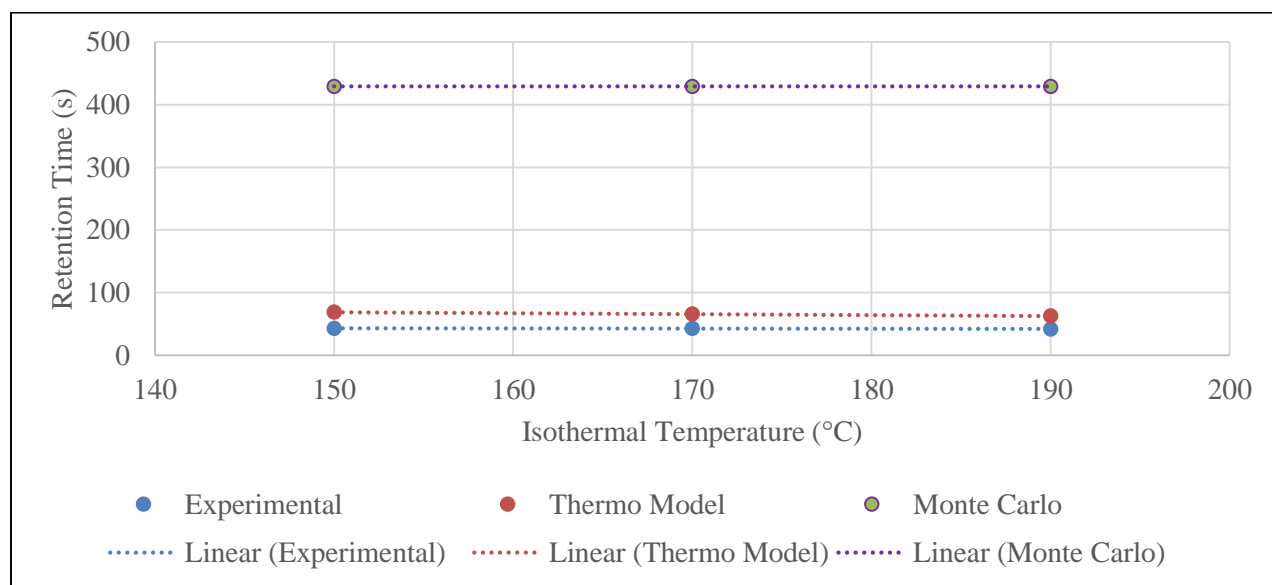


**Figure 5.19** Experimental vs. Theoretical Retention Times of Gd[hfac]<sub>4</sub> Samples

For the experimental setup outlined in this research, the thermodynamic model appears to much more closely resemble experimental data than the MC model output and is recommended for generating a first-order basis of expected retention times of the  $\text{Ln}[\text{hfac}]_4$  complexes.

*This section has been developed into a journal article and was submitted to the Journal of Radioanalytical and Nuclear Chemistry, where it will be published before this dissertation is publicly available.*



# CHAPTER 6

## CONCLUSION

### 6.1 Conclusion

The enthalpy and entropy of adsorption of twelve lanthanide hexafluoroacetylacetone chelates have been experimentally measured for the first time. Initial tests conducted with thermochromatographic methods showed promise for rapid gas-phase separations using these complexes.<sup>13</sup> Subsequently, several years were devoted to an isothermal approach to measure the thermodynamic properties of these compounds using a coupled gas chromatography inductively-coupled plasma time-of-flight mass spectrometer. Numerous issues with the connection between these two instruments, in addition to interference and disruptions caused by the introduction of such harsh complexes into a plasma torch designed for gentler substances, indicated that a different approach would be required to measure the thermodynamic properties of these complexes in a timely manner. Following that conclusion, a variant of thermochromatography was used to successfully measure (albeit with larger experimental error) the entropy and enthalpy of adsorption of twelve  $\text{Ln}(\text{hfac})_3$  complexes on a quartz column. These values were calculated using equations derived for a temperature ramping method of chromatography, and thus, a simulated temperature ramping procedure was adapted in order to use these equations for the samples under interrogation. The resulting thermodynamic properties are generally in line with sublimation enthalpy values calculated with thermogravimetric analysis, and a new relationship relating these two properties has been derived as a part of this work. Additionally, the newly-measured thermodynamic properties were implemented in both Monte Carlo and theoretical thermodynamic models to optimize conditions for a large-scale gas-phase separation procedure

separating the complexes with enhanced speed and resolution. However, as discussed in the previous chapter, the hypothesis of viable separations between these complexes under isothermal operating conditions was proven infeasible in both the theoretical model simulations and in the experimental isothermal data. In conclusion:

- 1) Twenty-four new thermodynamic properties have been measured to more completely characterize lanthanide hexafluoroacetylacetonates;
- 2) A new equation relating the enthalpy of adsorption to the enthalpy of sublimation of  $\text{Ln}[\text{hfac}]_4$  complexes has been derived;
- 3) Heavy fission products cannot be used in conjunction with hexafluoroacetylacetonate for gas-phase separations under isothermal conditions;
- 4) Thermochromatographic operations hold promise for gas-phase separations of lanthanide hexafluoroacetylacetonates; and
- 5) Further investigation into gas-phase separations of lanthanide chlorides and oxides is highly recommended to advance post-detonation nuclear forensic science.

## **6.2 Areas of Continuation**

A realistic sample of post-detonation nuclear melt glass contains a huge number of fission and activation products that must be identified and quantified for accurate attribution.<sup>8</sup> This work has only employed and measured the thermodynamics of thirteen fission products (La, Pr, Nd, Gd, Tm, Dy, Sm, Eu, Tb, Ho, Er, Yb, and Lu), and it is therefore necessary to measure the remaining fission products for a complete analytic capability. Additionally, many other ligands such as hfod

and hdpm, both of which we have attached to lanthanide metals in our lab, are available for metal volatilization and should be explored to identify the optimal ligand for this operation. In order for this work to be complete, the entropy and entropy of adsorption for all fission products and weapon fuels should be measured for a complete optimization of a large-matrix gas-phase separation.

This work employs gas-phase chemistry to separate heavy fission products for the sole purpose of increasing the speed and accuracy of post-detonation nuclear forensic analysis. The synthesis process to volatilize the complexes is timely (on the order of several hours) and is an undesirable component of this process. To address this issue, future work will aim to remove the volatilization process and separate pure chlorides and oxides in the gas phase. This work will be modeled after work performed in Dubna, Russia primarily used for the synthesis and detection of superheavy elements.<sup>37</sup>

Preliminary components of the new chloride/oxide separation systems are currently in development, as shown in figures 6.1 – 6.5.

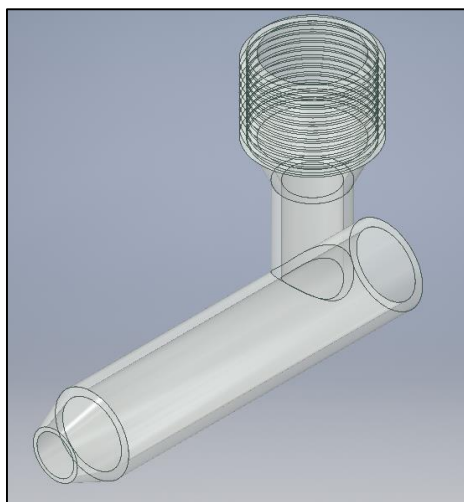


**Figure 6.1** Injection Port Rendering

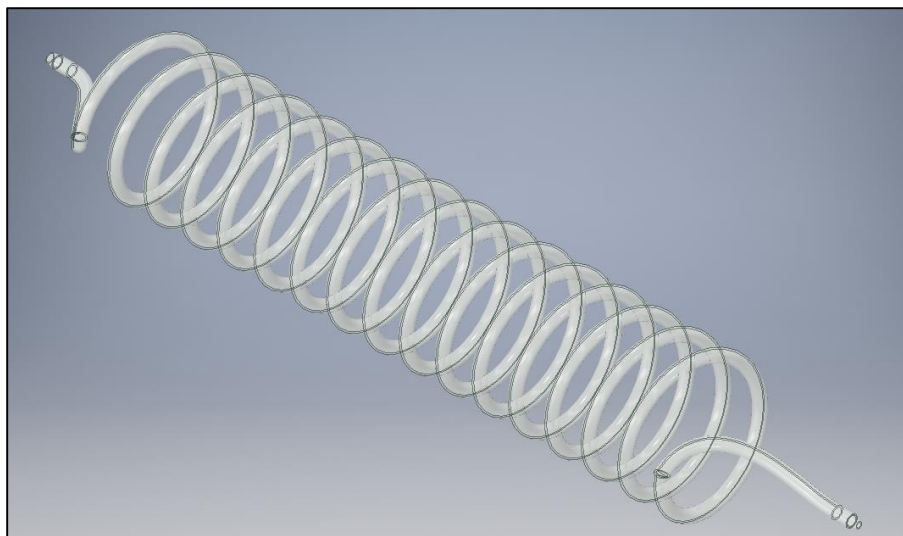


**Figure 6.2** Quartz Separations Column Rendering

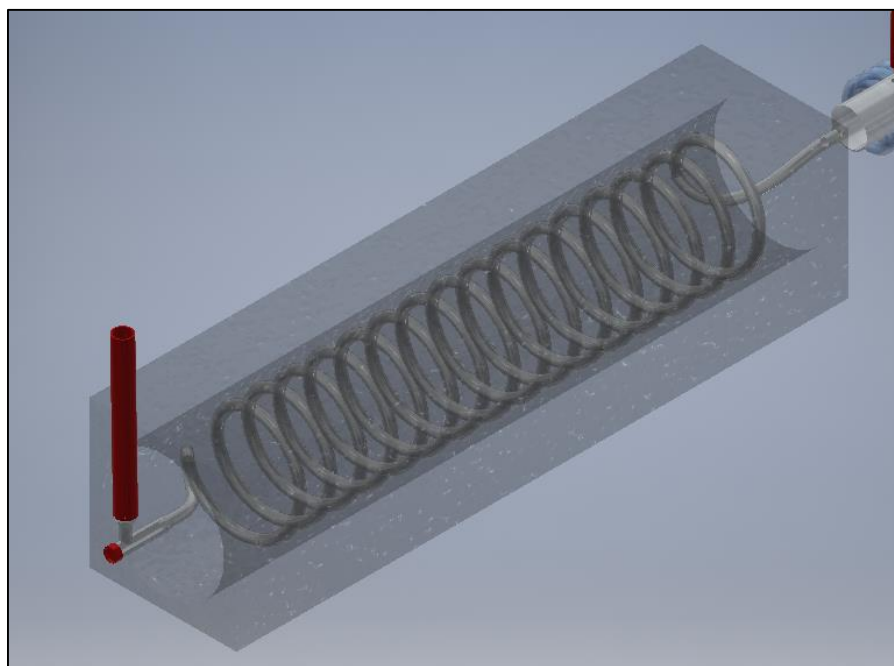


**Figure 6.3** Tube Furnace Assembly Rendering

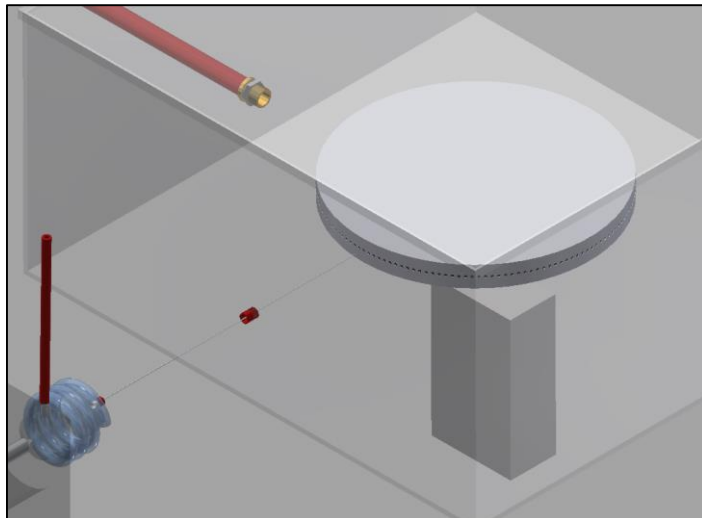


**Figure 6.4** Vacuum Chamber Rendering

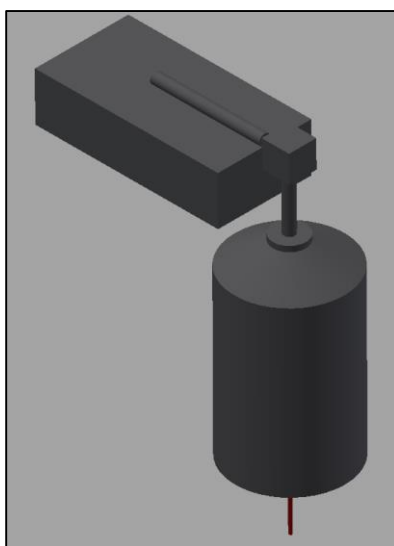


**Figure 6.5** KCl Injector Rendering

Most of these components will have to withstand temperatures exceeding 1500°C in order to volatilize the oxide complexes injected into the system. Material selection will play a large role in the considerable difficulty associated with separating oxides using isothermal

chromatography, and will likely involve high-temperature metal and quartz components. Though many obstacles will necessarily need to be addressed during the design process, a successful instrument will remove the timely ligand synthesis component of the current organometallic complexes. This reduction in destructive analysis time will greatly speed the technical forensics analysis component of the attribution cycle.

### **6.3 Legal Disclaimers and Acknowledgements**

This work was performed under grant number DE-NA0001983 from the Stewardship Science Academic Alliances (SSAA) Program of the National Nuclear Security Administration (NNSA). The views expressed are those of the authors and do not necessarily reflect those of the DOE or NNSA.

This material is also based upon work supported by the U.S. Department of Homeland Security under Grant Award Number, 2012-DN-130-NF0001. The views and conclusions contained in this document are those of the authors and should not be interpreted as representing the official policies, either expressed or implied, of the U.S. Department of Homeland Security.

## **REFERENCES**

- (1) Molgaaard, J. J.; Auxier, J. D.; Hall, H. L. Novel Synthetic Nuclear Melt Glass and Methods Thereof. 62/002,202, 2014.
- (2) Congress. *Nuclear Forensics and Attributions Act*; Congress, 2010.
- (3) Gowadia, H. A.; Mardigras, B. S. *Int. J. Nucl. Secur.* **2015**, *1* (1), 1–8.
- (4) Molgaard, J. J.; Auxier, J. D.; Giminaro, A. V.; Oldham, C. J.; Cook, M. T.; Young, S. A.; Hall, H. L. *J. Radioanal. Nucl. Chem.* **2015**, *304* (3), 1293–1301.
- (5) Giminaro, A. V.; Stratz, S. A.; Gill, J. A.; Auxier, J. P.; Oldham, C. J.; Cook, M. T.; Auxier, J. D.; Molgaard, J. J.; Hall, H. L. *J. Radioanal. Nucl. Chem.* **2015**.
- (6) Allison, G. *Nuclear Terrorism: The Ultimate Preventable Catastrophe*; Macmillan, 2004.
- (7) Ferguson, C. D.; Potter, W. C.; Sands, A.; Spector, L. S.; Wehling, F. L. *The Four Faces of Nuclear Terrorism*; 2004.
- (8) Moody, K. J.; Grant, P. M.; Hutcheon, I. D. *Nuclear Forensic Analysis*, 2nd Editio.; Taylor & Francis Group, LLC, 2015.
- (9) Auxier II, J. D.; Hanson, D. E.; Marsh, M. L.; Hall, H. L. Thermochromatographic Separations of Fission and Activation Products. 62/028,199, 2014.
- (10) Tse, B. P. *United States Geol. Surv.* **2011**, *Ope-File R*.
- (11) Chunhua, Y. A. N.; Jiangtao, J. I. A.; Chunsheng, L. *Tsinghua Sci. Technol.* **2006**, *11* (2).
- (12) Garrison, J. R.; Hanson, D. E.; Hall, H. L. *J. Radioanal. Nucl. Chem.* **2011**, *291* (3), 885–894.
- (13) Hanson, D. E.; Garrison, J. R.; Hall, H. L. *J. Radioanal. Nucl. Chem.* **2011**.



- (14) Stratz, S. A.; Gill, J. A.; Auxier II, J. D.; Hall, H. L. *Int. J. Nucl. Secur.* **2016**.
- (15) Auxier, J. D.; Stratz, S. A.; Hanson, D. E.; Marsh, M. L.; Jordan, J. A.; Cressy, D.; Jenkins, D. M.; Hall, H. L. **2015**.
- (16) Marin, R. C.; Sarkis, J. E. S.; Pestana, R. C. B. 2013.
- (17) Smith, D. K.; Kristo, M. J.; Niemeyer, S.; Dudder, G. B. *J. Radioanal. Nucl. Chem.* **2008**, 276 (2), 415–419.
- (18) Chiao, L. Discussions on Space, Exploration and Life  
<http://leroychiao.blogspot.com/2010/05/trinity-test-site.html>.
- (19) Carney, K. P.; Finck, M. R.; McGrath, C. a.; Martin, L. R.; Lewis, R. R. *J. Radioanal. Nucl. Chem.* **2013**, 299 (1), 363–372.
- (20) Carney, K.; Finck, M.; McGrath, C.; Brush, B.; Jansen, D.; Dry, D.; Brooks, G.; Chamberlain, D. *J. Radioanal. Nucl. Chem.* **2012**, 296 (2), 769–773.
- (21) Cook, M. T.; Auxier, J. D.; Giminaro, A. V.; Molgaard, J. J.; Knowles, J. R.; Hall, H. L. *J. Radioanal. Nucl. Chem.* **2015**.
- (22) Mills, J. 70 Years in the Nuclear Age <https://history.denverlibrary.org/news/70-years-nuclear-age>.
- (23) Molgaard, J. J. Production of Nuclear Debris Surrogates for Forensic Methods Development, University of Tennessee, 2014.
- (24) Montgomery, J.; Jeffery, R. Asymmetrical Fission Products  
<http://www.unclear2nuclear.com/asymFission.php>.
- (25) Binnemans, K. **2005**, 35 (05), 107–272.

- (26) Lanthanides <http://chemistry.tutorcircle.com/inorganic-chemistry/lanthanides.html>.
- (27) Tompkins, E. R.; Mayer, S. W. *J. Am. Chem. Soc.* **1947**.
- (28) Street, K.; Seaborg, G. *J. Am. Chem. Soc.* **1949**, 72 (19), 2790–2792.
- (29) Pin, C.; Francisco, J.; Zaldueguilb, S. *Anal. Chim. Acta* **1997**.
- (30) Resin in Pulp (RIP) Technology [http://www.ion-exchange.com.au/ix\\_technology.html](http://www.ion-exchange.com.au/ix_technology.html).
- (31) Ion Exchange Resin [http://www.mlball.com/Ion\\_Exchange\\_Resin.htm](http://www.mlball.com/Ion_Exchange_Resin.htm).
- (32) Baltus, R. E.; Counce, R. M.; Culbertson, B. H.; Luo, H.; DePaoli, D. W.; Dai, S.; Duckworth, D. C. *Sep. Sci. Technol.* **2005**, 40 (1-3), 525–541.
- (33) Pressure Swing Adsorption: A Ubiquitous Gas Separation Technology  
<http://www.aiche.org/academy/webinars/pressure-swing-adsorption-ubiquitous-gas-separation-technology>.
- (34) Eichler, R.; Brüchle, W.; Buda, R.; Bürger, S.; Dressler, R.; Düllmann, C. E.; Dvorak, J.; Eberhardt, K.; Eichler, B.; Folden, C. M.; Gäggeler, H. W.; Gregorich, K. E.; Haenssler, F.; Hoffman, D. C.; Hummrich, H.; Jäger, E.; Kratz, J. V.; Kuczewski, B.; Liebe, D.; Nayak, D.; Nitsche, H.; Piguet, D.; Qin, Z.; Rieth, U.; Schädel, M.; Schausten, B.; Schimpf, E.; Semchenkov, a.; Soverna, S.; Sudowe, R.; Trautmann, N.; Thörle, P.; Türlér, a.; Wierczinski, B.; Wiehl, N.; Wilk, P. a.; Wirth, G.; Yakushev, a. B.; von Zweidorf, a. *Radiochim. Acta* **2006**, 94 (4/2006), 181–191.
- (35) Eichler, R.; Soverna, S. *Phys. At. Nucl.* **2003**, 66 (6), 1146–1151.
- (36) Schädel, M.; Shaughnessy, D. A. *The Chemistry of Superheavy Elements*; 2013.
- (37) Zvara, I. *The Inorganic Radiochemistry of Heavy Elements*; Springer, 2008.

- (38) Even, J.; Yakushev, A.; Düllmann, C. E.; Haba, H.; Asai, M.; Sato, T. K.; Brand, H.; Di Nitto, A.; Eichler, R.; Fan, F. L.; Hartmann, W.; Huang, M.; Jager, E.; Kaji, D.; Kanaya, Y.; Khuyagbaatar, J.; Kindler, B.; Kratz, J. V.; Krier, J.; Kudou, Y.; Kurz, N.; Lommel, B.; Miyashita, S.; Morimoto, K.; Morita, K.; Murakami, M.; Nagame, Y.; Nitsche, H.; Ooe, K.; Qin, Z.; Schadel, M.; Steiner, J.; Sumita, T.; Takeyama, M.; Tanaka, K.; Toyoshima, A.; Tsukada, K.; Turler, A.; Usoltsev, I.; Wkabayashi, Y.; Wang, Y.; Wiehl, N.; Yamaki, S. *Science* (80-. ). **2014**, *345* (6203), 1491–1494.
- (39) Discovery of Elements 113 and 115 <https://plslnl.gov/research-and-development/nuclear-science/project-highlights/livermorium/elements-113-and-115>.
- (40) Yakushev, A.; Gates, J. M.; Türler, A.; Schädel, M.; Düllmann, C. E.; Ackermann, D.; Andersson, L.-L.; Block, M.; Bruchle, W.; Dvorak, J.; Eberhardt, K.; Essel, H. G.; Even, J.; Forsberg, U.; Gorshkov, A.; Graeger, R.; Gregorich, K. E.; Hartmann, W.; Herzberg, R.-D.; Hessberger, F. P.; Hild, D.; Hübner, A.; Jäger, E.; Khuyagbaatar, J.; Kindler, B.; Kratz, J. V.; Krier, J.; Kurz, N.; Lommel, B.; Niewisch, L. J.; Nitsche, H.; Omtvedt, J. P.; Parr, E.; Qin, Z.; Rudolph, D.; Runke, J.; Schausten, B.; Schimpf, E.; Semchenkov, A.; Steiner, J.; Thörle-Pospiech, P.; Uusitalo, J.; Wegrzecki, M.; Wiehl, N. *Inorg. Chem.* **2014**, *53* (3), 1624–1629.
- (41) Miller, J. M. *Chromatography: concepts and contrasts*; John Wiley & Sons Ltd, 2005.
- (42) Schadel, M.; Bruchle, W.; Dressler, R.; Eichler, B.; Gaggeler, H. W.; Gunther, R.; Gregorich, K. E.; Hoffman, D. C.; Hubener, S.; Jost, D. T.; Kratz, J. V.; Paulus, W.; Schumann, D.; Timokhin, S.; Trautmann, N.; Turler, A.; Wirth, G.; Yakushev, A. *Lett. to Nat.* **1997**, *58* (May), 220–222.

- (43) Swain Jr., H. A.; Karraker, D. G. *Inorg. Chem.* **1970**, 9 (7), 1766–1769.
- (44) Greulich, N.; Hickmann, U.; Trautmann, N.; Herrmann, G. *Fresenius' Zeitschrift für Anal. Chemie* **1986**, 323 (8), 839–845.
- (45) Nikitenko, S. I.; Moisy, P.; Tcharushnikova, I. A.; Blanc, P.; Madic, C. *Ultrason. Sonochem.* **2000**, 7, 177–182.
- (46) Fedoseev, E. V.; Aizenberg, M. I.; Timokhin, S. N.; Travnikov, S. S.; Zvara, I.; Davydov, a. V.; Myasedov, B. F. *J. Radioanal. Nucl. Chem. Artic.* **1990**, 142 (2), 459–465.
- (47) Leggitt, J.; Inn, K.; Goldberg, S.; Essex, R.; LaMont, S.; Chase, S. *J. Radioanal. Nucl. Chem.* **2009**, 282 (3), 997–1001.
- (48) *Daubert et ux., individually and as guardians ad litem for Daubert, et al. v. Merrell Dow Pharmaceuticals , Inc.*; 1993; pp 585–589.
- (49) *Federal Rules of Evidence*; 2014.
- (50) Merwin, S. E.; Moeller, D. W.; William E. Kennedy, J.; Moeller, M. P. *Heal. Phys. J.* **2001**, 81 (6), 670–677.
- (51) Masten, J.; Strzelczyk, J. *Heal. Phys. J.* **2001**, 81 (6), 678–682.
- (52) Hileman, B. *Chemical and Engineering News*. 2003.
- (53) Johnson, A. A.; Storey, R. J. 2015.
- (54) IAEA. 2002; pp 21–23.
- (55) Eichler, B.; Zvara, I. *Radiochim. Acta* **1982**, 30, 233–238.
- (56) Rudolph, J.; Bachmann, K. *J. Chromatogr.* **1979**, 178, 459–469.

- (57) Steffen, A.; Bachmann, K. *Thermochromatographic Investig.* **1978**, 25, 677–683.
- (58) ICP-TOF Explore <http://www.gbcsscientific.com/icptofexplore.html>.
- (59) Chuburkov, Y. T.; Seb, H. H.; Alpert, L. K. *Radiochemistry* **1995**.
- (60) Shahbazi, S.; Stratz, S. A.; Auxier, J. D.; Hanson, D. E.; Marsh, M. L.; Hall, H. L. *J. Radioanal. Nucl. Chem.* **2016**.
- (61) Auxier II, J. D.; Jordan, J. A.; Stratz, S. A.; Shahbazi, S.; Hanson, D. E.; Cressy, D.; Hall, H. L. *J. Radioanal. Nucl. Chem.* **2015**.

## **APPENDICES**

# **APPENDIX A**

## **CHARACTERIZATION OF NH<sub>4</sub>[LN(HFAC)<sub>4</sub>] COMPLEXES**

**(EXCERPT FROM CO-AUTHORED PUBLICATION<sup>15</sup>)**

### **A.1 Characterization of Sm[hfac]<sub>4</sub> (1), Gd[hfac]<sub>4</sub> (2), Dy[hfac]<sub>4</sub> (3), and Tm[hfac]<sub>4</sub> (4)**

The following characterization information was taken from a publication co-authored by J.D. Auxier, S.A. Stratz, D.E. Hanson, M.L. Marsh, J.A. Jordan, D. Cressy, D.M. Jenkins, and H.L. Hall with the intention of being published in the Journal of the American Chemical Society in 2016.

Determination of crystal structure was only achieved for Gd[hfac]<sub>3</sub>. Following data collection, reflections were sampled from all regions of the Ewald sphere to re-determine unit cell parameters for data integration. Following exhaustive review of collected frames the resolution of the dataset was judged, and, if necessary, regions of the frames where no coherent scattering was observed were removed from consideration for data integration using the Bruker SAINTplus program. Data was integrated using a narrow frame algorithm and was subsequently corrected for absorption. Absorption corrections were performed for both samples using the SADABS program. Space group determination and tests for merohedral twinning were carried out using XPREP. The highest possible space group was chosen.

The final model was refined anisotropically (with the exception of H atoms). Hydrogen atoms were not placed on solvent molecules due to disorder. The structure was examined using

The ORTEP diagram shows the molecular structure of 2,2,2-trifluoroethyl 2,2,2-trifluoroethyl phosphonate. The central phosphorus atom (P) is bonded to two ethyl groups (CH<sub>2</sub>CH<sub>3</sub>) and two trifluoromethyl groups (CF<sub>3</sub>). The ethyl groups are represented by black and white spheres, while the trifluoromethyl groups are represented by green spheres. The phosphorus atom is shown as a blue sphere. The structure is displayed with thermal ellipsoids at the 50% probability level, and the hydrogen atoms are shown as small spheres of arbitrary radii.

## 37. N 4.06, F N/A. For 2.1



### A.3 FTIR

For **1**. (ATR cm<sup>-1</sup>): 3184 (br), 1644 (w), 1563 (w), 1538 (w), 1440 (m), 1252 (m), 1194 (m), 1179 (m), 1130 (br, s), 805 (w), 744 (m). For **2**. (ATR cm<sup>-1</sup>): 3127 (br), 3040 (br), 1645 (s), 1611 (w), 1563 (w), 1537 (m), 1502 (w), 1472 (w), 1405 (m), 1349 (w), 1253 (s), 1201 (s), 1136 (s), 1096 (s), 804 (s), 768 (w), 744 (s), 752 (w), 661 (s). For **3**. (ATR cm<sup>-1</sup>) 3211 (br), 1645 (w), 1564 (w), 1535 (w), 1459 (m), 1253 (m), 1196 (s), 1177 (s), 1123 (s), 800 (m), 738 (m). For **4**. (ATR cm<sup>-1</sup>) 3149 (br), 1649 (w), 1564 (w), 1537 (w), 1473 (m), 1251 (m), 1203 (s), 1177 (s), 1132 (s), 804 (m), 744 (m).

### A.4 NMR

For **1**: <sup>1</sup>H NMR (500 MHz, 1,4-Dioxane-d<sub>8</sub>)  $\delta$  7.26 (s, 1H), 5.34 (s, 1H), 2.64 (s, 2H). <sup>19</sup>F NMR (470 MHz, dioxane)  $\delta$  -76.50, -76.98, -77.41. For **2**: <sup>1</sup>H NMR (500 MHz, dioxane)  $\delta$  6.91, 2.37. <sup>19</sup>F NMR (470 MHz, dioxane)  $\delta$  -78.02, -79.70, -80.93. For **3**: <sup>1</sup>H NMR (500 MHz, dioxane)  $\delta$  1.03, 0.97. <sup>19</sup>F NMR (470 MHz, dioxane)  $\delta$  -71.83, -75.13, -76.22, -77.42, -78.24. For **4**: <sup>1</sup>H NMR (500 MHz, 1,4-Dioxane-d<sub>8</sub>)  $\delta$  4.72 (s, 1H). <sup>19</sup>F NMR (470 MHz, dioxane)  $\delta$  -77.49, -108.66, -109.94.

### A.5 Melting Points

Table A.1 gives the mean melting points of the NH<sub>4</sub>[Ln(hfac)<sub>4</sub>] samples, taken with four measurements per sample and averaged, as shown in Figure A.2.



**Figure A.2** Melting Point Measurements of  $\text{Pr}(\text{hfac})_4$

Melting point analyses were performed using a Mettler Toledo MP50 melting point system and four samples of each compound were measured simultaneously.

### **A.5 TGA**

Thermogravimetric analysis (TGA) and differential thermogravimetric analysis (DTA) were used to analyze decomposition methods for the complexes. DTA was generated via numerical differentiation of existing TGA data and was used to calculate the value for  $T_s$ . Kinetic parameters can be calculated from published equations and yield the activation energy,  $E^*$ , A or Z (functionally similar pre-exponential factors), reaction order, n, and entropy, enthalpy, and

Gibbs free energy of sublimation. The temperature ranges were chosen to capture the curvature of the TGA curves. Resulting parameters are shown in Table A.2.

**Table A.1** Melting Points of  $\text{NH}_4[\text{Ln}(\text{hfac})_4]$  Complexes

Hfac Complex	Mean Melting Point ( C )
Lanthanum (La)	143.0625
Praseodymium (Pr)	181.5
Neodymium (Nd)	172.6
Samarium (Sm)	192.95
Europium (Eu)	180.75
Gadolinium (Gd)	182.375
Terbium (Tb)	198.75
Dysprosium (Dy)	207.75
Holmium (Ho)	221.5
Erbium (Er)	223
Thulium (Tm )	207.81
Ytterbium (Yb)	217.075
Lutetium (Lu)	219
Ammonium ( $\text{NH}_4$ )	88.69

**Table A.2** Kinetic Thermodynamic Parameters of Complexes 1 – 4 using Coats-Redfern, Horowitz-Metzger, and Freeman Carroll

Compound	Method	T <sub>s</sub> (K)	Range (K)	E* (kJ/mol)	A or Z (1/s)	ΔS (kJ/mol*K)	ΔH (kJ/mol)	ΔG (kJ/mol)
Sm(hfac)	CR	464.97	450-469	55.0	12118	-0.170	51.2	130.4
	HM			64.3	99127	-0.153	60.4	131.5
	FC			214.3	1.67E+22	0.177	210.4	128.2
Dy(hfac)	CR	504.01	455.8- 498.5	69.7	1.12E+05	-0.153	65.5	142.4
	HM			87.0	7.10E+06	-0.118	82.8	142.3
	FC			139.6	5.30E+12	-0.006	135.4	138.3
Tm(hfac)	CR	522.34	475-522	70.7	82533	-0.155	66.3	147.5
	HM			87.3	3.44E+06	-0.124	82.9	148.0
	FC			163.9	5.12E+14	0.032	159.6	142.9
Gd(hfac)	CR	488	456-496	37.0	44.76	-0.217	32.9	139.0
	HM			48.3	600.4	-0.196	44.2	139.8
	FC			194.6	1.43E+19	0.118	190.6	133.1

## APPENDIX B

### ICP-MS SAMPLE INTEGRITY OF Ln[hfac]<sub>x</sub> COMPLEXES

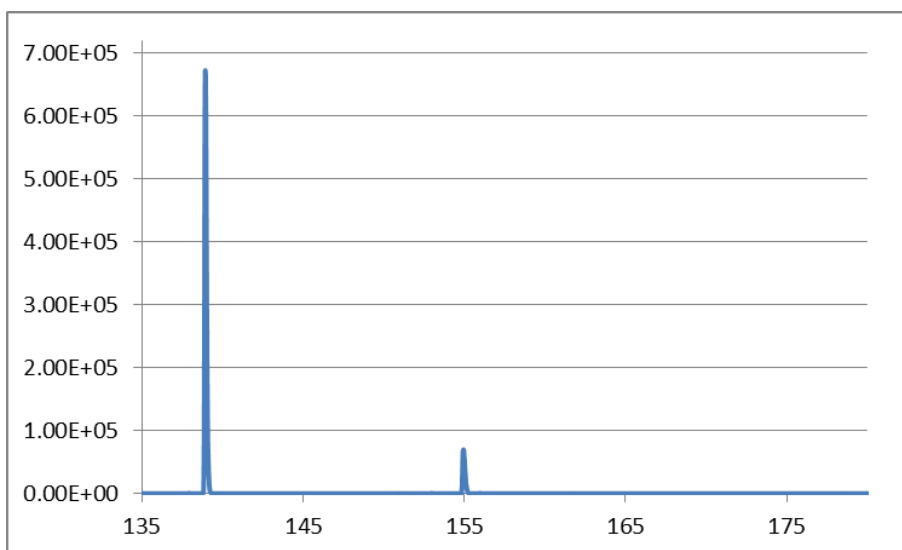


**Figure B.1** La[hfac]<sub>4</sub> Mass Spectrum

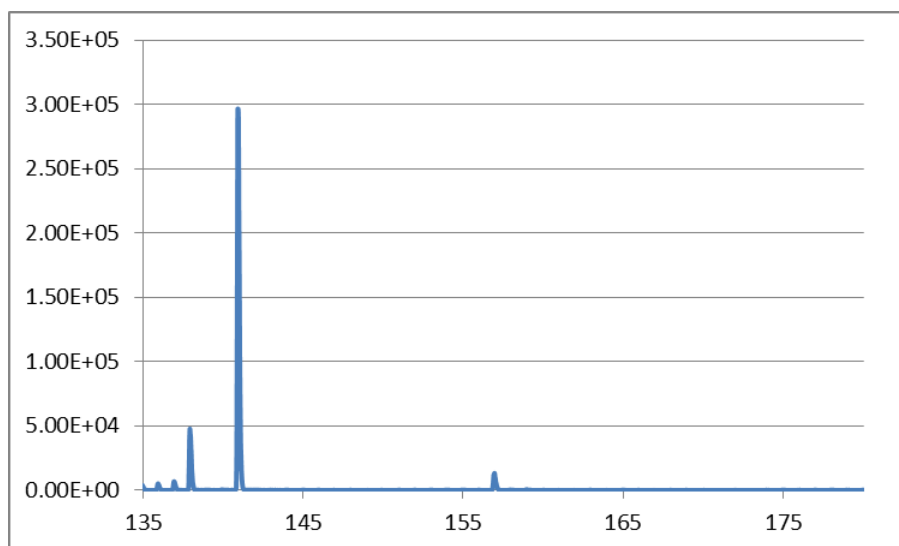


**Figure B.2** Pr[hfac]<sub>4</sub> Mass Spectrum

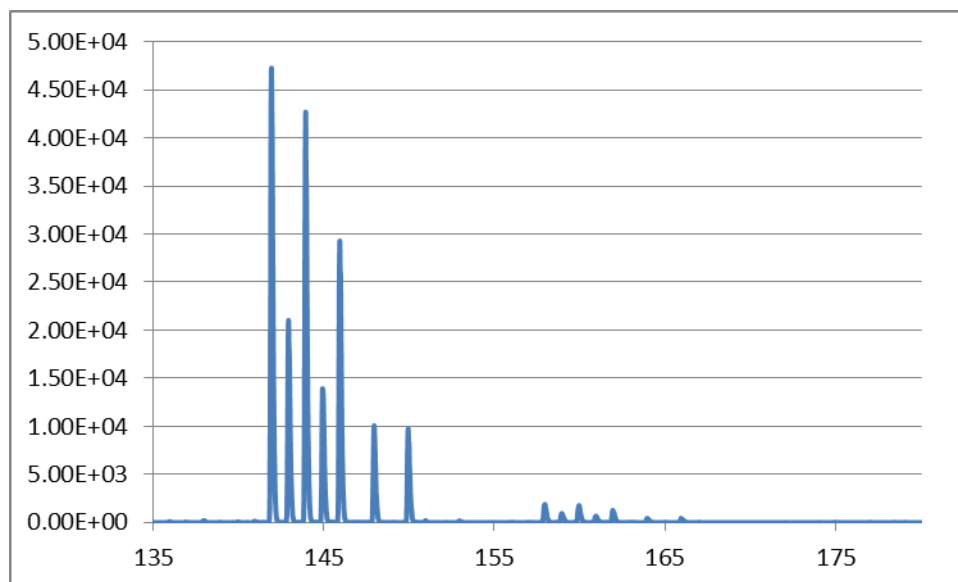


**Figure B.3** Nd[hfac]<sub>4</sub> Mass Spectrum

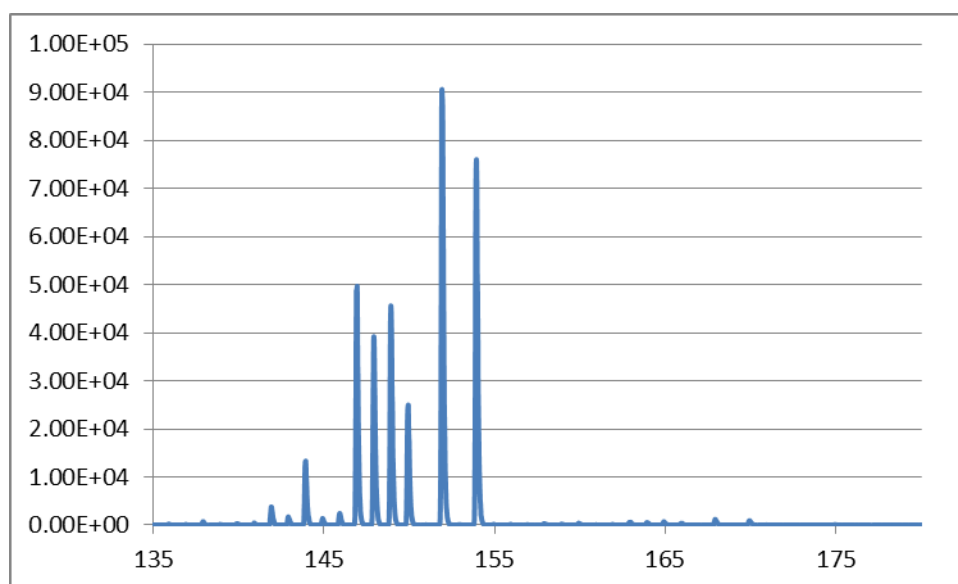


**Figure B.4** Sm[hfac]<sub>4</sub> Mass Spectrum

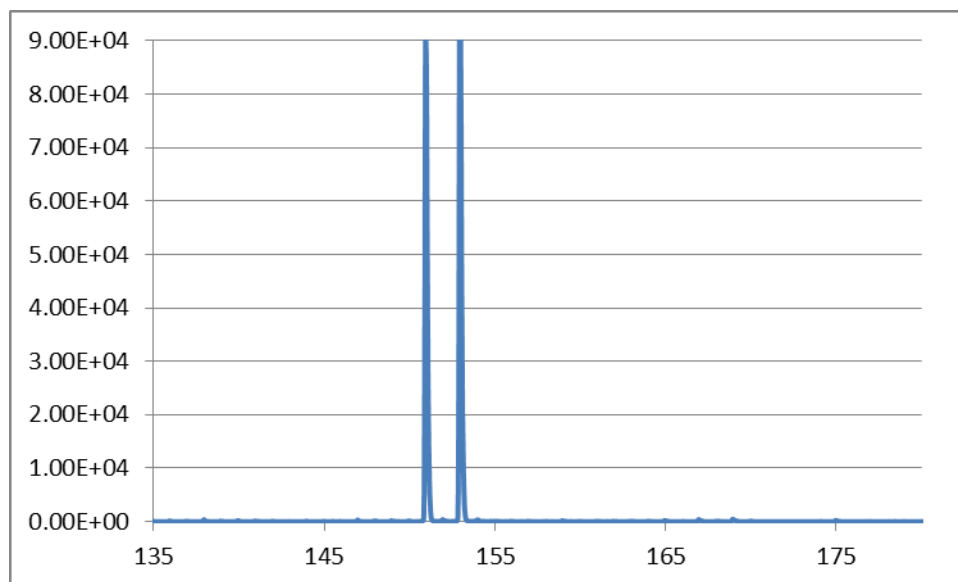


**Figure B.5** Eu[hfac]<sub>4</sub> Mass Spectrum

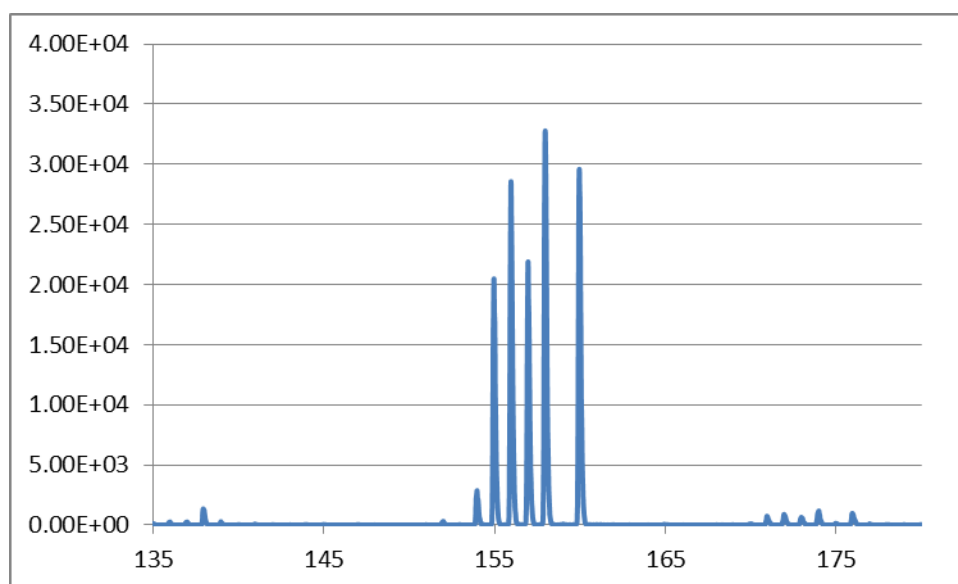


**Figure B.6** Gd[hfac]<sub>4</sub> Mass Spectrum

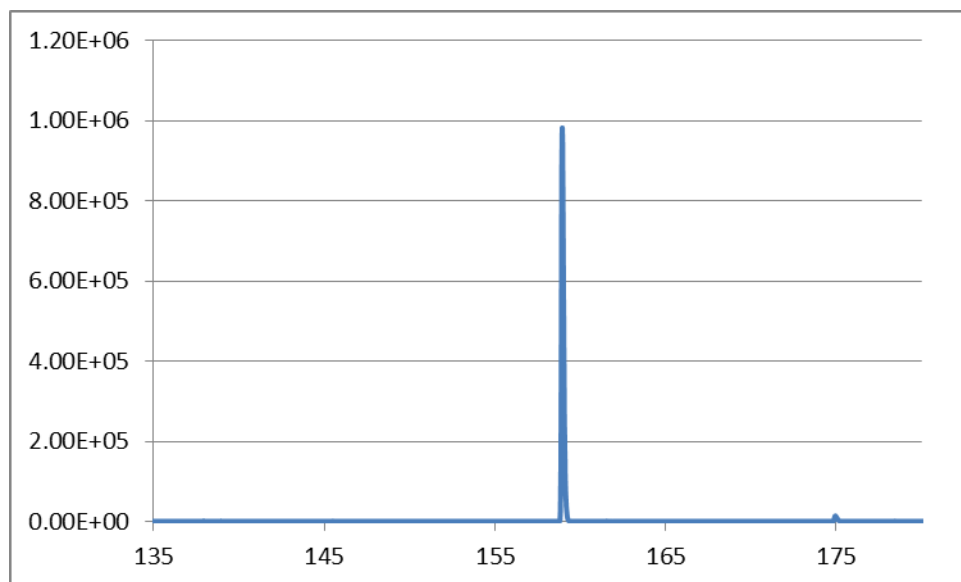


**Figure B.7** Tb[hfac]<sub>4</sub> Mass Spectrum

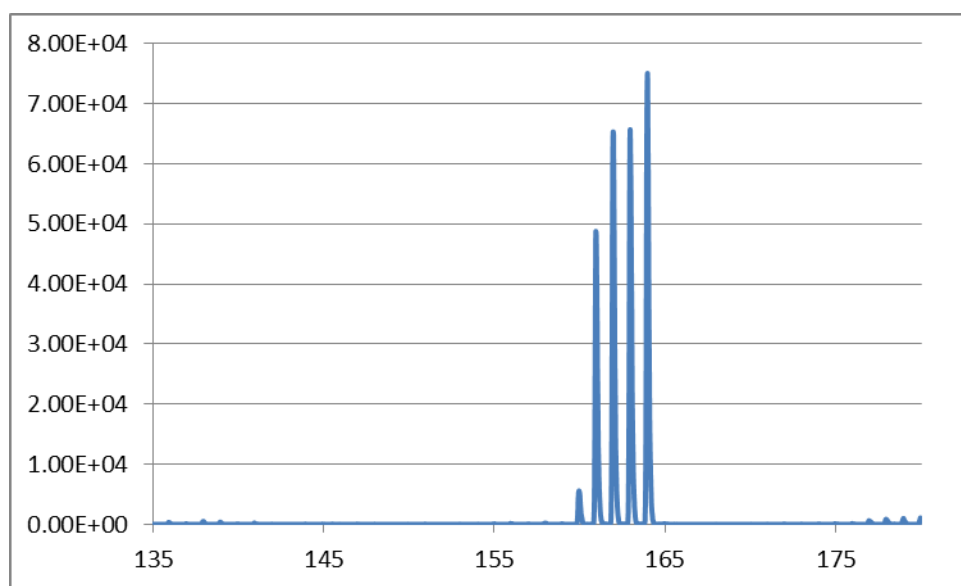


**Figure B.8** Dy[hfac]<sub>4</sub> Mass Spectrum



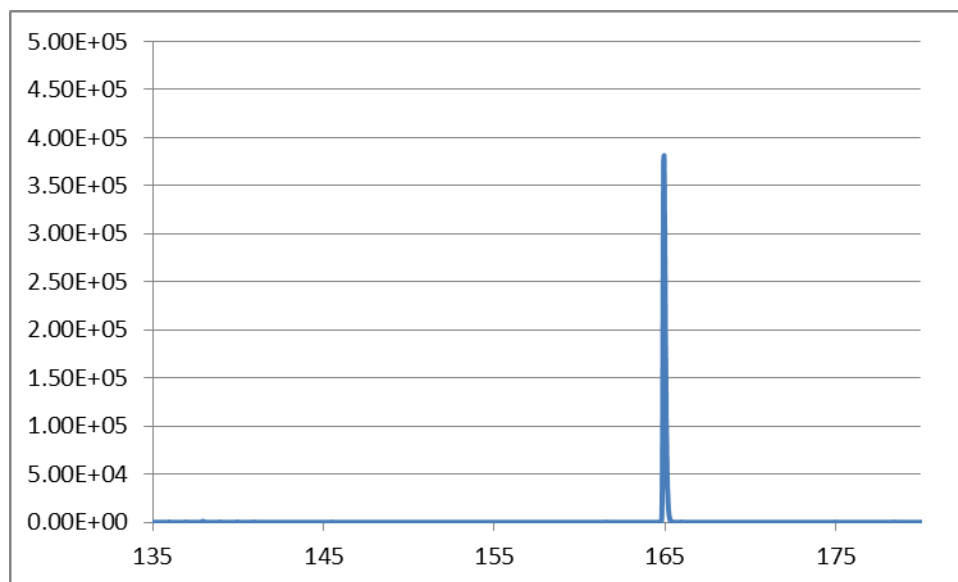


**Figure B.9** Ho[hfac]<sub>4</sub> Mass Spectrum

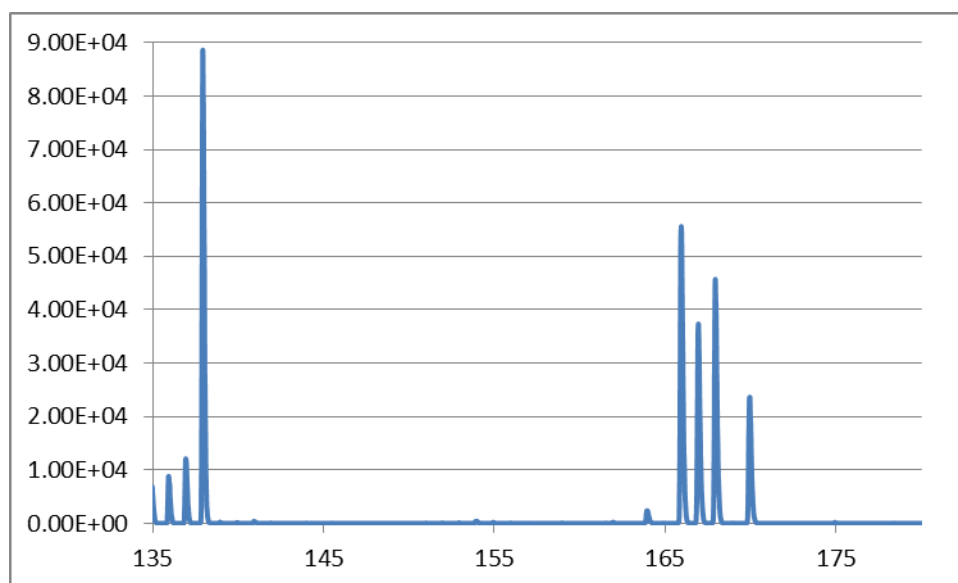


**Figure B.10** Er[hfac]<sub>4</sub> Mass Spectrum

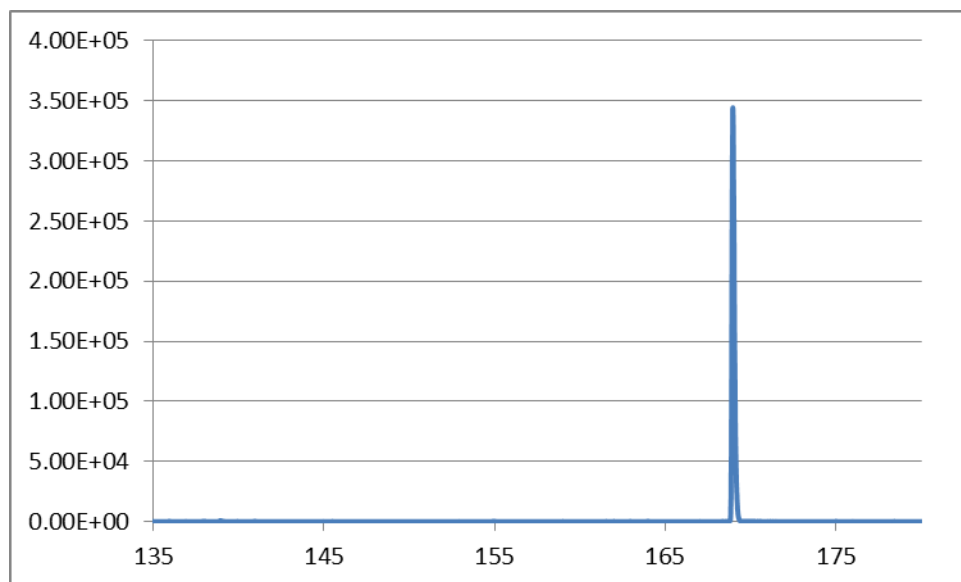


**Figure B.11** Tm[hfac]<sub>4</sub> Mass Spectrum

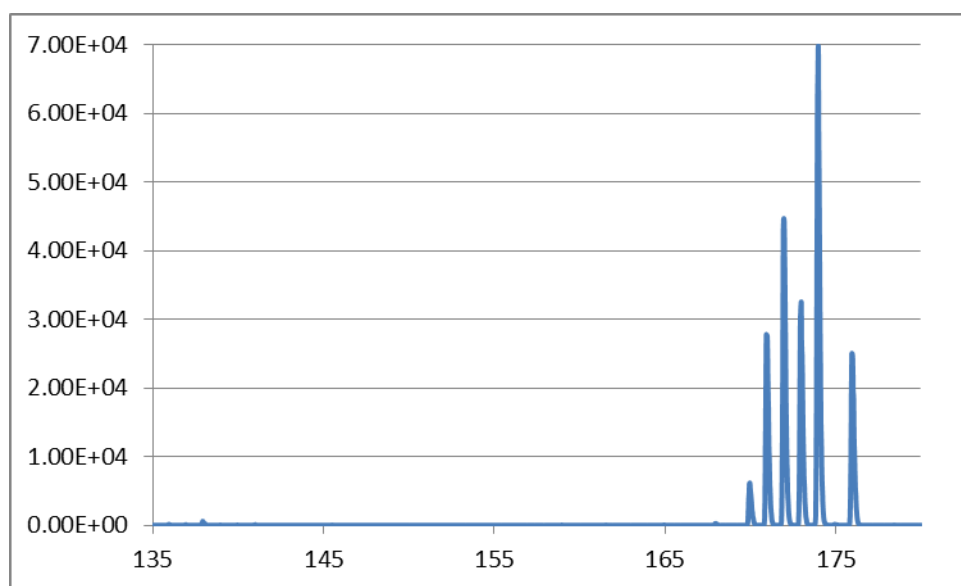


**Figure B.12** Yb[hfac]<sub>4</sub> Mass Spectrum

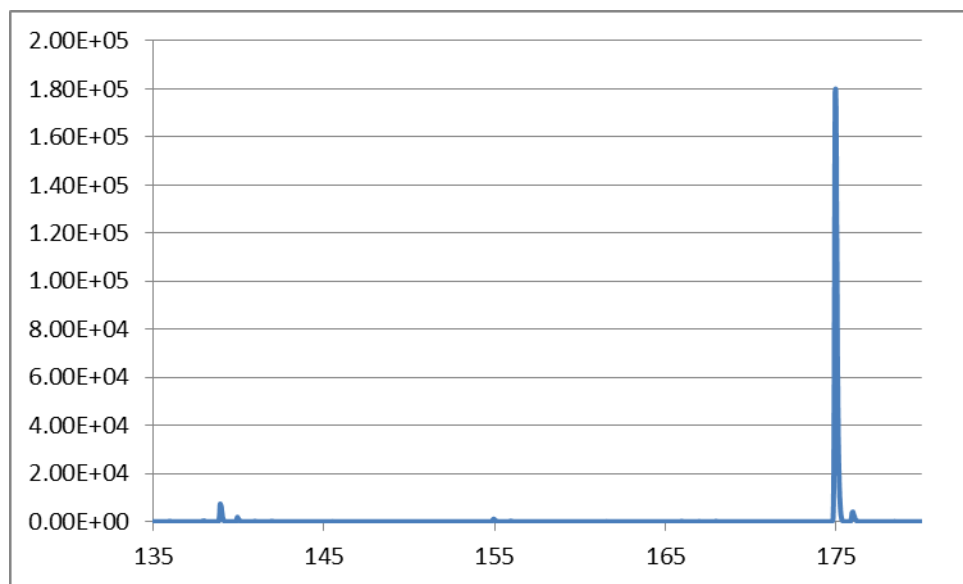


**Figure B.13** Lu[hfac]<sub>4</sub> Mass Spectrum

# APPENDIX C

## MATLAB CODES AND MODELS

### C.1 GCMS Readout Analysis

%%% This program plots GCMS data from .csv files and computes retention time %%%

```
clear all;
```

```
close all;
```

```
clc;
```

```
filename = 'GdHfac 170 290min Run1.dat'; % Locate dataset
```

```
M = csvread(filename); % Read in dataset
```

```
isotope = 142; % mass number of interest
```

```
Scan_Number = M(1:end,1); % Scan time (Row 5 to end, column 1)
```

```
Mass_Number = M(1,2:end); % Mass number (Row 5, column 2 to end)
```

```
sample = M(2:end, isotope); % pull out isotope intensity column
```

```
surf(M); % Generate the 3D Map
```

```
% Axis Properties %
```

```
title(filename)
```

```

xlabel('Mass Number (amu)')

ylabel('Scan Number (165/min)')

zlabel('Intensity (arb. u.)')

axis([280 290 3 M(end,1) 3 5000 3 5000]) % (xmin, xmax, y, y, z, z, color, color)

% Color Ramp %

shading interp % vertical color ramp

colormap jet(40) % colormap selection

% Peak Retention Time %

scans = M(end,1); % total number of scans

mult = 0; % initialize variable 'mult'

for i=1:scans

    mult = i*sample(i,1)+mult;

end

sum_intensity = sum(sample); % sums all intensities over time of isotope

retention_time = (mult/sum_intensity)/165; %  $t = (m \cdot t)/m / 165$  scans/min

avg_int = mean(sample);

max_sample = max(sample);

max_time = 0; % initialize

```

```
%find time of max elution
```

```
for i=1:scans
```

```
    if sample(i) == max_sample
```

```
        max_time = i/165;
```

```
    end
```

```
end
```

```
%find time of first elution of isotope
```

```
first_time = 0;
```

```
for i=1:scans
```

```
    if sample(i)>0 && first_time == 0
```

```
        first_time = i/165;
```

```
    end
```

```
end
```

```
%calculate first moment of peak (for retention time of tailing peak)
```

```
A = mult/165;          % area (minute*Intensity)
```

```
h = max_sample;        % max peak height (Intensity)
```

```
F = 0.7;               % carrier gas flow rate (cm3/min)
```

```
M = A*F;              % M=AF = volume (cm3) injected
```

```
sdt = A/(h*sqrt(2*3.14159)) % standard deviation of time
```

```

tr = 0;           % retention time (min)

t = 0;           % time (min)


tr_LHS = tr;

tr_RHS = 0;

k=0;


%for tr=1:scans

    %if k ==0

        %for t = 1:scans

            % tr_LHS = tr;

            % tr_RHS = tr_RHS + (1/(sdt*sqrt(2*3.14159)))*exp((-0.5)*((tr-t)/sdt)^2);

            % if tr_RHS > tr_LHS-0.001 && tr_RHS < tr_LHS+0.001

                % k=1

                % break

            % end

        % end

    % end

%end

%end

%tr_RHS;

%tr_LHS;


disp(' ')

```

```

disp(['The average intensity of mass ' sprintf('%0f',isotope) ' is ' sprintf('%0.2f',avg_int)])

disp(' ')

disp(['The average retention time of mass ' sprintf('%0f',isotope) ' is '

sprintf('%0.2f',retention_time) ' min'])

disp(' ')

disp(['The maximum intensity of mass ' sprintf('%0f',isotope) ' is at ' sprintf('%0.2f',max_time) '

min'])

disp(' ')

disp(['The first elution of mass ' sprintf('%0f',isotope) ' is at ' sprintf('%0.2f',first_time) ' min'])

disp(' ')

```

## C.2 Thermodynamic Model

% Retention time calculator

```
clear all;
```

```
close all;
```

```
clc;
```

% Define variables

```
L = 2600;          % Length of column (cm)
```

```
T_0 = 298.15;     % Standard T (K)
```

```
theta = 0.0005;   % Free open cross section area (cm^2)
```

```
V_0 = 6.00;       % Carrier gas flow rate (mL/min) CHANGE
```

```
s = 3.9;          % Open surface of column per 1m length (mc^2)
```



$v = 0.005$ ;      % Open volume of column per 1m length ( $\text{cm}^3$ )  
 $V = 1.8$ ;      % Inner volume of column ( $\text{cm}^3$ )  
 $R = 8.314$ ;      % Ideal gas constant ( $\text{J/mol}\cdot\text{K}$ )  
 $A = 3.96$ ;      % Inner surface per 1m length ( $\text{cm}^2$ )  
 $M_a = 60.0843$ ; % Mass of adsorbing material (amu)  
 $v_b = 880$ ;      % Phonon frequency of quartz ( $\text{s}^{-1}$ )

%Table of Enthalpy of sublimation, -J/mol % +/- error

$H_{\text{sub\_la}} = 104000$ ; %6600  
 $H_{\text{sub\_pr}} = 117500$ ; %7400  
 $H_{\text{sub\_nd}} = 137800$ ; %8000  
 $H_{\text{sub\_sm}} = 81100$ ; %6000  
 $H_{\text{sub\_eu}} = 73100$ ; %6000  
 $H_{\text{sub\_gd}} = 83800$ ; %6200  
 $H_{\text{sub\_tb}} = 83900$ ; %6200  
 $H_{\text{sub\_dy}} = 111600$ ; %9200, 7100  
 $H_{\text{sub\_ho}} = 85000$ ; %6900  
 $H_{\text{sub\_er}} = 94500$ ; %6600  
 $H_{\text{sub\_tm}} = 78600$ ; %6300  
 $H_{\text{sub\_yb}} = 90200$ ; %6600  
 $H_{\text{sub\_lu}} = 95600$ ; %6700

%Hads values, experimental

Hads\_pr = 139000; %J/mol\*K

Hads\_nd = 139000;

Hads\_sm = 76000;

Hads\_eu = 43000;

Hads\_gd = 34000;

Hads\_tb = 83000;

Hads\_dy = 118000;

Hads\_ho = 109000;

Hads\_er = 39000;

Hads\_tm = 53000;

Hads\_yb = 33000;

Hads\_lu = 38000;

%Hads standard deviation

sd\_Hads\_pr = 4000; %J/mol\*K

sd\_Hads\_nd = 5000;

sd\_Hads\_sm = 17000;

sd\_Hads\_eu = 20000;

sd\_Hads\_gd = 3000;

sd\_Hads\_tb = 49000;

sd\_Hads\_dy = 8000;

sd\_Hads\_ho = 21000;

sd\_Hads\_er = 10000;

```
sd_Hads_tm = 25000;
```

```
sd_Hads_yb = 3000;
```

```
sd_Hads_lu = 11000;
```

```
%Sads values, experimental
```

```
Sads_pr = 519; %J/mol
```

```
Sads_nd = 518;
```

```
Sads_sm = 359;
```

```
Sads_eu = 281;
```

```
Sads_gd = 262;
```

```
Sads_tb = 399;
```

```
Sads_dy = 474;
```

```
Sads_ho = 453;
```

```
Sads_er = 276;
```

```
Sads_tm = 306;
```

```
Sads_yb = 257;
```

```
Sads_lu = 268;
```

```
%Sads standard deviation
```

```
sd_Sads_pr = 19; %J/mol
```

```
sd_Sads_nd = 23;
```

```
sd_Sads_sm = 52;
```

```
sd_Sads_eu = 57;
```

```
sd_Sads_gd = 18;  
sd_Sads_tb = 142;  
sd_Sads_dy = 29;  
sd_Sads_ho = 64;  
sd_Sads_er = 34;  
sd_Sads_tm = 70;  
sd_Sads_yb = 16;  
sd_Sads_lu = 38;
```

%Select Element

```
H_ads = Hads_lu;  
sd_Hads = sd_Hads_lu;  
S_ads = Sads_lu;  
sd_Sads = sd_Sads_lu;
```

```
M_comp = 832+175; % Mass of organometallic complex  CHANGE
```

```
T_iso = 273+193; % Isothermal column temperature (K) CHANGE
```

% Temperature Range (sublimation - decomposition) C

%la 153-237 C

%pr 147-220 C

%nd 147-224 C

%sm 137-200 C

%eu 140-220 C

%gd 141-210 C

%tb 141-205 C

%dy 135-200 C

%ho 142-193 C

%er 143-205 C

%tm 139-200 C

%yb 143-200 C

%lu 144-195 C

$H_{\max} = H_{\text{ads}} + sd_{\text{Hads}};$

$H_{\min} = H_{\text{ads}} - sd_{\text{Hads}};$

$S_{\max} = S_{\text{ads}} + sd_{\text{Sads}};$

$S_{\min} = S_{\text{ads}} - sd_{\text{Sads}};$

% Calculate retention time

$\text{term1} = ((L * T_0 * \theta) / (V_0 * T_{\text{iso}}));$

$\text{term2} = (V / (100 * A));$

$t_{\min} = 60 * \text{term1} * (1 + (s/v) * \text{term2} * \exp((H_{\max} / (R * T_{\text{iso}}))) * \exp(-S_{\min} / R));$

$t_{\max} = 60 * \text{term1} * (1 + (s/v) * \text{term2} * \exp((H_{\min} / (R * T_{\text{iso}}))) * \exp(-S_{\max} / R));$

```

disp(' ')
disp(['Maximum retention time of mass ' sprintf('%.0f',M_comp) ': ' sprintf('%.2f',t_min) ' sec'])
disp(' ')
disp(['Minimum retention time of mass ' sprintf('%.0f',M_comp) ': ' sprintf('%.2f',t_max) ' sec'])
disp(' ')

```

### C.3 Monte Carlo Model<sup>12</sup>

```

clc, clear, clf

format long g;

tic

%Hads values, experimental
Hads_pr = 139000; %J/mol*K
Hads_nd = 139000;
Hads_sm = 76000;
Hads_eu = 43000;
Hads_gd = 34000;
Hads_tb = 83000;
Hads_dy = 118000;
Hads_ho = 109000;
Hads_er = 39000;
Hads_tm = 53000;

```

Hads\_yb = 33000;

Hads\_lu = 38000;

%Hads standard deviation

sd\_Hads\_pr = 4000; %J/mol\*K

sd\_Hads\_nd = 5000;

sd\_Hads\_sm = 17000;

sd\_Hads\_eu = 20000;

sd\_Hads\_gd = 3000;

sd\_Hads\_tb = 49000;

sd\_Hads\_dy = 8000;

sd\_Hads\_ho = 21000;

sd\_Hads\_er = 10000;

sd\_Hads\_tm = 25000;

sd\_Hads\_yb = 3000;

sd\_Hads\_lu = 11000;

%Molecular weight of pure tracer (g/mol)

M\_pr = 140.9;

M\_nd = 144.2;

M\_sm = 150.36;

M\_eu = 151.96;

M\_gd = 157.25;

M\_tb = 158.93;

M\_dy = 162.5;

M\_ho = 164.93;

M\_er = 167.26;

M\_tm = 168.93;

M\_yb = 173.05;

M\_lu = 174.97;

% Density of pure room temp tracer metal (g/cc)

rho\_pr = 6.77;

rho\_nd = 7.01;

rho\_sm = 7.52;

rho\_eu = 5.26;

rho\_gd = 7.90;

rho\_tb = 8.23;

rho\_dy = 8.54;

rho\_ho = 8.79;

rho\_er = 9.07;

rho\_tm = 9.32;

rho\_yb = 6.90;

rho\_lu = 9.84;

M1=M\_lu; %molecular weight of pure tracer (g/mol) \*\*\*\*\*



$M_2=39.948$ ; %molar mass of carrier gas (g/mol) Argon  
 $M_{\text{hfac}}=208.06$ ; %(g/mol)  
 $M_{\text{fod}}=296.182$ ; %(g/mol)  
 $M_{\text{dpm}}=184.279$ ; %(g/mol)  
 $M_{\text{ligand}}=M_{\text{hfac}}$ ; %choose ligand: Mhfac, Mfod, or Mdpm  
 $\text{coord}=4$ ; %choose coordination number of element-ligand complex  
 $M=M_1+(M_{\text{ligand}}*\text{coord})$ ;  
  
 $\rho=\rho_{\text{lu}}$ ; %density of pure room temp tracer metal (g/cc) \*\*\*\*\*  
 $\rho_2=1.784\text{e-}3$ ; %density of carrier gas (g/cc) Argon  
 $\mu_2=2\text{e-}4$ ; %dynamic viscosity of carrier gas (Poise) Argon  
 $d_m=3.66\text{e-}8$ ; %carrier collision diameter (cm) [ref 9, pg 40] Argon  
  
 $R=8.3145\text{e}7$ ; %gas constant (erg/mol/K)  
 $R_2=8.3145\text{e-}3$ ; %gas constant (kJ/mol/K)  
 $N_{\text{avo}}=6.022\text{e}23$ ; %avogradros number (atoms/mol)  
  
 $i_d=0.53$ ; %inside diameter (mm)  
 $r=(i_d/10)/2$ ; %inner column radius (cm)  
  
 $T_{\text{emp}}=193$ ; %isothermal temperature (deg C)  
 $T=T_{\text{emp}}+273.15$ ; %isothermal temperature of column (K)

$\tau_0=1e-13$ ; %oscillatory period of molecule in adsorbed state (s)[ref 9, pg 42]

Length=2600; %column length (cm)

%Delta\_H\_a = -(Hads\_ho)/1000; %adsorption enthalpy (kJ/mol)\*\*\*\*\*

Delta\_H\_a = -(Hads\_lu-sd\_Hads\_lu)/1000; %adsorption enthalpy (kJ/mol)\*\*\*\*\*

% reference 9, Zvara: Calculate Diffusion Coefficient

% Collision Diameters of Carrier and Tracer

% If pure element, choose first one; if chloride or oxychloride choose 2nd

%  $dm1=(\sqrt{2}) * M / (N_{avo} * \rho))^{(1/3)}$ ; %tracer collision diameter for pure (cm)

$dm1=(2e-11) * M + 5e-8$ ; %tracer collision diameter for complexes (cm)

$w12=(dm1+dm2)/2$ ; %collision diameter (cm)

P=2.275; %pressure of column (bar) --- use pressure flow calculator software to find gauge  
pressure

u=45.45; %average linear flow velocity (cm/s) --- from pressure flow calculator

$Q=\pi * (r^2) * u$ ; %volumetric flow rate calculated from average flow velocity (cc/s)

%  $Q1=Q*60$  % (cc/min)

Q1=6.0;

% check if carrier is large laminar flow

$Re=2*r*u*rho2/mu2$ ; %Re number for carrier flow, must be large but <2300 for large laminar flow

$n2=(7.24e21)*P/T$ ; %atomic concentration of carrier gas (1/cc)

$M12=(M*M2)/(M+M2)$ ; %(g/mol)

$lambdam1=1/(pi*n2*(w12^2))$ ; %(cm)

$u12=sqrt(8*R*T/(pi*M12))$ ; %(cm/s)

$D=u12*lambdam1/2$ ; %diffusion coefficient (cm<sup>2</sup>/s)

$N=50$ ; %number of molecules observed

$tau\_a\_bar=tau\_0*exp(-Delta\_H\_a/(R2*T))$  %avg time molecule spends in the adsorbed state (s)

$nu\_1=(r/Q)*sqrt((2*pi*R*T)/M)$ ; %(1/cm)

$phi=(1/u)/((1/u)+(nu\_1*tau\_a\_bar))$ ; %ratio of carrier gas velocity to mean migration velocity of zone

$eta\_bar=(pi*(r^2)*D/Q)+(11-16*phi+6*(phi^2))*(Q/(48*pi*D))+(1/(2*nu\_1))$  %average jump length (cm)

%simulation

$m=0$ ; % counter for the number of molecules

$tau\_s\_m=zeros(1,m)$ ; %place holder for vector creation

$x\_m=zeros(1,m)$ ; % " "

while  $m < N$

```

m=m+1; %adds one each loop

x=0; %initial x coordinate

%calculation of adsorption residence times

i=0; %counter for the number of jumps per molecule

tauvec=zeros(1,i); %place holder for residence times filled below

while x<Length

    i=i+1; %jump counter

    eta=-eta_bar*log(1-rand); % random jump length (cm)

    x=x+eta; %new x coordinate after jump

    %randomizing residence time resulting from adsorptions

    tau_mu = nu_1*tau_a_bar*eta_bar;

    tau_a = -tau_mu*log(1-rand);

    tau_g = (eta*pi*(r^2))/Q;

    tau_ag = tau_a + tau_g;

    %creating a vector of residence times

    tauvec(i)=tau_ag;

    tau_s=sum(tauvec); %sum of residence times

end

```

```

%vector of final x coordinates for all molecules

x_m(m)=x;

%vector of total residence times for all molecules

tau_s_m(m)=tau_s;

end

%plot vectors pulled from loop for efficiency

%time_La=linspace(0,max(tau_s_m));

%j_La=hist(tau_s_m,time_La);

%plot(time_La,j_La)

retention_time_in_seconds=mean(tau_s_m)

retention_time_standard_deviation=std(tau_s_m);

%xlswrite('All_Lats',La,'Lanthanides','B2');

%xlswrite('All_Lats',La_std,'Lanthanides','C2');

toc;

```

**\*Special thanks to Mr. Shayan Shahbazi**

## C.4 Experimental Data Analysis

%%% This program uses temperature ramping in a GC column to converge

%%% enthalpy and entropy of adsorption values

clear all;

close all;

clc;

R = 0.008314; % Gas constant (KJ/K\*mol)

s = 0.66; % Surface of stationary phase (cm<sup>2</sup>)

a = 0.5; % Temperature ramp rate (K/min)

Vg = 0.009; % Free column volume (cm<sup>3</sup>)(assuming 4cm length)

u0\_12 = 1023; % Linear gas velocity at standard temperature (cm/min)12 psi

u0\_22 = 1682; % Linear gas velocity at standard temperature (cm/min)22 psi

u0\_33 = 2727; % Linear gas velocity at standard temperature (cm/min)33 psi

u0\_42 = 3355; % Linear gas velocity at standard temperature (cm/min)42 psi

ta = 6 ; % Time of deposition (min)

T0\_12 = 273+115; % Initial column temperature (K) 12 psi

Ta\_12 = 273+110; % Elution temperature (K) 12 psi

```

T0_22 = 273+100; % Initial column temperature (K) 22 psi
Ta_22 = 273+96; % Elution temperature (K) 22 psi

T0_33 = 273+96; % Initial column temperature (K) 33 psi
Ta_33 = 273+92; % Elution temperature (K) 33 psi

%T0_42 = 273+110; % Elution temperature (K) 42 psi
%Ta_42 = 273+105; % Elution temperature (K) 42 psi

syms Hads_12; % Enthalpy of adsorption (KJ/mol) 12 psi
syms Hads_22; % Enthalpy of adsorption (KJ/mol) 22 psi
syms Hads_33; % Enthalpy of adsorption (KJ/mol) 33 psi
syms Hads_42; % Enthalpy of adsorption (KJ/mol) 42 psi

Sads = linspace(-0.1, -1.1, 5); % Entropy of adsorption range (KJ/mol*K)

for i = 1:5

    eqn12 = log10(ta) == (-1*Hads_12/(2.3*R*Ta_12)) + (Sads(i)/(2.3*R)) +
log10(3.6E10*R*T0_12*s/(a*u0_12*Vg));

    H_12(i) = double(solve(eqn12, Hads_12))

    eqn22 = log10(ta) == (-1*Hads_22/(2.3*R*Ta_22)) + (Sads(i)/(2.3*R)) +
log10(3.6E10*R*T0_22*s/(a*u0_22*Vg));

    H_22(i) = double(solve(eqn22, Hads_22))

```

```

eqn33 = log10(ta) == (-1*Hads_33/(2.3*R*Ta_33)) + (Sads(i)/(2.3*R)) +
log10(3.6E10*R*T0_33*s/(a*u0_33*Vg));

H_33(i) = double(solve(eqn33, Hads_33))

%eqn42 = log10(ta) == (-1*Hads_42/(2.3*R*Ta_42)) + (Sads(i)/(2.3*R)) +
log10(3.6E10*R*T0_42*s/(a*u0_42*Vg));

%H_42(i) = double(solve(eqn42, Hads_42))

i=i+1;

end

scatter(1000*Sads(:), H_12(:)) % Associate elements of Sads to respective H elements
scatter(1000*Sads(:), H_22(:)) % Associate elements of Sads to respective H elements
scatter(1000*Sads(:), H_33(:)) % Associate elements of Sads to respective H elements
%scatter(1000*Sads(:), H_42(:)) % Associate elements of Sads to respective H elements

p = plot(1000*Sads(:), H_12(:), 1000*Sads(:), H_22(:), 1000*Sads(:), H_33(:)) % Plot scatter
graphs

p(1).LineWidth = 2; % Set line widths on graph
p(2).LineWidth = 2;
p(3).LineWidth = 2;
%p(4).LineWidth = 2;

title('Enthalpy and Entropy of Adsorption: Individual Ln[hfac]4 Complexes')

```



```
xlabel('Entropy of Adsorption (J/mol)') % x-axis label  
ylabel('Enthalpy of Adsorption (Kj/mol*K)') % y-axis label  
legend('12 psi','22 psi', '33 psi', 'Location','southeast')
```

# APPENDIX D

## FRAGMENTATION PATTERNS

**Table D.1** Possible FID Fragmentation Patterns of  $\text{NH}_4[\text{Ln}(\text{hfac})_4]$  Complexes\*

<u>ISOTOPE NAME</u>	<b>Hfac</b>	<b>208</b>	<b>La-139 hfac</b>	<b>139</b>	<b>Pr-141 hfac</b>	<b>141</b>
<b><u>POSSIBLE FRAGMENTS</u></b>	$\text{CF}_3\text{C}(\text{O})\text{CH}_2\text{C}(\text{O})\text{CF}_3$	208	$\text{La-CF}_3\text{C}(\text{O})\text{CH}_2\text{C}(\text{O})\text{CF}_3$	347	$\text{Pr-CF}_3\text{C}(\text{O})\text{CH}_2\text{C}(\text{O})\text{CF}_3$	349
	$\text{CF}_3$	69	$\text{CF}_3$	69	$\text{CF}_3$	69
	$\text{C}(\text{O})\text{CH}_2\text{C}(\text{O})\text{CF}_3$	139	$\text{La-C}(\text{O})\text{CH}_2\text{C}(\text{O})\text{CF}_3$	278	$\text{Pr-C}(\text{O})\text{CH}_2\text{C}(\text{O})\text{CF}_3$	280
	$\text{CF}_3\text{C}(\text{O})$	97	$\text{CF}_3\text{C}(\text{O})$	97	$\text{CF}_3\text{C}(\text{O})$	97
	$\text{CH}_2\text{C}(\text{O})\text{CF}_3$	111	$\text{CH}_2\text{C}(\text{O})\text{CF}_3$	111	$\text{CH}_2\text{C}(\text{O})\text{CF}_3$	111
	-	-	La	139	Pr	141
	$\text{O}_2$	32	$\text{La-O}_2$	171	$\text{Pr-O}_2$	173
	$\text{CCH}_2\text{C}(\text{O})\text{CF}_3$	123	$\text{CCH}_2\text{C}(\text{O})\text{CF}_3$	123	$\text{CCH}_2\text{C}(\text{O})\text{CF}_3$	123
<b><u>UNLIKELY FRAGMENTS</u></b>	$\text{CF}_3\text{C}(\text{O})$	97	$\text{La-CF}_3\text{C}(\text{O})$	236	$\text{Pr-CF}_3\text{C}(\text{O})$	238
	$\text{CH}_2\text{C}(\text{O})\text{CF}_3$	111	$\text{La-CH}_2\text{C}(\text{O})\text{CF}_3$	250	$\text{Pr-CH}_2\text{C}(\text{O})\text{CF}_3$	252
	$\text{CF}_3\text{C}(\text{O})\text{CHC}(\text{O})\text{CF}_3$	207	$\text{La-CF}_3\text{C}(\text{O})\text{CHC}(\text{O})\text{CF}_3$	346	$\text{Pr-CF}_3\text{C}(\text{O})\text{CHC}(\text{O})\text{CF}_3$	348
	$\text{CF}_3\text{C}(\text{O})\text{CH}_2\text{C}(\text{O})\text{CF}_2$	189	$\text{La-CF}_3\text{C}(\text{O})\text{CH}_2\text{C}(\text{O})\text{CF}_2$	328	$\text{Pr-CF}_3\text{C}(\text{O})\text{CH}_2\text{C}(\text{O})\text{CF}_2$	330
	$\text{OCCF}_3$	97	$\text{La-OCCF}_3$	236	$\text{Pr-OCCF}_3$	238
	$\text{CCH}_2\text{C}(\text{O})\text{CF}_3$	123	$\text{La-CCH}_2\text{C}(\text{O})\text{CF}_3$	262	$\text{Pr-CCH}_2\text{C}(\text{O})\text{CF}_3$	264
	$\text{CF}_3\text{CCH}_2\text{C}(\text{O})\text{CF}_3$	192	$\text{La-CF}_3\text{CCH}_2\text{C}(\text{O})\text{CF}_3$	331	$\text{Pr-CF}_3\text{CCH}_2\text{C}(\text{O})\text{CF}_3$	333
	$\text{CF}_3\text{CCH}_2\text{C}(\text{O})\text{CF}_3$	192	$\text{CF}_3\text{CCH}_2\text{C}(\text{O})\text{CF}_3$	192	$\text{CF}_3\text{CCH}_2\text{C}(\text{O})\text{CF}_3$	192

<b>Nd-142 hfac</b>	<b>142</b>	<b>Nd-143 hfac</b>	<b>143</b>	<b>Nd-144 hfac</b>	<b>144</b>	<b>Nd-145 hfac</b>	<b>145</b>
$\text{Nd-CF}_3\text{C}(\text{O})\text{CH}_2\text{C}(\text{O})\text{CF}_3$	350	$\text{Nd-CF}_3\text{C}(\text{O})\text{CH}_2\text{C}(\text{O})\text{CF}_3$	351	$\text{Nd-CF}_3\text{C}(\text{O})\text{CH}_2\text{C}(\text{O})\text{CF}_3$	352	$\text{Nd-CF}_3\text{C}(\text{O})\text{CH}_2\text{C}(\text{O})\text{CF}_3$	353
$\text{CF}_3$	69	$\text{CF}_3$	69	$\text{CF}_3$	69	$\text{CF}_3$	69
$\text{Nd-C}(\text{O})\text{CH}_2\text{C}(\text{O})\text{CF}_3$	281	$\text{Nd-C}(\text{O})\text{CH}_2\text{C}(\text{O})\text{CF}_3$	282	$\text{Nd-C}(\text{O})\text{CH}_2\text{C}(\text{O})\text{CF}_3$	283	$\text{Nd-C}(\text{O})\text{CH}_2\text{C}(\text{O})\text{CF}_3$	284
$\text{CF}_3\text{C}(\text{O})$	97	$\text{CF}_3\text{C}(\text{O})$	97	$\text{CF}_3\text{C}(\text{O})$	97	$\text{CF}_3\text{C}(\text{O})$	97
$\text{CH}_2\text{C}(\text{O})\text{CF}_3$	111	$\text{CH}_2\text{C}(\text{O})\text{CF}_3$	111	$\text{CH}_2\text{C}(\text{O})\text{CF}_3$	111	$\text{CH}_2\text{C}(\text{O})\text{CF}_3$	111
Nd	142	Nd	143	Nd	144	Nd	145
$\text{Nd-O}_2$	174	$\text{Nd-O}_2$	175	$\text{Nd-O}_2$	176	$\text{Nd-O}_2$	177

CCH <sub>2</sub> C(O)CF <sub>3</sub>	123	CCH <sub>2</sub> C(O)CF <sub>3</sub>	123	CCH <sub>2</sub> C(O)CF <sub>3</sub>	123	CCH <sub>2</sub> C(O)CF <sub>3</sub>	123
Nd-CF <sub>3</sub> C(O)	239	Nd-CF <sub>3</sub> C(O)	240	Nd-CF <sub>3</sub> C(O)	241	Nd-CF <sub>3</sub> C(O)	242
Nd-CH <sub>2</sub> C(O)CF <sub>3</sub>	253	Nd-CH <sub>2</sub> C(O)CF <sub>3</sub>	254	Nd-CH <sub>2</sub> C(O)CF <sub>3</sub>	255	Nd-CH <sub>2</sub> C(O)CF <sub>3</sub>	256
Nd-CF <sub>3</sub> C(O)CHC(O)CF <sub>3</sub>	349	Nd-CF <sub>3</sub> C(O)CHC(O)CF <sub>3</sub>	350	Nd-CF <sub>3</sub> C(O)CHC(O)CF <sub>3</sub>	351	Nd-CF <sub>3</sub> C(O)CHC(O)CF <sub>3</sub>	352
Nd-CF <sub>3</sub> C(O)CH <sub>2</sub> C(O)CF <sub>2</sub>	331	Nd-CF <sub>3</sub> C(O)CH <sub>2</sub> C(O)CF <sub>2</sub>	332	Nd-CF <sub>3</sub> C(O)CH <sub>2</sub> C(O)CF <sub>2</sub>	333	Nd-CF <sub>3</sub> C(O)CH <sub>2</sub> C(O)CF <sub>2</sub>	334
Nd-OCCF <sub>3</sub>	239	Nd-OCCF <sub>3</sub>	240	Nd-OCCF <sub>3</sub>	241	Nd-OCCF <sub>3</sub>	242
Nd-CCH <sub>2</sub> C(O)CF <sub>3</sub>	265	Nd-CCH <sub>2</sub> C(O)CF <sub>3</sub>	266	Nd-CCH <sub>2</sub> C(O)CF <sub>3</sub>	267	Nd-CCH <sub>2</sub> C(O)CF <sub>3</sub>	268
Nd-CF <sub>3</sub> CCH <sub>2</sub> C(O)CF <sub>3</sub>	334	Nd-CF <sub>3</sub> CCH <sub>2</sub> C(O)CF <sub>3</sub>	335	Nd-CF <sub>3</sub> CCH <sub>2</sub> C(O)CF <sub>3</sub>	336	Nd-CF <sub>3</sub> CCH <sub>2</sub> C(O)CF <sub>3</sub>	337
CF <sub>3</sub> CCH <sub>2</sub> C(O)CF <sub>3</sub>	192	CF <sub>3</sub> CCH <sub>2</sub> C(O)CF <sub>3</sub>	192	CF <sub>3</sub> CCH <sub>2</sub> C(O)CF <sub>3</sub>	192	CF <sub>3</sub> CCH <sub>2</sub> C(O)CF <sub>3</sub>	192

<b>Nd-146 hfac</b>	<b>146</b>	<b>Nd-148 Hfac</b>	<b>148</b>	<b>Nd-150 hfac</b>	<b>150</b>	<b>Sm-147 hfac</b>	<b>147</b>
Nd-CF <sub>3</sub> C(O)CH <sub>2</sub> C(O)CF <sub>3</sub>	354	Nd-CF <sub>3</sub> C(O)CH <sub>2</sub> C(O)CF <sub>3</sub>	356	Nd-CF <sub>3</sub> C(O)CH <sub>2</sub> C(O)CF <sub>3</sub>	358	Sm-CF <sub>3</sub> C(O)CH <sub>2</sub> C(O)CF <sub>3</sub>	355
CF <sub>3</sub>	69	CF <sub>3</sub>	69	CF <sub>3</sub>	69	CF <sub>3</sub>	69
Nd-C(O)CH <sub>2</sub> C(O)CF <sub>3</sub>	285	Nd-C(O)CH <sub>2</sub> C(O)CF <sub>3</sub>	287	Nd-C(O)CH <sub>2</sub> C(O)CF <sub>3</sub>	289	Sm-C(O)CH <sub>2</sub> C(O)CF <sub>3</sub>	286
CF <sub>3</sub> C(O)	97	CF <sub>3</sub> C(O)	97	CF <sub>3</sub> C(O)	97	CF <sub>3</sub> C(O)	97
CH <sub>2</sub> C(O)CF <sub>9</sub>	111	CH <sub>2</sub> C(O)CF <sub>3</sub>	111	CH <sub>2</sub> C(O)CF <sub>3</sub>	111	CH <sub>2</sub> C(O)CF <sub>3</sub>	111
Nd	146	Nd	148	Nd	150	Sm	147
Nd-O <sub>2</sub>	178	Nd-O <sub>2</sub>	180	Nd-O <sub>2</sub>	182	Sm-O <sub>2</sub>	179
CCH <sub>2</sub> C(O)CF <sub>3</sub>	123	CCH <sub>2</sub> C(O)CF <sub>3</sub>	123	CCH <sub>2</sub> C(O)CF <sub>3</sub>	123	CCH <sub>2</sub> C(O)CF <sub>3</sub>	123
Nd-CF <sub>3</sub> C(O)	243	Nd-CF <sub>3</sub> C(O)	245	Nd-CF <sub>3</sub> C(O)	247	Sm-CF <sub>3</sub> C(O)	244
Nd-CH <sub>2</sub> C(O)CF <sub>3</sub>	257	Nd-CH <sub>2</sub> C(O)CF <sub>3</sub>	259	Nd-CH <sub>2</sub> C(O)CF <sub>3</sub>	261	Sm-CH <sub>2</sub> C(O)CF <sub>3</sub>	258
Nd-CF <sub>3</sub> C(O)CHC(O)CF <sub>3</sub>	353	Nd-CF <sub>3</sub> C(O)CHC(O)CF <sub>3</sub>	355	Nd-CF <sub>3</sub> C(O)CHC(O)CF <sub>3</sub>	357	Sm-CF <sub>3</sub> C(O)CHC(O)CF <sub>3</sub>	354
Nd-CF <sub>3</sub> C(O)CH <sub>2</sub> C(O)CF <sub>2</sub>	335	Nd-CF <sub>3</sub> C(O)CH <sub>2</sub> C(O)CF <sub>2</sub>	337	Nd-CF <sub>3</sub> C(O)CH <sub>2</sub> C(O)CF <sub>2</sub>	339	Sm-CF <sub>3</sub> C(O)CH <sub>2</sub> C(O)CF <sub>2</sub>	336
Nd-OCCF <sub>3</sub>	243	Nd-OCCF <sub>3</sub>	245	Nd-OCCF <sub>3</sub>	247	Sm-OCCF <sub>3</sub>	244
Nd-CCH <sub>2</sub> C(O)CF <sub>3</sub>	269	Nd-CCH <sub>2</sub> C(O)CF <sub>3</sub>	271	Nd-CCH <sub>2</sub> C(O)CF <sub>3</sub>	273	Sm-CCH <sub>2</sub> C(O)CF <sub>3</sub>	270
Nd-CF <sub>3</sub> CCH <sub>2</sub> C(O)CF <sub>3</sub>	338	Nd-CF <sub>3</sub> CCH <sub>2</sub> C(O)CF <sub>3</sub>	340	Nd-CF <sub>3</sub> CCH <sub>2</sub> C(O)CF <sub>3</sub>	342	Sm-CF <sub>3</sub> CCH <sub>2</sub> C(O)CF <sub>3</sub>	339
CF <sub>3</sub> CCH <sub>2</sub> C(O)CF <sub>3</sub>	192	CF <sub>3</sub> CCH <sub>2</sub> C(O)CF <sub>3</sub>	192	CF <sub>3</sub> CCH <sub>2</sub> C(O)CF <sub>3</sub>	192	CF <sub>3</sub> CCH <sub>2</sub> C(O)CF <sub>3</sub>	192

<b>Sm-148 hfac</b>	<b>148</b>	<b>Sm-149 hfac</b>	<b>149</b>	<b>Sm-150 hfac</b>	<b>150</b>	<b>Sm-152 hfac</b>	<b>152</b>
Sm-CF <sub>3</sub> C(O)CH <sub>2</sub> C(O)CF <sub>3</sub>	356	Sm-CF <sub>3</sub> C(O)CH <sub>2</sub> C(O)CF <sub>3</sub>	357	Sm-CF <sub>3</sub> C(O)CH <sub>2</sub> C(O)CF <sub>3</sub>	358	Sm-CF <sub>3</sub> C(O)CH <sub>2</sub> C(O)CF <sub>3</sub>	360
CF <sub>3</sub>	69	CF <sub>3</sub>	69	CF <sub>3</sub>	69	CF <sub>3</sub>	69

Sm-C(O)CH <sub>2</sub> C(O)CF <sub>3</sub>	287	Sm-C(O)CH <sub>2</sub> C(O)CF <sub>3</sub>	288	Sm-C(O)CH <sub>2</sub> C(O)CF <sub>3</sub>	289	Sm-C(O)CH <sub>2</sub> C(O)CF <sub>3</sub>	291
CF <sub>3</sub> C(O)	97	CF <sub>3</sub> C(O)	97	CF <sub>3</sub> C(O)	97	CF <sub>3</sub> C(O)	97
CH <sub>2</sub> C(O)CF <sub>3</sub>	111	CH <sub>2</sub> C(O)CF <sub>3</sub>	111	CH <sub>2</sub> C(O)CF <sub>3</sub>	111	CH <sub>2</sub> C(O)CF <sub>3</sub>	111
Sm	148	Sm	149	Sm	150	Sm	152
Sm-O <sub>2</sub>	180	Sm-O <sub>2</sub>	181	Sm-O <sub>2</sub>	182	Sm-O <sub>2</sub>	184
CCH <sub>2</sub> C(O)CF <sub>3</sub>	123	CCH <sub>2</sub> C(O)CF <sub>3</sub>	123	CCH <sub>2</sub> C(O)CF <sub>3</sub>	123	CCH <sub>2</sub> C(O)CF <sub>3</sub>	123
Sm-CF <sub>3</sub> C(O)	245	Sm-CF <sub>3</sub> C(O)	246	Sm-CF <sub>3</sub> C(O)	247	Sm-CF <sub>3</sub> C(O)	249
Sm-CH <sub>2</sub> C(O)CF <sub>3</sub>	259	Sm-CH <sub>2</sub> C(O)CF <sub>3</sub>	260	Sm-CH <sub>2</sub> C(O)CF <sub>3</sub>	261	Sm-CH <sub>2</sub> C(O)CF <sub>3</sub>	263
Sm-CF <sub>3</sub> C(O)CHC(O)CF <sub>3</sub>	355	Sm-CF <sub>3</sub> C(O)CHC(O)CF <sub>3</sub>	356	Sm-CF <sub>3</sub> C(O)CHC(O)CF <sub>3</sub>	357	Sm-CF <sub>3</sub> C(O)CHC(O)CF <sub>3</sub>	359
Sm-CF <sub>3</sub> C(O)CH <sub>2</sub> C(O)CF <sub>2</sub>	337	Sm-CF <sub>3</sub> C(O)CH <sub>2</sub> C(O)CF <sub>2</sub>	338	Sm-CF <sub>3</sub> C(O)CH <sub>2</sub> C(O)CF <sub>2</sub>	339	Sm-CF <sub>3</sub> C(O)CH <sub>2</sub> C(O)CF <sub>2</sub>	341
Sm-OCCF <sub>3</sub>	245	Sm-OCCF <sub>3</sub>	246	Sm-OCCF <sub>3</sub>	247	Sm-OCCF <sub>3</sub>	249
Sm-CCH <sub>2</sub> C(O)CF <sub>3</sub>	271	Sm-CCH <sub>2</sub> C(O)CF <sub>3</sub>	272	Sm-CCH <sub>2</sub> C(O)CF <sub>3</sub>	273	Sm-CCH <sub>2</sub> C(O)CF <sub>3</sub>	275
Sm-CF <sub>3</sub> CCH <sub>2</sub> C(O)CF <sub>3</sub>	340	Sm-CF <sub>3</sub> CCH <sub>2</sub> C(O)CF <sub>3</sub>	341	Sm-CF <sub>3</sub> CCH <sub>2</sub> C(O)CF <sub>3</sub>	342	Sm-CF <sub>3</sub> CCH <sub>2</sub> C(O)CF <sub>3</sub>	344
CF <sub>3</sub> CCH <sub>2</sub> C(O)CF <sub>3</sub>	192	CF <sub>3</sub> CCH <sub>2</sub> C(O)CF <sub>3</sub>	192	CF <sub>3</sub> CCH <sub>2</sub> C(O)CF <sub>3</sub>	192	CF <sub>3</sub> CCH <sub>2</sub> C(O)CF <sub>3</sub>	192

<b>Sm-154 hfac</b>	<b>154</b>	<b>Eu-151 hfac</b>	<b>151</b>	<b>Eu-153 hfac</b>	<b>153</b>	<b>Gd-155 hfac</b>	<b>155</b>
Sm-CF <sub>3</sub> C(O)CH <sub>2</sub> C(O)CF <sub>3</sub>	362	Eu-CF <sub>3</sub> C(O)CH <sub>2</sub> C(O)CF <sub>3</sub>	359	Eu-CF <sub>3</sub> C(O)CH <sub>2</sub> C(O)CF <sub>3</sub>	361	Gd-CF <sub>3</sub> C(O)CH <sub>2</sub> C(O)CF <sub>3</sub>	363
CF <sub>3</sub>	69	CF <sub>3</sub>	69	CF <sub>3</sub>	69	CF <sub>3</sub>	69
Sm-C(O)CH <sub>2</sub> C(O)CF <sub>3</sub>	293	Eu-C(O)CH <sub>2</sub> C(O)CF <sub>3</sub>	290	Eu-C(O)CH <sub>2</sub> C(O)CF <sub>3</sub>	292	Gd-C(O)CH <sub>2</sub> C(O)CF <sub>3</sub>	294
CF <sub>3</sub> C(O)	97	CF <sub>3</sub> C(O)	97	CF <sub>3</sub> C(O)	97	CF <sub>3</sub> C(O)	97
CH <sub>2</sub> C(O)CF <sub>3</sub>	111	CH <sub>2</sub> C(O)CF <sub>3</sub>	111	CH <sub>2</sub> C(O)CF <sub>3</sub>	111	CH <sub>2</sub> C(O)CF <sub>3</sub>	111
Sm	154	Eu	151	Eu	153	Gd	155
Sm-O <sub>2</sub>	186	Eu-O <sub>2</sub>	183	Eu-O <sub>2</sub>	185	Gd-O <sub>2</sub>	187
CCH <sub>2</sub> C(O)CF <sub>3</sub>	123	CCH <sub>2</sub> C(O)CF <sub>3</sub>	123	CCH <sub>2</sub> C(O)CF <sub>3</sub>	123	CCH <sub>2</sub> C(O)CF <sub>3</sub>	123
Sm-CF <sub>3</sub> C(O)	251	Eu-CF <sub>3</sub> C(O)	248	Eu-CF <sub>3</sub> C(O)	250	Gd-CF <sub>3</sub> C(O)	252
Sm-CH <sub>2</sub> C(O)CF <sub>3</sub>	265	Eu-CH <sub>2</sub> C(O)CF <sub>3</sub>	262	Eu-CH <sub>2</sub> C(O)CF <sub>3</sub>	264	Gd-CH <sub>2</sub> C(O)CF <sub>3</sub>	266
Sm-CF <sub>3</sub> C(O)CHC(O)CF <sub>3</sub>	361	Eu-CF <sub>3</sub> C(O)CHC(O)CF <sub>3</sub>	358	Eu-CF <sub>3</sub> C(O)CHC(O)CF <sub>3</sub>	360	Gd-CF <sub>3</sub> C(O)CHC(O)CF <sub>3</sub>	362
Sm-CF <sub>3</sub> C(O)CH <sub>2</sub> C(O)CF <sub>2</sub>	343	Eu-CF <sub>3</sub> C(O)CH <sub>2</sub> C(O)CF <sub>2</sub>	340	Eu-CF <sub>3</sub> C(O)CH <sub>2</sub> C(O)CF <sub>2</sub>	342	Gd-CF <sub>3</sub> C(O)CH <sub>2</sub> C(O)CF <sub>2</sub>	344
Sm-OCCF <sub>3</sub>	251	Eu-OCCF <sub>3</sub>	248	Eu-OCCF <sub>3</sub>	250	Gd-OCCF <sub>3</sub>	252
Sm-CCH <sub>2</sub> C(O)CF <sub>3</sub>	277	Eu-CCH <sub>2</sub> C(O)CF <sub>3</sub>	274	Eu-CCH <sub>2</sub> C(O)CF <sub>3</sub>	276	Gd-CCH <sub>2</sub> C(O)CF <sub>3</sub>	278

Sm-CF <sub>3</sub> CCH <sub>2</sub> C(O)CF <sub>3</sub>	346	Eu-CF <sub>3</sub> CCH <sub>2</sub> C(O)CF <sub>3</sub>	343	Eu-CF <sub>3</sub> CCH <sub>2</sub> C(O)CF <sub>3</sub>	345	Gd-CF <sub>3</sub> CCH <sub>2</sub> C(O)CF <sub>3</sub>	347
CF <sub>3</sub> CCH <sub>2</sub> C(O)CF <sub>3</sub>	192	CF <sub>3</sub> CCH <sub>2</sub> C(O)CF <sub>3</sub>	192	CF <sub>3</sub> CCH <sub>2</sub> C(O)CF <sub>3</sub>	192	CF <sub>3</sub> CCH <sub>2</sub> C(O)CF <sub>3</sub>	192

<b>Gd-156 hfac</b>	<b>156</b>	<b>Gd-157 hfac</b>	<b>157</b>	<b>Gd-158 hfac</b>	<b>158</b>	<b>Gd-160 hfac</b>	<b>160</b>
Gd-CF <sub>3</sub> C(O)CH <sub>2</sub> C(O)CF <sub>3</sub>	364	Gd-CF <sub>3</sub> C(O)CH <sub>2</sub> C(O)CF <sub>3</sub>	365	Gd-CF <sub>3</sub> C(O)CH <sub>2</sub> C(O)CF <sub>3</sub>	366	Gd-CF <sub>3</sub> C(O)CH <sub>2</sub> C(O)CF <sub>3</sub>	368
CF <sub>3</sub>	69	CF <sub>3</sub>	69	CF <sub>3</sub>	69	CF <sub>3</sub>	69
Gd-C(O)CH <sub>2</sub> C(O)CF <sub>3</sub>	295	Gd-C(O)CH <sub>2</sub> C(O)CF <sub>3</sub>	296	Gd-C(O)CH <sub>2</sub> C(O)CF <sub>3</sub>	297	Gd-C(O)CH <sub>2</sub> C(O)CF <sub>3</sub>	299
CF <sub>3</sub> C(O)	97	CF <sub>3</sub> C(O)	97	CF <sub>3</sub> C(O)	97	CF <sub>3</sub> C(O)	97
CH <sub>2</sub> C(O)CF <sub>3</sub>	111	CH <sub>2</sub> C(O)CF <sub>3</sub>	111	CH <sub>2</sub> C(O)CF <sub>3</sub>	111	CH <sub>2</sub> C(O)CF <sub>3</sub>	111
Gd	156	Gd	157	Gd	158	Gd	160
Gd-O <sub>2</sub>	188	Gd-O <sub>2</sub>	189	Gd-O <sub>2</sub>	190	Gd-O <sub>2</sub>	192
CCH <sub>2</sub> C(O)CF <sub>3</sub>	123	CCH <sub>2</sub> C(O)CF <sub>3</sub>	123	CCH <sub>2</sub> C(O)CF <sub>3</sub>	123	CCH <sub>2</sub> C(O)CF <sub>3</sub>	123
Gd-CF <sub>3</sub> C(O)	253	Gd-CF <sub>3</sub> C(O)	254	Gd-CF <sub>3</sub> C(O)	255	Gd-CF <sub>3</sub> C(O)	257
Gd-CH <sub>2</sub> C(O)CF <sub>3</sub>	267	Gd-CH <sub>2</sub> C(O)CF <sub>3</sub>	268	Gd-CH <sub>2</sub> C(O)CF <sub>3</sub>	269	Gd-CH <sub>2</sub> C(O)CF <sub>3</sub>	271
Gd-CF <sub>3</sub> C(O)CHC(O)CF <sub>3</sub>	363	Gd-CF <sub>3</sub> C(O)CHC(O)CF <sub>3</sub>	364	Gd-CF <sub>3</sub> C(O)CHC(O)CF <sub>3</sub>	365	Gd-CF <sub>3</sub> C(O)CHC(O)CF <sub>3</sub>	367
Gd-CF <sub>3</sub> C(O)CH <sub>2</sub> C(O)CF <sub>2</sub>	345	Gd-CF <sub>3</sub> C(O)CH <sub>2</sub> C(O)CF <sub>2</sub>	346	Gd-CF <sub>3</sub> C(O)CH <sub>2</sub> C(O)CF <sub>2</sub>	347	Gd-CF <sub>3</sub> C(O)CH <sub>2</sub> C(O)CF <sub>2</sub>	349
Gd-OCCF <sub>3</sub>	253	Gd-OCCF <sub>3</sub>	254	Gd-OCCF <sub>3</sub>	255	Gd-OCCF <sub>3</sub>	257
Gd-CCH <sub>2</sub> C(O)CF <sub>3</sub>	279	Gd-CCH <sub>2</sub> C(O)CF <sub>3</sub>	280	Gd-CCH <sub>2</sub> C(O)CF <sub>3</sub>	281	Gd-CCH <sub>2</sub> C(O)CF <sub>3</sub>	283
Gd-CF <sub>3</sub> CCH <sub>2</sub> C(O)CF <sub>3</sub>	348	Gd-CF <sub>3</sub> CCH <sub>2</sub> C(O)CF <sub>3</sub>	349	Gd-CF <sub>3</sub> CCH <sub>2</sub> C(O)CF <sub>3</sub>	350	Gd-CF <sub>3</sub> CCH <sub>2</sub> C(O)CF <sub>3</sub>	352
CF <sub>3</sub> CCH <sub>2</sub> C(O)CF <sub>3</sub>	192	CF <sub>3</sub> CCH <sub>2</sub> C(O)CF <sub>3</sub>	192	CF <sub>3</sub> CCH <sub>2</sub> C(O)CF <sub>3</sub>	192	CF <sub>3</sub> CCH <sub>2</sub> C(O)CF <sub>3</sub>	192

<b>Tb-159 hfac</b>	<b>159</b>	<b>Dy-161 hfac</b>	<b>161</b>	<b>Dy-162 hfac</b>	<b>162</b>	<b>Dy-163 hfac</b>	<b>163</b>
Tb-CF <sub>3</sub> C(O)CH <sub>2</sub> C(O)CF <sub>3</sub>	367	Dy-CF <sub>3</sub> C(O)CH <sub>2</sub> C(O)CF <sub>3</sub>	369	Dy-CF <sub>3</sub> C(O)CH <sub>2</sub> C(O)CF <sub>3</sub>	370	Dy-CF <sub>3</sub> C(O)CH <sub>2</sub> C(O)CF <sub>3</sub>	371
CF <sub>3</sub>	69	CF <sub>3</sub>	69	CF <sub>3</sub>	69	CF <sub>3</sub>	69
Tb-C(O)CH <sub>2</sub> C(O)CF <sub>3</sub>	298	Dy-C(O)CH <sub>2</sub> C(O)CF <sub>3</sub>	300	Dy-C(O)CH <sub>2</sub> C(O)CF <sub>3</sub>	301	Dy-C(O)CH <sub>2</sub> C(O)CF <sub>3</sub>	302
CF <sub>3</sub> C(O)	97	CF <sub>3</sub> C(O)	97	CF <sub>3</sub> C(O)	97	CF <sub>3</sub> C(O)	97
CH <sub>2</sub> C(O)CF <sub>3</sub>	111	CH <sub>2</sub> C(O)CF <sub>3</sub>	111	CH <sub>2</sub> C(O)CF <sub>3</sub>	111	CH <sub>2</sub> C(O)CF <sub>3</sub>	111
Tb	159	Dy	161	Dy	162	Dy	163
Tb-O <sub>2</sub>	191	Dy-O <sub>2</sub>	193	Dy-O <sub>2</sub>	194	Dy-O <sub>2</sub>	195

CCH <sub>2</sub> C(O)CF <sub>3</sub>	123	CCH <sub>2</sub> C(O)CF <sub>3</sub>	123	CCH <sub>2</sub> C(O)CF <sub>3</sub>	123	CCH <sub>2</sub> C(O)CF <sub>3</sub>	123
Tb-CF <sub>3</sub> C(O)	256	Dy-CF <sub>3</sub> C(O)	258	Dy-CF <sub>3</sub> C(O)	259	Dy-CF <sub>3</sub> C(O)	260
Td-CH <sub>2</sub> C(O)CF <sub>3</sub>	270	Dy-CH <sub>2</sub> C(O)CF <sub>3</sub>	272	Dy-CH <sub>2</sub> C(O)CF <sub>3</sub>	273	Dy-CH <sub>2</sub> C(O)CF <sub>3</sub>	274
Tb-CF <sub>3</sub> C(O)CHC(O)CF <sub>3</sub>	366	Dy-CF <sub>3</sub> C(O)CHC(O)CF <sub>3</sub>	368	Dy-CF <sub>3</sub> C(O)CHC(O)CF <sub>3</sub>	369	Dy-CF <sub>3</sub> C(O)CHC(O)CF <sub>3</sub>	370
Tb-CF <sub>3</sub> C(O)CH <sub>2</sub> C(O)CF <sub>2</sub>	348	Dy-CF <sub>3</sub> C(O)CH <sub>2</sub> C(O)CF <sub>2</sub>	350	Dy-CF <sub>3</sub> C(O)CH <sub>2</sub> C(O)CF <sub>2</sub>	351	Dy-CF <sub>3</sub> C(O)CH <sub>2</sub> C(O)CF <sub>2</sub>	352
Tb-OCCF <sub>3</sub>	256	Dy-OCCF <sub>3</sub>	258	Dy-OCCF <sub>3</sub>	259	Dy-OCCF <sub>3</sub>	260
Tb-CCH <sub>2</sub> C(O)CF <sub>3</sub>	282	Dy-CCH <sub>2</sub> C(O)CF <sub>3</sub>	284	Dy-CCH <sub>2</sub> C(O)CF <sub>3</sub>	285	Dy-CCH <sub>2</sub> C(O)CF <sub>3</sub>	286
Tb-CF <sub>3</sub> CCH <sub>2</sub> C(O)CF <sub>3</sub>	351	Dy-CF <sub>3</sub> CCH <sub>2</sub> C(O)CF <sub>3</sub>	353	Dy-CF <sub>3</sub> CCH <sub>2</sub> C(O)CF <sub>3</sub>	354	Dy-CF <sub>3</sub> CCH <sub>2</sub> C(O)CF <sub>3</sub>	355
CF <sub>3</sub> CCH <sub>2</sub> C(O)CF <sub>3</sub>	192	CF <sub>3</sub> CCH <sub>2</sub> C(O)CF <sub>3</sub>	192	CF <sub>3</sub> CCH <sub>2</sub> C(O)CF <sub>3</sub>	192	CF <sub>3</sub> CCH <sub>2</sub> C(O)CF <sub>3</sub>	192

<b>Dy-164 hfac</b>	<b>164</b>	<b>Ho-165 hfac</b>	<b>165</b>	<b>Er-166 hfac</b>	<b>166</b>	<b>Er-167 hfac</b>	<b>167</b>
Dy-CF <sub>3</sub> C(O)CH <sub>2</sub> C(O)CF <sub>3</sub>	372	Ho-CF <sub>3</sub> C(O)CH <sub>2</sub> C(O)CF <sub>3</sub>	373	Er-CF <sub>3</sub> C(O)CH <sub>2</sub> C(O)CF <sub>3</sub>	374	Er-CF <sub>3</sub> C(O)CH <sub>2</sub> C(O)CF <sub>3</sub>	375
CF <sub>3</sub>	69	CF <sub>3</sub>	69	CF <sub>3</sub>	69	CF <sub>3</sub>	69
Dy-C(O)CH <sub>2</sub> C(O)CF <sub>3</sub>	303	Ho-C(O)CH <sub>2</sub> C(O)CF <sub>3</sub>	304	Er-C(O)CH <sub>2</sub> C(O)CF <sub>3</sub>	305	Er-C(O)CH <sub>2</sub> C(O)CF <sub>3</sub>	306
CF <sub>3</sub> C(O)	97	CF <sub>3</sub> C(O)	97	CF <sub>3</sub> C(O)	97	CF <sub>3</sub> C(O)	97
CH <sub>2</sub> C(O)CF <sub>3</sub>	111	CH <sub>2</sub> C(O)CF <sub>3</sub>	111	CH <sub>2</sub> C(O)CF <sub>3</sub>	111	CH <sub>2</sub> C(O)CF <sub>3</sub>	111
Dy	164	Ho	165	Er	166	Er	167
Dy-O <sub>2</sub>	196	Ho-O <sub>2</sub>	197	Er-O <sub>2</sub>	198	Er-O <sub>2</sub>	199
CCH <sub>2</sub> C(O)CF <sub>3</sub>	123	CCH <sub>2</sub> C(O)CF <sub>3</sub>	123	CCH <sub>2</sub> C(O)CF <sub>3</sub>	123	CCH <sub>2</sub> C(O)CF <sub>3</sub>	123
Dy-CF <sub>3</sub> C(O)	261	Ho-CF <sub>3</sub> C(O)	262	Er-CF <sub>3</sub> C(O)	263	Er-CF <sub>3</sub> C(O)	264
Dy-CH <sub>2</sub> C(O)CF <sub>3</sub>	275	Ho-CH <sub>2</sub> C(O)CF <sub>3</sub>	276	Er-CH <sub>2</sub> C(O)CF <sub>3</sub>	277	Er-CH <sub>2</sub> C(O)CF <sub>3</sub>	278
Dy-CF <sub>3</sub> C(O)CHC(O)CF <sub>3</sub>	371	Ho-CF <sub>3</sub> C(O)CHC(O)CF <sub>3</sub>	372	Er-CF <sub>3</sub> C(O)CHC(O)CF <sub>3</sub>	373	Er-CF <sub>3</sub> C(O)CHC(O)CF <sub>3</sub>	374
Dy-CF <sub>3</sub> C(O)CH <sub>2</sub> C(O)CF <sub>2</sub>	353	Ho-CF <sub>3</sub> C(O)CH <sub>2</sub> C(O)CF <sub>2</sub>	354	Er-CF <sub>3</sub> C(O)CH <sub>2</sub> C(O)CF <sub>2</sub>	355	Er-CF <sub>3</sub> C(O)CH <sub>2</sub> C(O)CF <sub>2</sub>	356
Dy-OCCF <sub>3</sub>	261	Ho-OCCF <sub>3</sub>	262	Er-OCCF <sub>3</sub>	263	Er-OCCF <sub>3</sub>	264
Dy-CCH <sub>2</sub> C(O)CF <sub>3</sub>	287	Ho-CCH <sub>2</sub> C(O)CF <sub>3</sub>	288	Er-CCH <sub>2</sub> C(O)CF <sub>3</sub>	289	Er-CCH <sub>2</sub> C(O)CF <sub>3</sub>	290
Dy-CF <sub>3</sub> CCH <sub>2</sub> C(O)CF <sub>3</sub>	356	Ho-CF <sub>3</sub> CCH <sub>2</sub> C(O)CF <sub>3</sub>	357	Er-CF <sub>3</sub> CCH <sub>2</sub> C(O)CF <sub>3</sub>	358	Er-CF <sub>3</sub> CCH <sub>2</sub> C(O)CF <sub>3</sub>	359
CF <sub>3</sub> CCH <sub>2</sub> C(O)CF <sub>3</sub>	192	CF <sub>3</sub> CCH <sub>2</sub> C(O)CF <sub>3</sub>	192	CF <sub>3</sub> CCH <sub>2</sub> C(O)CF <sub>3</sub>	192	CF <sub>3</sub> CCH <sub>2</sub> C(O)CF <sub>3</sub>	192

<b>Er-168 hfac</b>	<b>168</b>	<b>Er-170 hfac</b>	<b>170</b>	<b>Tm-169 hfac</b>	<b>169</b>	<b>Yb-171 hfac</b>	<b>171</b>
--------------------	------------	--------------------	------------	--------------------	------------	--------------------	------------

Er-CF <sub>3</sub> C(O)CH <sub>2</sub> C(O)CF <sub>3</sub>	376	Er-CF <sub>3</sub> C(O)CH <sub>2</sub> C(O)CF <sub>3</sub>	378	Tm-CF <sub>3</sub> C(O)CH <sub>2</sub> C(O)CF <sub>3</sub>	377	Yb-CF <sub>3</sub> C(O)CH <sub>2</sub> C(O)CF <sub>3</sub>	379
CF <sub>3</sub>	69	CF <sub>3</sub>	69	CF <sub>3</sub>	69	CF <sub>3</sub>	69
Er-C(O)CH <sub>2</sub> C(O)CF <sub>3</sub>	307	Er-C(O)CH <sub>2</sub> C(O)CF <sub>3</sub>	309	Tm-C(O)CH <sub>2</sub> C(O)CF <sub>3</sub>	308	Yb-C(O)CH <sub>2</sub> C(O)CF <sub>3</sub>	310
CF <sub>3</sub> C(O)	97	CF <sub>3</sub> C(O)	97	CF <sub>3</sub> C(O)	97	CF <sub>3</sub> C(O)	97
CH <sub>2</sub> C(O)CF <sub>3</sub>	111	CH <sub>2</sub> C(O)CF <sub>3</sub>	111	CH <sub>2</sub> C(O)CF <sub>3</sub>	111	CH <sub>2</sub> C(O)CF <sub>3</sub>	111
Er	168	Er	170	Tm	169	Yb	171
Er-O <sub>2</sub>	200	Er-O <sub>2</sub>	202	Tm-O <sub>2</sub>	201	Yb-O <sub>2</sub>	203
CCH <sub>2</sub> C(O)CF <sub>3</sub>	123	CCH <sub>2</sub> C(O)CF <sub>3</sub>	123	CCH <sub>2</sub> C(O)CF <sub>3</sub>	123	CCH <sub>2</sub> C(O)CF <sub>3</sub>	123
Er-CF <sub>3</sub> C(O)	265	Er-CF <sub>3</sub> C(O)	267	Tm-CF <sub>3</sub> C(O)	266	Yb-CF <sub>3</sub> C(O)	268
Er-CH <sub>2</sub> C(O)CF <sub>3</sub>	279	Er-CH <sub>2</sub> C(O)CF <sub>3</sub>	281	Tm-CH <sub>2</sub> C(O)CF <sub>3</sub>	280	Yb-CH <sub>2</sub> C(O)CF <sub>3</sub>	282
Er-CF <sub>3</sub> C(O)CHC(O)CF <sub>3</sub>	375	Er-CF <sub>3</sub> C(O)CHC(O)CF <sub>3</sub>	377	Tm-CF <sub>3</sub> C(O)CHC(O)CF <sub>3</sub>	376	Yb-CF <sub>3</sub> C(O)CHC(O)CF <sub>3</sub>	378
Er-CF <sub>3</sub> C(O)CH <sub>2</sub> C(O)CF <sub>2</sub>	357	Er-CF <sub>3</sub> C(O)CH <sub>2</sub> C(O)CF <sub>2</sub>	359	Tm-CF <sub>3</sub> C(O)CH <sub>2</sub> C(O)CF <sub>2</sub>	358	Yb-CF <sub>3</sub> C(O)CH <sub>2</sub> C(O)CF <sub>2</sub>	360
Er-OCCF <sub>3</sub>	265	Er-OCCF <sub>3</sub>	267	Tm-OCCF <sub>3</sub>	266	Yb-OCCF <sub>3</sub>	268
Er-CCH <sub>2</sub> C(O)CF <sub>3</sub>	291	Er-CCH <sub>2</sub> C(O)CF <sub>3</sub>	293	Tm-CCH <sub>2</sub> C(O)CF <sub>3</sub>	292	Yb-CCH <sub>2</sub> C(O)CF <sub>3</sub>	294
Er-CF <sub>3</sub> CCH <sub>2</sub> C(O)CF <sub>3</sub>	360	Er-CF <sub>3</sub> CCH <sub>2</sub> C(O)CF <sub>3</sub>	362	Tm-CF <sub>3</sub> CCH <sub>2</sub> C(O)CF <sub>3</sub>	361	Yb-CF <sub>3</sub> CCH <sub>2</sub> C(O)CF <sub>3</sub>	363
CF <sub>3</sub> CCH <sub>2</sub> C(O)CF <sub>3</sub>	192	CF <sub>3</sub> CCH <sub>2</sub> C(O)CF <sub>3</sub>	192	CF <sub>3</sub> CCH <sub>2</sub> C(O)CF <sub>3</sub>	192	CF <sub>3</sub> CCH <sub>2</sub> C(O)CF <sub>3</sub>	192

<b>Yb-172 hfac</b>	<b>172</b>	<b>Yb-173 hfac</b>	<b>173</b>	<b>Yb-174 hfac</b>	<b>174</b>	<b>Yb-176 hfac</b>	<b>176</b>
Yb-CF <sub>3</sub> C(O)CH <sub>2</sub> C(O)CF <sub>3</sub>	380	Yb-CF <sub>3</sub> C(O)CH <sub>2</sub> C(O)CF <sub>3</sub>	381	Yb-CF <sub>3</sub> C(O)CH <sub>2</sub> C(O)CF <sub>3</sub>	382	Yb-CF <sub>3</sub> C(O)CH <sub>2</sub> C(O)CF <sub>3</sub>	384
CF <sub>3</sub>	69	CF <sub>3</sub>	69	CF <sub>3</sub>	69	CF <sub>3</sub>	69
Yb-C(O)CH <sub>2</sub> C(O)CF <sub>3</sub>	311	Yb-C(O)CH <sub>2</sub> C(O)CF <sub>3</sub>	312	Yb-C(O)CH <sub>2</sub> C(O)CF <sub>3</sub>	313	Yb-C(O)CH <sub>2</sub> C(O)CF <sub>3</sub>	315
CF <sub>3</sub> C(O)	97	CF <sub>3</sub> C(O)	97	CF <sub>3</sub> C(O)	97	CF <sub>3</sub> C(O)	97
CH <sub>2</sub> C(O)CF <sub>3</sub>	111	CH <sub>2</sub> C(O)CF <sub>3</sub>	111	CH <sub>2</sub> C(O)CF <sub>3</sub>	111	CH <sub>2</sub> C(O)CF <sub>3</sub>	111
Yb	172	Yb	173	Yb	174	Yb	176
Yb-O <sub>2</sub>	204	Yb-O <sub>2</sub>	205	Yb-O <sub>2</sub>	206	Yb-O <sub>2</sub>	208
CCH <sub>2</sub> C(O)CF <sub>3</sub>	123	CCH <sub>2</sub> C(O)CF <sub>3</sub>	123	CCH <sub>2</sub> C(O)CF <sub>3</sub>	123	CCH <sub>2</sub> C(O)CF <sub>3</sub>	123
Yb-CF <sub>3</sub> C(O)	269	Yb-CF <sub>3</sub> C(O)	270	Yb-CF <sub>3</sub> C(O)	271	Yb-CF <sub>3</sub> C(O)	273
Yb-CH <sub>2</sub> C(O)CF <sub>3</sub>	283	Yb-CH <sub>2</sub> C(O)CF <sub>3</sub>	284	Yb-CH <sub>2</sub> C(O)CF <sub>3</sub>	285	Yb-CH <sub>2</sub> C(O)CF <sub>3</sub>	287
Yb-CF <sub>3</sub> C(O)CHC(O)CF <sub>3</sub>	379	Yb-CF <sub>3</sub> C(O)CHC(O)CF <sub>3</sub>	380	Yb-CF <sub>3</sub> C(O)CHC(O)CF <sub>3</sub>	381	Yb-CF <sub>3</sub> C(O)CHC(O)CF <sub>3</sub>	383
Yb-CF <sub>3</sub> C(O)CH <sub>2</sub> C(O)CF <sub>2</sub>	361	Yb-CF <sub>3</sub> C(O)CH <sub>2</sub> C(O)CF <sub>2</sub>	362	Yb-CF <sub>3</sub> C(O)CH <sub>2</sub> C(O)CF <sub>2</sub>	363	Yb-CF <sub>3</sub> C(O)CH <sub>2</sub> C(O)CF <sub>2</sub>	365
Yb-OCCF <sub>3</sub>	269	Yb-OCCF <sub>3</sub>	270	Yb-OCCF <sub>3</sub>	271	Yb-OCCF <sub>3</sub>	273
Yb-CCH <sub>2</sub> C(O)CF <sub>3</sub>	295	Yb-CCH <sub>2</sub> C(O)CF <sub>3</sub>	296	Yb-CCH <sub>2</sub> C(O)CF <sub>3</sub>	297	Yb-CCH <sub>2</sub> C(O)CF <sub>3</sub>	299

Yb-CF <sub>3</sub> CCH <sub>2</sub> C(O)CF <sub>3</sub>	364	Yb-CF <sub>3</sub> CCH <sub>2</sub> C(O)CF <sub>3</sub>	365	Yb-CF <sub>3</sub> CCH <sub>2</sub> C(O)CF <sub>3</sub>	366	Yb-CF <sub>3</sub> CCH <sub>2</sub> C(O)CF <sub>3</sub>	368
CF <sub>3</sub> CCH <sub>2</sub> C(O)CF <sub>3</sub>	192	CF <sub>3</sub> CCH <sub>2</sub> C(O)CF <sub>3</sub>	192	CF <sub>3</sub> CCH <sub>2</sub> C(O)CF <sub>3</sub>	192	CF <sub>3</sub> CCH <sub>2</sub> C(O)CF <sub>3</sub>	192

<b>Lu-175 hfac</b>	<b>175</b>
Lu-CF <sub>3</sub> C(O)CH <sub>2</sub> C(O)CF <sub>3</sub>	383
CF <sub>3</sub>	69
Lu-C(O)CH <sub>2</sub> C(O)CF <sub>3</sub>	314
CF <sub>3</sub> C(O)	97
CH <sub>2</sub> C(O)CF <sub>3</sub>	111
Lu	175
Lu-O <sub>2</sub>	207
CCH <sub>2</sub> C(O)CF <sub>3</sub>	123
Lu-CF <sub>3</sub> C(O)	272
Lu-CH <sub>2</sub> C(O)CF <sub>3</sub>	286
Lu-CF <sub>3</sub> C(O)CHC(O)CF <sub>3</sub>	382
Lu-CF <sub>3</sub> C(O)CH <sub>2</sub> C(O)CF <sub>2</sub>	364
Lu-OCCF <sub>3</sub>	272
Lu-CCH <sub>2</sub> C(O)CF <sub>3</sub>	298
Lu-CF <sub>3</sub> CCH <sub>2</sub> C(O)CF <sub>3</sub>	367
CF <sub>3</sub> CCH <sub>2</sub> C(O)CF <sub>3</sub>	192

**\*Special thanks to Mr. Austin Mullen for his hard work in compiling this fragmentation database**



## APPENDIX E

### THERMOGRAVIMETRIC ANALYSIS

The following is taken from the article “Thermodynamic Analysis of Volatile Organometallic Fission Products” in the *Journal of Radioanalytical and Nuclear Chemistry* of which I am a co-author.<sup>61</sup>

**Table E.1** Thermogravimetric Predictions of Enthalpy of Adsorption

	Atomic Radius (A)	H <sub>sub</sub> (-KJ/mol)	+/-	H <sub>ads</sub> (-KJ/mol)	+/-
<b>La</b>	7.25E-05	119.86	15.92	93.42	11.28
<b>Pr</b>	7.29E-05	191.87	27.11	136.62	17.74
<b>Nd</b>	7.34E-05	161.95	2.68	118.67	6.78
<b>Sm</b>	7.44E-05	201.91	8.68	142.64	8.93
<b>Eu</b>	7.47E-05	150.44	2.92	111.77	6.65
<b>Gd</b>	7.55E-05	196.04	21.46	139.12	14.72
<b>Tb</b>	7.58E-05	195.45	6.60	138.77	8.16
<b>Dy</b>	7.65E-05	188.84	6.39	134.81	8.00
<b>Ho</b>	7.68E-05	118.72	17.49	92.73	12.08
<b>Er</b>	7.71E-05	82.32	3.49	70.89	5.97
<b>Tm</b>	7.74E-05	155.52	11.53	114.81	9.49
<b>Yb</b>	7.80E-05	146.56	7.00	109.43	7.62
<b>Lu</b>	7.83E-05	98.03	0.57	80.32	5.76

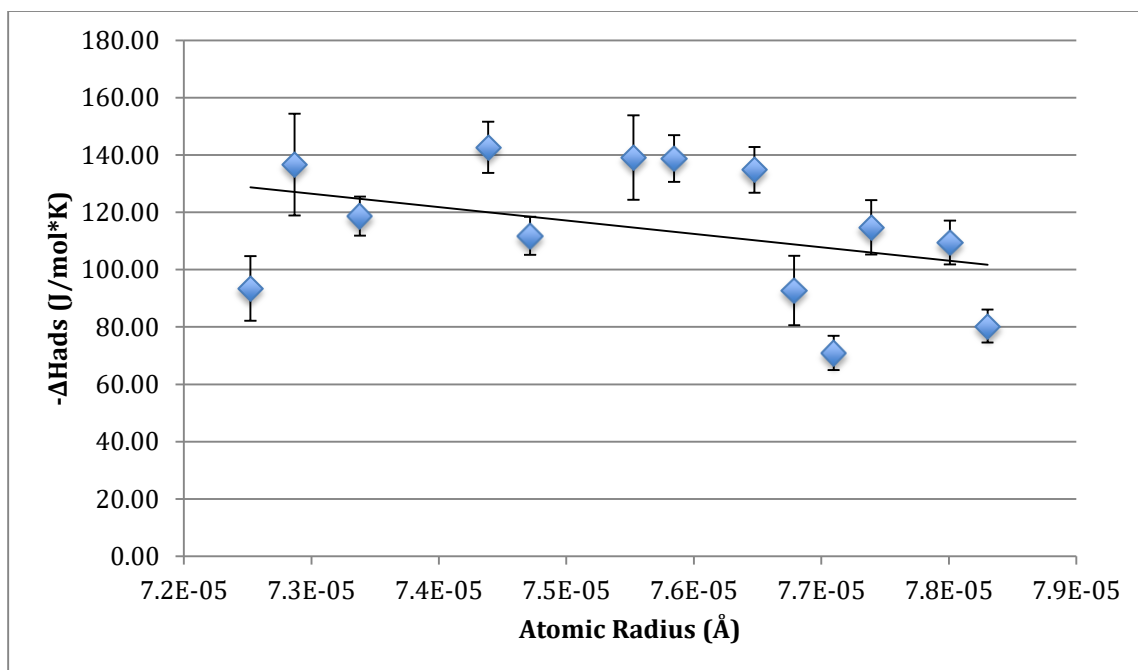


**Figure E.1** Predicted Adsorption Enthalpy vs Atomic Radius

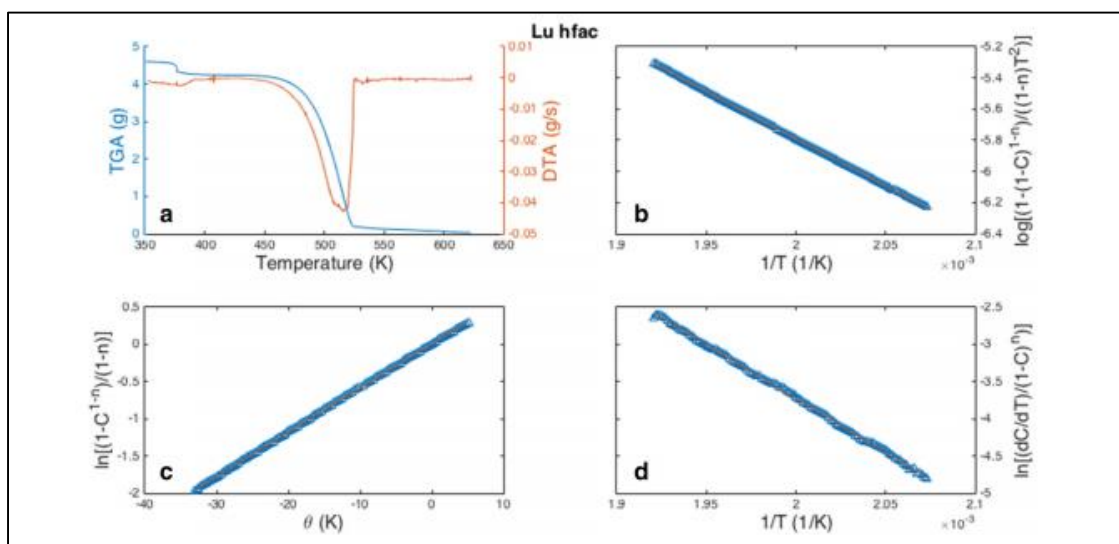


**Figure E.2** (a) The TGA/DSC data for the  $\text{NH}_4\text{Lu}[\text{hfac}]_4$  compounds, (b) Coats-Redfern method, (c) Horowitz-Metzger method, and (d) Freeman Carroll method

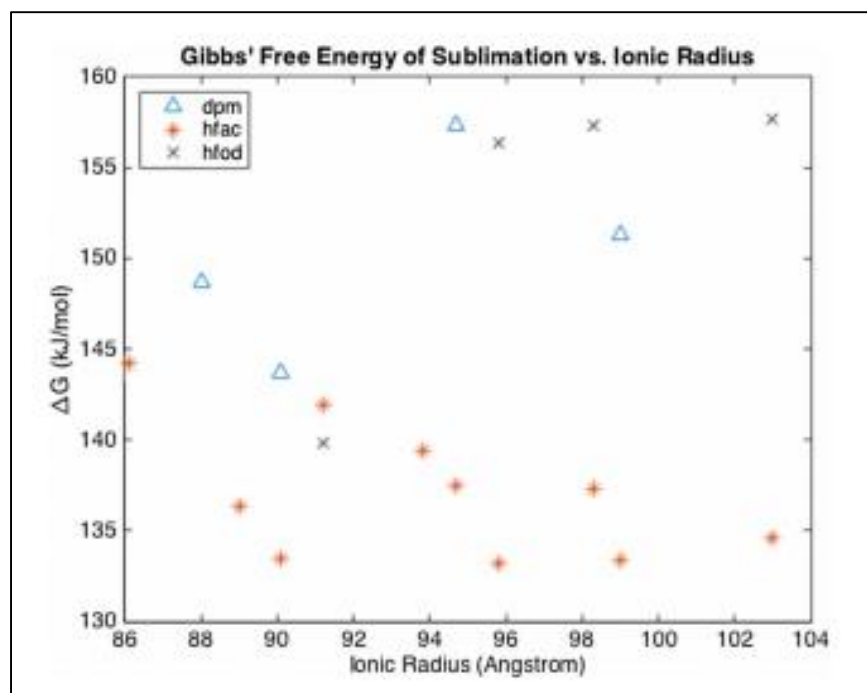


**Figure E.3** The average (of the HM and CR methods) Gibbs' free energy of sublimation (ordinate) is plotted as a function of the ionic radius (abscissa)

The following methodology section was co-written by Mr. Shayan Shahbazi and Mr. Jake Jordan in our co-authored paper, *Thermodynamic Analysis of Volatile Organometallic Fission Products*.<sup>61</sup>

The thermodynamic data can be used to predict the retention times in thermochromatographic experiments as noted by Eichler et al.<sup>34</sup>

$$t_r = \frac{LT_0\phi}{\bar{V}_0 T_{iso}} \times \left( 1 + \frac{s}{v} \times \frac{V}{100A} \times \exp\left(-\frac{\Delta H_{ads}^0}{RT_{iso}}\right) \times \exp\left(\frac{\Delta S_{ads}^0}{R}\right) \right)$$

### Equation E.1

where  $L$  is the length of the column,  $T_0$  is standard temperature 298.15 K,  $\phi$  is the free open cross-sectional area of the column,  $\bar{V}_0$  is the carrier gas flow at STP (standard temperature and pressure),  $T_{iso}$  is the isothermal column temperature,  $s$  is the open surface of column per 1 m column length,  $v$  is the open volume of the column per 1 m column length,  $V$  is the inner volume of the column,  $A$  is the inner surface per 1 m of column length, and  $R$  is the ideal gas constant. The entropy of adsorption can be calculated from the previous equation, while the enthalpy of adsorption can be found using:

$$-\Delta H_{ads}^0 = (2.9 \pm 16) + (.73 \pm .1) \times \Delta H_{subl}^0$$

### Equation E.2

where the enthalpy of sublimation was taken from the thermodynamic models mentioned previously. The Coats-Redfern and the Horowitz-Metzger methods were used for calculation of the parameter, while the Freeman-Carroll was not used due to the inconsistent nature of parameter values obtained from the method. The calculation of  $\Delta S_{ads}^0$  can be done using:

$$\Delta S_{ads}^0 = R \left( \ln \left( \frac{100A}{V \times v_b} \right) \times \sqrt{\frac{R \times T}{2 \times \pi \times M_a} + \frac{1}{2}} \right)$$

### Equation E.3

where the entropy of adsorption is related to  $R$ , the ideal gas constant, the area of the column,  $A$ , the volume of the column,  $V$ , the phonon frequency of the column material (e.g., quartz, etc.),  $\nu_b$ , the temperature,  $T$ , and the mass of the adsorbing material,  $M_a$ . The approximate retention times using a thermochromatography unit fitted with a 30 m SiO<sub>2</sub> column operating at 150 C, with a flow rate of 0.8 cm/s and an inner diameter of 0.5 mm, were approximated.

## VITA

Adam was born in Nashville, TN and graduated from Father Ryan High School in 2009. He received his undergraduate degree from Tennessee Technological University in Civil and Environmental Engineering with Summa Cum Laude standing and received his Master's degree from the same institution in Civil Engineering. He received the Rising Renaissance Engineering Award and Scholarship in his department as a senior engineering student. His research included the effects of climate change on fundamental hydrologic control variables used in the design of major hydraulic dams, projection of extreme precipitation patterns in dynamic climate systems, and dam fortification for post-construction developments in probable maximum precipitation patterns.

Adam was accepted to the University of Tennessee Department of Nuclear Engineering PhD program and moved to Knoxville to begin research at the Radiochemistry Center of Excellence and Institute for Nuclear Security. He was a teaching assistant for Introduction to Nuclear and Radiological Engineering and Principles of Health Physics in his first year, and in his second year, Adam was awarded a fellowship from the Department of Homeland Security Domestic Nuclear Detection Office in Nuclear Forensics. Adam received the local American Nuclear Society chapter's graduate student scholarship and the American Nuclear Society Decommissioning and Environmental Science Division national scholarship in 2015, and was granted a 10-week practicum at Lawrence Livermore National Laboratories in 2016, where he worked in prompt weapon diagnostic instrumentation. He has presented research at eleven national conferences and program reviews and has coauthored six publications in his field, both

published and in review. He will begin a postdoctoral fellowship with the National Nuclear Security Administration upon completion of his doctorate.